February 2012

Ph.D. Dissertation

Improving the systemic exposure of poorly bioavailable drugs via the nano drug delivery systems: Preparation and in vitro/in vivo characterization

Graduate School of Chosun University

Department of Pharmacy

Fu Qiang

February 2012 Ph.D. Dissertation Improving the systemic exposure of poorly bioavailable drugs via the nano drug delivery systems: Preparation and in vitro/in vivo Fu Qiang

February 2012

Ph.D. Dissertation

Improving the systemic exposure of poorly bioavailable drugs via the nano drug delivery systems: Preparation and in vitro/in vivo characterization

Graduate School of Chosun University

Department of Pharmacy

Fu Qiang

Improving the systemic exposure of poorly bioavailable drugs via the nano drug delivery systems: Preparation and in vitro/in vivo characterization

약물의 생체이용률 개선을 위한
나노약물전달시스템의 개발 및 이의 in vitro/in vivo 특성 평가

February 24 2012

Graduate School of Chosun University

Department of Pharmacy

Fu Qiang

Improving the systemic exposure of poorly bioavailable drugs via the nano drug delivery systems: Preparation and in vitro/in vivo characterization

Adviser Hoo-Kyun Choi

The Dissertation Submitted to The Graduate School of Chosun University in partial fulfillment of Requirements for the Degree of Ph.D. of Pharmacy

October 2011

Graduate School of Chosun University

Department of Pharmacy

Fu Qiang

부강의 박사학위논문을 인준함

위원장	동국대학교	교 수	한효경	인
위 원	조선대학교	교 수	최후균	인
위 원	조선대학교	교 수	최준식	인
위 원	조선대학교	교 수	이원재	인
위 원	조선대학교	교 수	유진욱	인

2011 년 12 월

조선대학교 대학원

CONTENTS

Chapter 1

Characterization of Nanoparticles intended for Drug Delivery

Chapter 2

Fexofenadine nanoliposomes for the enhanced intranasal systemic delivery: development and pharmacokinetic evaluation

Chapter 3

Enhanced dissolution and bioavailability of rebamipide via the preparation of organo-clay based drug delivery system

List of Figures

Chapter 1

Chapter 2

Chapter 3

List of Tables

Chapter 2

Chapter 3

국문초록

약물의 생체이용률 개선을 위한 나노약물전달시스템의 개발 및 이의 in vitro/in vivo 특성 평가

부강
지도교수: 최후균
약학과
조선대학교 대학원

Nanotechnology의 제품은 nanotechnology와 nanomedicine 연구를 지원하기 위하여 최근 과학진보 및 글로벌 계획에 의해 입증됨으로써 현대 약의 혁명을 일으킬 것으로 예상되고 있다. 약물 전달 분야는 이러한 발전의 직접적인 수혜자이다. 깊은 분자 표적 및 제어 약물 자료를 액세스하여 대상 조직에서의 표적으로 인해서 현재nanoparticles의 과제는 현대의 전달뿐만 아니라, 기존의 약물전달의 직면에 도움이 되고 있다. 약품의 대다수가 고체를 채택하기 때문에, nanoparticles에는 약품 발달에 대한 광범위한 영향이 있을 것으로 예상된다. 이 논문의 목적은 nanoparticles의 응용을 통해 제대로 bioavailable 약물의 전신 노출을 개선하는 실질적인 존재이다. 업계, 학계 및 규제 기관뿐만 아니라, 생물 의학 공학, 화학 공학, 약학 및 약물 전달에 관심이있는 다른 과학 분야의 나노 약물 전달 시스템에 적용될 수 있다. 이 논문은 세 부분으로 구성되어있다. 첫 번째 섹션은 이제 의학 나노기술의 응용 프로그램에서 실현되고있는 흥미로운 기회의 일부를 설명한다. 나노 약물 개발자에게 toolsets 공학의 유연성을 제공함으로써 전통적인 제약 디자인 혁명이라 볼 수 있다. nanoparticle에 대한 구별 기본 속성과 기술이 장에서는 의학

나노기술의 응용 프로그램의 광범위한 개요를 제공 논문 볼륨을 소개 역할을 하고, 나노기술 기반 nanoliposomes 및 nanoclay의 약물 전달의 유익한 측면의 일부를 설명한다. 우리는 나노기술을 정의하고 나노 약물 전달 응용 프로그램에서 사용 nanomaterials의 주요 클래스의 간단한 설명을 제공한다.

두 번째 섹션은 nanoliposome의 특성은 비강 전달 속성과 효과를 관련 설명한다. 이 작품의 목적은 비강 전달을 위해 nanoliposome의 개발과 저조한 흡수성 fexofenadine의 생체 이용률을 높이는 것이었다. Nanoliposome는 액셀러레이터 안정제와 같은 지질 핵심 소재 및 chitosnan로 DPPC, DPPG과 콜레스테롤을 사용하여 설계되었다. nanoliposome (Lip)와 공동 키토산 nanoliposome (CS - Lip)로 구성된 nanoliposome 시스템은 체외 마약 릴리스 셀 이해에서 입자 크기, 제타 전위, entrapment efficiency, 고체 연구에 의해 특징되었고, 비강 전달을 위해 개발되었다. mucin 흡착 및 저장 안정성. Pharmacokinetic 연구는 또한 SD rats 에서 수행되었다. 체외 연구에서, 그것은 Lip 및 CS - Lip 이 66% 근처에 좋은 약물 entrapment, 원하는 릴리스 및 mucin 흡착 특성, 구형 형상과 최대 저장 안정성이 있다고 관찰했다. 치료 분말에 비해 CS - Lip 은 긍정적인 결과에도 불구하고 장기 보존을 달성할 수 있다. 그 Lip 을 연구하고, CS - Lip 을 저장하고 이해 연구함으로써 약물 방출 속도를 제어하고 촬영 시간에 따른 릴리스 피할 수 있다. 또한, 비강 pharmacokinetic 연구는 CS - Lip ($P < 0.05$)은 치료 분말 제제에 비해 rats 에 대한 fexofenadine의 시스템 노출을 강화 시킨 것을 지적했다. CS - Lip 은 비강 경로에서 fexofenadine 버전을 제어하는 최적의 배합으로 발견되었다. 비강으로 2.0 mg / kg 용량으로 투여시 $T_{1/2}$는 6.8시간으로 연장되었고, 절대 생체이용율은 정맥 투여에 대비해 약 35%였다. 우리의 결과는 다음과 CS - Lip 공법은 fexofenadine 의 제어 약물 릴리스 전달을위한 효과적인 비강 투여 형태로 사용될 수 있다고 제안했다.

세 번째 섹션은 약물 전달에서 nanoparticles의 소설 AMP - Clay 를 제공한다. 이 연구는 점토 기반의 유기-무기 하이브리드 재료를 사용하여 경구 전달 시스템을 통해 rebamipide 의 해산과 생체 이용률을 향상시키기 위해 목표로 하고 있다. Aminopropyl 기능화 마그네슘 phyllosilicate가 phyllosilicate가 이후 rebamipide의 존재에 다시 모였다. 피부 박피를 양이온 organoclay의 분산 (AMP - Clay)를 준비하는

데 사용된 합성 organo 기능화 및 trioctahedral 마그네슘의 층간 aminopropyl 그룹의 protonation에 의해 준비되었고 통합되었다. intercalated nanocomposites 계층 (Reb - AMPclay). Reb - AMPclay 55 %의 약물 로딩 효율 합성되었으며, 그 구조 특성은 ^{1}H - NMR, FT - IR, XRD 및 TEM에 의해 확인되었다. organo - Clay 에서 rebamipide의 용해도 및 약물 릴리스의 특징은 2.0 ~ 10.0의 산도 범위 또한 시뮬레이션 위장이나 창자 체액에서 평가되었다. Reb - AMPclay의 경구투여에 의한 rebamipide의 전신 노출도 rats에서 조사되었다. 치료 분말에 비해 Reb - AMPclay rebamipide는 독립적인 약물 릴리스로 이어지는 용해도뿐만 아니라, 낮은 산도에서의 rebamipide의 약물 릴리스의 범위를 향상시켰다. 특히, Reb - AMPclay는 치료 가루에 비해, 가상 위액에 약 1000 폴드에 의해 rebamipide의 용해를 증가시켰다. 또한, 구두 pharmacokinetic 연구 Reb - AMPclay 은 크게 ($P < 0.05$) 치료 분말 제제 및 AMP - clay (Reb - mix - AMPclay)과 rebamipide의 physicalmixture에 비해 rats에서 rebamipide의 구두 노출 향상된 것을 지적했다. $T_{1/2}$ 에 상당한 변화가 없는 반면 Reb - AMPclay의 경구투여 (20 mg/kg rebamipide) 이후 rebamipide의 C_{max}와 AUC는 각각, 2.1, 1.8배 증가하였고 T_{max} 가 3.0로 감소했을 때 $t_{1/2}$ 는 변화가 없었다. Organo -Clay 와 결합한Reb는 산도에 독립적인 용해와 rats에서 rebamipide의 생체 이용률을 향상시키는데 효과적인 것으로 보였다.

Chapter 1

Characterization of Nanoparticles intended for Drug Delivery

1. Recent Developments of Nanotechnology to Drug Delivery

During the last few years terms like nanomaterials, nanocomposites and nanosystems have become fashionable. It seems that anything with 'nano' attached to it has nearly a magical effect – not so much on performance as on expectations. There is an extensive effort to introduce nanotechnology offers many potential benefits to medical research by making pharmaceuticals more efficacious and by decreasing their adverse side-effects. Preclinical characterization of nanoparticles intended for medical applications is complicated – due to the variety of materials used, their unique surface properties and multifunctional nature. This chapter serves as an introduction to the thesis volume, giving a broad overview of applications of nanotechnology to medicine, and describes some of the beneficial aspects of nanotechnology-based drug delivery. We define nanotechnology and provide brief descriptions of the major classes of nanomaterials used for medical applications[1].

Prior to an involved discussion for nanotechnology, a definition of terms is in order. The SI prefix "nano" means a billionth (10^{-9}) part, and a nanometer is thus a billionth of a meter (about one hundred thousandth the thickness of a sheet of paper) An object is nanoscale, then, when it is of a size convenient to measure in nanometers – generally less in size than a micron. The nanoscale is also the size scale at which the properties of a material are often different than they are for the bulk (or "macroscale") phase. For many materials, this is approximately in the 1–300 nm size range. In this size range, properties change because as things become very small, their surfaces shrink more slowly than their volumes, causing nanoscale materials ("nanomaterials") to have far larger surface-to-volume

ratios than larger objects. More surface area can mean that nanomaterials have higher reactivity; different elastic, tensile, and magnetic properties; increased conductivity; or increased tendency to reflect and refract light. The nanoscale is a size scale that a cellular biologist is quite familiar with – it is the size range of important cellular components, such as DNA (double-stranded DNA is about 2.5 nm in diameter), proteins (hemoglobin is about 5 nm in diameter), cell walls, cell membranes, and compartments. Biological macromolecules were known to display properties and behavior different than macroscale objects far before they were termed "nanoparticles." For example, the way in which proteins fold into globular forms is a process with no analog among larger objects. The US National Nanotechnology Initiative has defined the nanoscale as 1–100 nm. This includes particles which are naturally occurring, such as proteins, particles in smoke, volcanic ash, sea spray, and from anthropogenic sources such as industrial combustion products and automotive exhaust.

The term "nanotechnology" involves manipulating and controlling nanoscale objects. The particles themselves are often engineered, such as those created by chemical reactions, electron beam lithography, or single-molecule manipulation. These nanoparticles can be put to use in a broad spectrum of applications, including aerospace, energy, healthcare, transportation, defense and information technology. They are also found in food additives and sunscreens. Relevant to it, nanoparticles are used as medical devices, as imaging agents and diagnostics, and as drug carriers for therapeutics for many different types of diseases. For this latter application, molecules such as chemotherapeutic agents can be selectively adsorbed or attached to the nanoparticle surface or interior. The drug is affixed to the nanoparticle by covalent conjugation or noncovalent attachment (e.g., encapsulation). Polymer coatings can also be bound to nanoparticle drug carriers – to increase their solubility and biocompatibility. The major classes of nanoparticles used for nanotech medical applications include: liposomes, nanoshells (including quantum dots), metals and metal oxides, carbon-based particles (carbon nanotubes and fullerenes), nanoemulsions, nanocrystals, and polymer-based nanomaterials (including dendrimers). One reason why

nanotechnology is gaining popularity is that there are great benefits to being able to engineer at the scale of individual macromolecules. For medicine especially, building tiny molecular-scale devices capable of delivering drugs specifically to areas of disease can make conventional pharmaceuticals more efficacious and decrease their adverse side effects. A nanoparticle coated with hydrophilic molecules, for example, can be an effective carrier for an otherwise insoluble drug [2]. Similarly, nanoparticle drug carriers can improve therapeutic outcomes by modulating drug distribution to tumor target sites via passive and active targeting. Passive targeting refers to the process whereby nanoscaled particles accumulate in tumors or sites of inflammation simply due to their size. For tumors, this phenomenon is referred to as the enhanced permeability and retention (EPR) effect and is caused by the leaky vasculature and incomplete lymphatic system surrounding tumors of soft-tissue and epithelial cell origin [3, 4]. Nanotech-based drugs taking advantage of EPR are already demonstrating pronounced improvements in efficacy. Active targeting works through the attachment of biochemical moieties, such as monoclonal antibodies, which facilitate delivery to diseased tissues expressing biomarkers that distinguish it from the surrounding healthy tissue [5, 6]. Examples of these biomarkers include membrane receptors and mutated cellular proteins. Both and passive targeting can lower a drug's adverse effects by reducing its systemic exposure to healthy tissues and organ systems.

Most nanoparticle formulations include surfactants to promote dispersion (i.e., prevent agglomeration) of the primary particles. These compounds too can interfere with conventional characterization methods. Impurities and contaminants which adsorb to nanoparticle surfaces can also contribute to ambiguous analytical results. These difficulties tend to hamper the development of standards for characterization and the subsequent clinical application of nanoparticles.

An investigational new drug (IND) or investigative device exemption(IDE) application is the first step in the FDA approval candidate drug's therapeutic or diagnostic potential in humans. Preclinical testing data in the IND must demonstrate that the new drug will not expose humans to unreasonable risks during initial use, and, in the case of therapeutics,

that the drug exhibits sufficient pharmacological activity to justify first-in-man clinical trials. For small-molecule drugs, the FDA has criteria for the types of preclinical data which should be presented in an IND. For nanomaterials, an IND can be less straight forward, since there is no standardized set of characterization methods for these materials. Until such standards become available, nanotech developer shave to design an dvalidate their own novel characterization methods to assess safety, toxicity, and quality control. The FDA then faces the difficulty of interpreting data generated by a variety of unfamiliar techniques without a substantial history of acceptance in scientific literature. All of this complicates the preclinical development process and can increase the time preceding first-inman trials for nanotech-based drugs.

One of the chief complications for preclinical characterization is the multicomponent nature of many nanoparticle-based therapeutics. The nanoparticle can serve as a scaffold for attachment of chemical moieties that each perform a particular medical function (e.g., targeting ligands, hydrophilic coatings that improve solubility, imaging agents, drugs, etc.). The resulting nanoparticle therapeutic is a multipart, multifunctional entity with greater complexity than a conventional small-molecule drug. Assessing the safety and efficacy of such a complex entity can be a daunting task. Ultimately, the realization of the use of these multicomponent nanoparticles in clinical trials is highly dependent on rigorous preclinical characterization.

Thorough characterization is also key for evaluating the safety of nanoparticles for incidental exposure and addressing concerns about environmental health and safety (EHS). Whether or not nanomaterials are more toxic than their macroscale counterparts has been a matter of extensive debate in the EHS community. The scientific literature contains a wide range of research findings, which are often conflicting due to the variety of methods used and to subtle variations in test materials. Arriving at a definitive answer to this question will depend on thorough characterization using standardized methods and materials.

Certain nanotech reformulations of existing drugs show remarkably decreased toxicity in comparison to their free forms. An excellent example of this is a drug in development by

CytImmune Sciences, Inc. under the trade name Aurimune[7]. Aurimune consists of tumor necrosis factor alpha (TNF-a) bound to polyethylene glycol (PEG)-coated nanosized colloidal gold. Almost ten years ago, TNF-a in its free form was discontinued during clinical trials due to severe immunotoxicity. Using the nanotech formulation (Aurimune), this same quantity of TNF-a was given to patients – but with minimal ill effect. This illustrates the utility of nanoparticle platforms in decreasing toxicity and adverse side effects.

Another way a nanoparticle platform may be used to improve a drug formulation is through serving as an alternative to conventional administration vehicles, which are sometimes toxic. For example, the potent chemotherapeutic paclitaxel is not soluble in water. Under the trade name Taxol, paclitaxel is dissolved in Cremophor EL, a polyoxyethylated castor oil, which is toxic. Abraxane, an albumin-bound form of paclitaxel uses the nanotech platform of albumin as an alternative to Cremophor EL. Abraxane has been shown to be both more efficacious and less toxic than Taxol [8, 9].

A rational characterization strategy for biomedical nanoparticles contains three elements: physicochemical characterization, in vitro assays, and in vivo studies. Each of these is essential to a comprehensive understanding of nanoparticle safety and efficacy. For example, without physicochemical characterization there can be no meaningful interpretation of in vitro or in vivo biological data or interlaboratory comparison. The simplicity and amplified reactions of in vitro assays may help elucidate the biological mechanism of action of a therapeutic or toxicant. Testing in vitro physiological models can also give an initial estimate of formulation efficacy and toxicity. Realistically though, it is not possible for the laboratory bench to exactly match the complex biological interplay found in vivo. It is therefore necessary to characterize the absorption, distribution, metabolism, and excretion and toxicity (ADME) of a drug formulation in animal models.

In terms of physicochemical properties, traditional small molecule drugs are characterized by their molecular weight, chemical composition, purity, solubility, and stability. These data form the basis of the chemistry, manufacturing, and controls (CMC) section of the IND application with the FDA. For small molecules, the instrumentation to

ascertain these properties have been well established and the techniques are standardized. Techniques like nuclear magnetic resonance (NMR), mass spectrometry, ultraviolet-visible (UV-Vis) spectroscopy, infrared spectroscopy (IR), and gas chromatography (GC) can be run in a high-throughput fashion to analyze such molecules. For nanomaterials, alternate instrumentation is required to obtain information on the same properties (composition, purity, stability, etc.). These properties influence biological activity, and may depend on parameters such as particle size, size distribution, surface area, surface charge, surface functionality, shape, and aggregation state. Additionally, since many nanoparticle concepts are multifunctional (with targeting, imaging, and therapeutic components), the stability and distribution of these components can have dramatic effects on nanoparticle biological activity as well.

It is now widely acknowledged that physicochemical properties such as size and surface chemistry can dramatically affect nanoparticle behavior in biological systems [2–7] and influence biodistribution, safety and efficacy. For instance, a decrease in particle size leads to an exponential increase in surface area per unit mass, and a concomitant increase in the availability of reactive surface groups. Nanoparticles with cationic surfaces have a notably increased tendency to permeate (and perforate) cellular membranes compared to neutral or anionic nanoparticles [8].

Physicochemical characterization of properties such as size, surface area, surface chemistry, and aggregation state can provide the basis for better understanding of structure–activity relationships. In this volume, methods are presented for determining nanoparticle size in solution by dynamic light scattering (DLS), molecular weight via mass spectrometry, surface charge through zeta potential measurement and topology by atomic force microscopy (AFM). Methods are also presented for transmission electron microscopy (TEM) and scanning electron microscopy (SEM) examination of nanoparticle samples, and elemental identification using energy dispersive X-ray spectroscopy (EDX). Another important and challenging area of nanoparticle characterization is measurement under physiological conditions that resemble or mimic the physical state in vivo. Many properties

of nanoparticles are environment and condition dependent; for example, the particle's hydrodynamic size at physiological pH and ionic strength may differ from the size in water or the dry state. Surface charge may also depend on the pH and ionic strength of the suspending solution. Plasma proteins are known to bind nanoparticles in the blood, and the protein-bound size is expected to be a more relevant determinant of disposition and clearance than the free-particle size. The release profile of an encapsulated therapeutic may even be environment dependent [9]. That is, there may be faster or slower release of the therapeutic as the temperature, pH, and/or ionic strength of the solution surrounding the nanoparticle formulation is varied.

Because the results of in vitro biological assays often don't correlate with in vivo endpoints, in vitro characterization is performed to elucidate mechanisms, not necessarily to screen for biocompatibility. In vitro studies may also be used to identify areas requiring attention for in vivo animal studies. Unfortunately, nanoparticle-based therapeutics frequently interfere with conventional in vitro pharmacologic assays. For instance, many nanoparticles aggregate or adsorb proteins. Other nanoparticles scatter light or have optical properties, which may invalidate colorimetric assays that rely on absorbance measurements. Some nanoparticles have catalytic properties that may interfere with enzymatic tests, such as those that evaluate endotoxin contamination. These many interferences necessitate the use of inhibition and enhancement controls. These are control samples with known properties included in an in vitro assay along with analyte samples to ensure accurate results. For example, in tests to evaluate endotoxin contamination, known amounts of endotoxin can be spiked into nanoparticle samples. If the endotoxin assay reliably measures the true (i.e., known) amount then the researcher can be reasonably sure that the nanoparticles are not interfering with the test method. However, if the test returns a measurement substantially enhancement or inhibition than the true amount in the control samples, then the test must be modified before the results can be meaningful.

Finally, the ability to engineer at the nanoscale confers the ability to combine several beneficial features into one multicomponent, multifunctional nanoparticle. The nanoparticle

can serve as a scaffold for attachment of a variety of chemical moieties, each of which performs an individual medical function. For example, ligands for particular cellular receptors can be attached to the nanoparticle to facilitate active targeting to tissues expressing those receptors [10]. Additionally, hydrophilic molecules, such as polyethylene glycol, can be bound to the nanoparticle surface to increase solubility and biocompatibility. Finally, image contrast agents, such as chelated gadolinium, can be conjugated to the nanoparticles for diagnostic purposes. The resulting nanoparticle is a multifunctional entity engineered to have greater biocompatibility and efficacy than a conventional small-molecule drug. Because nanoparticle-based drugs represent novel medical entities, they pose novel challenges for scientists, developers, and regulatory agencies. In particular, the FDA and pharmaceutical industries have used standardized tests to assess material biocompatibility for several decades. Nanoparticle developers and manufacturers leverage these well-established methods whenever possible, but the unique properties of nanomaterials often complicate this seemingly straightforward process. Some of the challenges involved in nanoparticle characterization are detailed in the following two chapters. The remainder of the volume consists of protocols specifically developed for nanoparticle characterization, and intended for use by the research community, drug developers, and regulatory agencies. Such methods are needed to speed up the translation of nanoparticle drugs from discovery to development, accelerating the conversion of the benefits of nanotechnology to drug delivery and diagnostics into real benefits for patients.

2. Characterization of Nanoliposomes Preparation, Analysis and Evaluation

Nanoliposomes are nanometric version of liposomes, which are one of the most applied encapsulation and controlled release systems [11]. In order to have a better understanding of nanoliposomes, we need to know about the older technology they are developed from, i.e. liposomes. The word liposome derives from two Greek words, lipos (fat) and soma (body or structure), meaning a structure in which a fatty envelope encapsulates internal aqueous compartment(s) [12, 13]. Liposomes (also known as bilayer lipid vesicles) are ideal models of cells and biomembranes. Their resemblance to biological membranes makes them an ideal system, not only for the study of contemporary biomembranes, but also in studies investigating the emergence, functioning and evolution of primitive cell membranes [14, 15]. Furthermore, they are being used by the food, cosmetic, agricultural and pharmaceutical industries as carrier systems for the protection and delivery of different material including drugs, nutraceuticals, pesticides and genetic material. Liposomes are composed of one or more concentric or nonconcentric lipid and/or phospholipid bilayers and can contain other molecules such as proteins in their structure. They can be single or multilamellar, with respect to the number of bilayers they contain, and can accommodate hydrophilic, lipophilic and amphiphilic compounds in their aqueous and/or lipid compartments. Since the introduction of liposomes to the scientific community, around 40 years ago [16], there have been considerable advances in the optimisation of liposomal formulations and their manufacturing techniques. These include prolonged liposomal half-life in blood circulation, the development of ingenious strategies for tissue and cell targeting and the elimination of harmful solvents used during their preparation [17]. The term nanoliposome has recently been introduced to exclusively refer to nanoscale bilayer lipid vesicles since liposome is a general terminology covering many classes of vesicles whose diameters range from tens of nanometers to several micrometers [11]. In a broad sense, liposomes and nanoliposomes share the same chemical, structural and thermodynamic properties. However, compared to

liposomes, nanoliposomes provide more surface area and have the potential to increase solubility, enhance bioavailability, improve controlled release and enable precision targeting of the encapsulated material to a greater extent [18]. The first journal article on nanoliposome technology was published in 2002 [19] and the first book on nanoliposomes was published more recently in 2005 [11].

2.1 Physicochemical Properties

In order to realize the mechanism of nanoliposome formation and main points in their manufacture, we have to look at their physical and chemical characteristics along with the properties of their constituents.

2.1.1 Chemical Constituents

The main chemical ingredients of nanoliposomes are lipid and/or phospholipid molecules. Lipids are fatty acid derivatives with various head group moieties. When taken orally, lipids are subjected to conversion by gastrointestinal lipases to their constituent fatty acids and head groups. Triglycerides are lipids made from three fatty acids and a glycerol molecule (a three-carbon alcohol with a hydroxyl group [OH] on each carbon atom). Mono- and diglycerides are glyceryl mono- and di-esters of fatty acids. Phospholipids are similar to triglycerides except that the first hydroxyl of the glycerol molecule has a polar phosphate-containing group in place of the fatty acid. Phospholipids are amphiphilic, possessing both hydrophilic (water soluble) and hydrophobic (lipid soluble) groups. The head group of a phospholipid is hydrophilic and its fatty acid tail (acyl chain) is hydrophobic [20]. The phosphate moiety of the head group is negatively charged. If the acyl chains only contain single chemical bonds, the lipid is known as '*saturated*' and if there is one or more double bonds in the acyl chains, the lipid is known as '*unsaturated*'. Therefore, saturated lipids have the maximum number of hydrogen atoms.

In addition to lipid and/or phospholipid molecules, nanoliposomes may contain other

molecules such as sterols in their structure. Sterols are important components of most natural membranes, and incorporation of sterols into nanoliposome bilayers can bring about major changes in the properties of these vesicles. The most widely used sterol in the manufacture of the lipid vesicles is cholesterol (Chol). Cholesterol does not by itself form bilayer structures, but it can be incorporated into phospholipid membranes in very high concentrations, for example up to 1:1 or even 2:1 molar ratios of cholesterol to a phospholipid such as phosphatidylcholine (PC) [21]. Cholesterol is used in nanoliposome structures in order to increase the stability of the vesicles by modulating the fluidity of the lipid bilayer. In general, cholesterol modulates fluidity of phospholipid membranes by preventing crystallization of the acyl chains of phospholipids and providing steric hindrance to their movement. This contributes to the stability of nanoliposomes and reduces the permeability of the lipid membrane to solutes [22].

The amount of cholesterol to be used in the nanoliposomal formulations largely depends on the intended application. For liposomes in the form of multilamellar vesicles (MLV), we have found that both anionic (with dicetylphosphate, DCP, as a negatively charged ingredient) and neutral (without DCP) liposomes containing PC can interact with model membrane systems (in the form of fusion/aggregation) when containing a 10% molar ratio of Chol [23]. Anionic vesicles containing 10% Chol were also able to incorporate DNA molecules in the presence of calcium ions. Increasing cholesterol content of these vesicles from 10 to 40%, however, caused them to be unable to interact with model membranes and also unable to incorporate DNA molecules. We concluded that these types of liposomes with 40% or more Chol content couldn't be useful in gene and drug delivery applications. Studies have shown that lipid composition and cholesterol content are among the major parameters in the research and development (R&D) of nanoliposome formulations [23, 24].

2.1.2 Phase Transition Temperature

Physicochemical properties of nanoliposomes depend on several factors including pH, ionic strength and temperature. Generally, lipid vesicles show low permeability to the entrapped material. However, at elevated temperatures, they undergo a phase transition that alters their permeability. Phospholipid ingredients of nanoliposomes have an important thermal characteristic, i.e., they can undergo a phase transition (*T*c) at temperatures lower than their final melting point (*T*m). Also known as gel to liquid crystalline transition temperature, *T*c is a temperature at which the lipidic bilayer loses much of its ordered packing while its fluidity increases. Phase transition temperature of phospholipid compounds and lipid bilayers depends on the following parameters:

●● Polar head group;

●● Acyl chain length;

●● Degree of saturation of the hydrocarbon chains;

●● Nature and ionic strength of the suspension medium.

In general, *T*c is lowered by decreased chain length, by unsaturation of the acyl chains, as well as presence of branched chains and bulky head groups (e.g. cyclopropane rings) [25]. An understanding of phase transitions and fluidity of phospholipid membranes is essential both in the manufacture and exploitation of liposomes. This is due to the fact that the phase behaviour of liposomes and nanoliposomes determines important properties such as permeability, fusion, aggregation, deformability and protein binding, all of which can significantly affect the stability of lipid vesicles and their behaviour in biological systems [21]. Phase transition temperature of the lipid vesicles has been reported to affect the pharmacokinetics of the encapsulated drugs such as doxorubicin [26].

Liposomes made of pure phospholipids will not form at temperatures below *T*c of the phospholipid. This temperature requirement is reduced to some extent, but not eliminated, by the addition of cholesterol [27]. In some cases, it is recommended that liposome

preparation be carried out at temperatures well above *T*c of the vesicles. For instance, in the case of vesicles containing dipalmitoyl phosphatidylcholine (DPPC, *T*c = 41°C), it has been suggested that the liposome preparation procedure be carried out at 10 °C higher than the *T*c at 51°C[28, 29]. This is in order to make sure that all the phospholipids are dissolved in the suspension medium homogenously and have sufficient flexibility to align themselves in the structure of lipid vesicles. Following termination of the preparation procedure, usually nanoliposomes are allowed to anneal and stabilize for certain periods of time (e.g. 30–60 min), at a temperature above *T*c, before storage.

2.2 Methods

2.2.1 Liposome Preparation

In general, elastic liposomes are prepared using similar methods to conventional liposomes, most commonly using the conventional rotary evaporation extrusion method [36]. A typical preparation method is outlined:

1. Ensure all equipment is clean and dry.
2. Place phosphatidylcholine and sodium cholate (85:15 for final concentration 50 mg/ml lipid) in the round bottom flask of the rotary evaporator that is activated at low speed, at a tilt of approximately 45°.
3. Add 10 ml ethanol (containing estradiol; 1 mg/ml) to dissolve the phospholipid and surfactant.
4. Remove ethanol by rotary evaporation, under a nitrogen stream, at a suitable temperature above the lipid transition temperature. Room temperature is suitable for this formulation. This will leave a film of lipids deposited on the wall of the flask.
5. Final traces of organic solvent can be removed under vacuum for 12 h or overnight.
6. Hydrate the deposited film with water by rotation for 2–4 h without vacuum .
7. Allow the resulting liposome suspension to swell for a further 2–4 h at 4°C temperature.

9. Extrude the resulting suspension through a sandwich of 200 and 100 nm polycarbonate membranes up to ten times.

2.2.2 Sonication Technique

Sonication is a simple method for reducing the size of liposomes and manufacture of nanoliposomes [31, 32]. The common laboratory method involves treating hydrated vesicles for several minutes with a titanium-tipped probe sonicator in a temperature controlled environment as explained in the following section.

1. Dissolve a suitable combination of the phospholipid components, with or without cholesterol, in either chloroform or in chloroform–methanol mixture (usually 2:1 v/v).
2. Filter the mixture to remove minor insoluble components or ultrafilter to reduce or eliminate pyrogens.
3. Transfer the solution to a pear-shaped or a round-bottom flask and, employing a rotary evaporator, remove the solvents at temperatures above *T*c under negative pressure, leaving a thin layer of dried lipid components in the flask.

Other methods of drying the lipid ingredients include lyophilization and spray drying [33].

4. Remove traces of the organic solvents using a vacuum pump, usually overnight at pressures below 0.1 Pa. Alternatively, traces of the organic solvents may be removed by flushing the flask with an inert gas, such as nitrogen or argon.
5. After drying the lipid ingredients, small quantity of glass beads (e.g. with 500 mm diameter) are added to the flask containing the dried lipids following by the addition of a suitable aqueous phase such as distilled water or buffer. Alternative hydration mediums are saline or nonelectrolytes such as a sugar solution. For an in vivo preparation, physiological osmolality (290 mol/kg) is recommended and can be achieved using 0.6% saline, 5% dextrose, or 10% sucrose solution[34]. The aqueous medium can contain salts, chelating agents, stabilizers, cryo-protectants (e.g. glycerol) and the drug to be entrapped.
6. The dried lipids can be dispersed into the hydration fluid by hand shaking the flask or vortex mixing for 1–5 min. At this stage, micrometric MLV type liposomes are formed.
7. Transfer the flask containing MLV either to a bath-type sonicator or a probe (tip)

sonicator (Fig.1). For probe sonication, place the tip of the sonicator in the MLV flask and sonicate the sample with 20 s ON, 20 s OFF intervals (to avoid over-heating), for a total period of 10–15 min. At this stage, nanoliposomes are formed, which are predominantly in the form of small unilamellar vesicles (SUV). Alternatively, nanoliposomes can be produced using a bath sonicator as explained in the following section.

8. Fill the bath sonicator with room temperature water mixed with a couple of drops of liquid detergent. Using a ring stand and test tube clamp, suspend the MLV flask in the bath sonicator. The liquid level inside the flask should be equal to that of outside the flask. Sonicate for a time period of 20–40 min.

9. Store the final product at temperatures above *T*c under an inert atmosphere such as nitrogen or argon for 1 h to allow the annealing process to come to completion. Mean size and polydispersity index of vesicles is influenced by lipid composition and concentration, temperature, sonication time and power, sample volume, and sonicator tuning. Since sonication process is difficult to reproduce, size variation between batches produced at different times is not uncommon.

10. Residual large particles remaining in the sample can be removed by centrifugation to yield a clear suspension of nanoliposomes.

2.2.3 Extrusion Method

Extrusion is a process by which micrometric liposomes (e.g. MLV) are structurally modified to large unilamellar vesicles (LUV) or nanoliposomes depending on the pore-size of the filters used [35–37]. Vesicles are physically extruded under pressure through polycarbonate filters of defined pore sizes. A protocol for using a small-sized extruder (Fig. 2) is described in the following section. A mini extruder device (e.g. from Avanti Polar Lipids, Inc., Alabaster, AL, USA; or Avestin Inc., Mannheim, Germany), with 0.5 ml or 1 ml gas-tight syringes can be employed in this procedure.

1. Prepare a liposome sample, such as MLV, as explained earlier.

2. Place one or two-stacked polycarbonate filters into the stainless steel filter-holder of the extruder (Fig. 2).

3. Place the extruder stand/heating block onto a hot plate. Insert a thermometer into the well provided in the heating block. Switch the hot plate on and allow the temperature to reach a temperature above *T*c of the lipids.

4. In order to reduce the dead volume, pre-wet the extruder parts by passing a syringe full of buffer through the extruder and then discard the buffer.

5. Load the liposome suspension into one of the syringes (donor syringe) of the mini extruder and carefully place the syringe into one end of the extruder by applying a gentle twisting.

6. Place the second syringe (receiver syringe) into the other end of the extruder. Make sure the receiver syringe plunger is set to zero.

7. Insert the fully assembled extruder device into the extruder stand. Insert the stainless-steel hexagonal nut in such a way that any two opposing apexes fall in the vertical plane. Use the swing-arm clips to hold the syringes in good thermal contact with the heating block.

8. Allow the temperature of the liposome suspension to reach the temperature of the heating block (approximately 5–10 min).

9. Gently push the plunger of the filled syringe until the liposome suspension is completely transferred to the empty syringe.

10. Gently push the plunger of the alternate syringe to transfer the suspension back to the original syringe.

11. Repeat the extrusion process for a minimum of seven passes through the filters. In general, the more passes though the filters, the more homogenous the sample becomes. In order to reduce the possibility of sample contamination with larger particles or foreign material, the final extrusion should fill the receiver syringe. Therefore, an odd number of passages through the filters should be performed.

12. Carefully remove the extruder from the heating block. Remove the filled syringe from

the extruder and inject the nanoliposome sample into a clean vial.
13. The extruder components can be cleaned by first rinsing with ethanol (or leaving the extruder parts in warm 70% ethanol for few hours) and then rinsing with distilled water.
14. Keep the final product at temperatures above *T*c under an inert atmosphere such as nitrogen or argon for 1 h to allow the sample to anneal and stabilize.

2.3 Characterization and Analysis of Nanoliposomes

Following preparation of nanoliposomes, especially when using a new technique, characterization is required to ensure adequate quality of the product. Methods of characterization have to be meaningful and preferably rapid. Several techniques such as electron microscopy, radiotracers, fluorescence quenching, ultrasonic absorption, electron spin resonance spectroscopy, and nuclear magnetic resonance spectroscopy may be used to characterize nanoliposome formulations. Each technique has characteristic advantages and possible disadvantages. The most important parameters of nanoliposome characterization include visual appearance, size distribution, stability, Zeta potential, lamellarity and entrapment efficiency.

2.3.1 Size Determination

Size and size distribution (polydispersity) of the formulated nanoliposomes are of particular importance in their characterization. Maintaining a constant size and/or size distribution for a prolonged period of time is an indication of liposome stability. Electron microscopic methods are widely used for establishing the morphology, size and stability of liposomes. With respect to a statistically meaningful analysis of size distribution of the lipid vesicles, methods such as light scattering, which measure the size of large number of vesicles in an aqueous medium, are more appropriate than microscopic techniques. Ideally, these two techniques need to be employed along with other inexpensive and routine laboratory techniques, such as gel permeation chromatography, to provide a comprehensive

and reliable characterization of the nanoliposomal formulations [11, 38].

Each of the currently used particle size determination techniques has its own advantages and disadvantages. Light scattering, for example, provides cumulative average information of the size of a large number of nanoliposomes simultaneously. However, it does not provide information on the shape of the lipidic system (e.g. oval, spherical, cylindrical, etc.) and it assumes any aggregation of more than one vesicle as one single particle. Electron microscopic techniques, on the other hand, make direct observation possible; hence provide information on the shape of the vesicles as well as presence/absence of any aggregation and/ or fusion. The drawback of the microscopic investigations is that the number of particles that can be studied at any certain time is limited. Therefore, the general approach for the determination of size distribution of nanoliposomal formulations should be to use as many different techniques as possible.

2.3.2 Zeta Potential

The other important parameter in liposome characterisation is zeta potential. Zeta potential is the overall charge a lipid vesicle acquires in a particular medium. It is a measure of the magnitude of repulsion or attraction between particles in general and lipid vesicles in particular. Evaluation of the zeta potential of a nanoliposome preparation can help to predict the stability and in vivo fate of liposomes. Any modification of the nanoliposome surface, e.g. surface covering by polymer(s) to extend blood circulation life, can also be monitored by measurement of the zeta potential. Generally, particle size and zeta potential are the two most important properties that determine the fate of intravenously injected liposomes. Knowledge of the zeta potential is also useful in controlling the aggregation, fusion and precipitation of nanoliposomes, which are important factors affecting the stability of nanoliposomal formulations [11].

2.3.3 Transmission Electron Microscopy Determination

(a) A droplet of the ML suspension, adjusted to about 5 mM Fe, is deposited on a Formvar-coated grid.

(b) After 5 min, excess fluid is drained away with a piece of filter paper and the sample is stained with a drop of 0.5% uranylacetate (UCB, Belgium) in Milli Q water.

(c) After dehydration, the grid samples are examined in the electron microscope. A representative sample of an electron micrograph, clearly showing the translucent ML envelope.

2.3.4 Encapsulation Efficiency

Encapsulation efficiency is commonly measured by encapsulating a hydrophilic marker (i.e. radioactive sugar, ion, fluorescent dye), sometimes using single-molecule detection. The techniques used for this quantification depend on the nature of the entrapped material and include spectrophotometry, fluorescence spectroscopy, enzymebased methods, and electrochemical techniques [32, 34].

If a separation technique such as HPLC or FFF (Field Flow Fractionation) is applied, the percent entrapment can be expressed as the ratio of the unencapsulated peak area to that of a reference standard of the same initial concentration. This method can be applied if the nanoliposomes do not undergo any purification (e.g. size exclusion chromatography, dialysis, centrifugation, etc.) following the preparation. Any of the purification technique serves to separate nanoliposome encapsulated materials from those that remain in the suspension medium. Therefore, they can also be used to monitor the storage stability of nanoliposomes in terms of leakage or the effect of various disruptive conditions on the retention of encapsulants. In the latter case, total lysis can be induced by the addition of a surfactant such as Triton X100.

Drug entrapment efficiency is calculated as follows:

Entrapment Efficiency (%) = (Total amount drug- Amount of free drug)/ Total amount drug ×100

2.4 In Vitro Drug Release

The experimental setup for the release study comprises a dialysis membrane tube and a glass vessel with diameter just larger than the membrane tube. This is placed in a water bath that is maintained at 37°C.

1. Place buffered saline (pH 2.0/7.4/10.0)/ serum/medium solution in the glass vessel and allow to stand in the water bath until equilibrated to 37°C.
2. Tie one end of the dialysis membrane tube tightly to ensure no leakage.
3. Place the liposome suspension in PBS in the dialysis tube and seal the other end.
4. Suspend the dialysis tube within the glass vessel.
5. Remove samples of the buffer solution at time intervals up to 24 h, replacing each sample with fresh pre-warmed PBS.
6. At 24 h, remove the liposome suspension and lyse the liposomes, as previously described, to liberate the estradiol remaining in the liposomes.
7. Measure the estradiol content in all samples by HPLC using a validated assay.

2.5 In Vitro Cell Culture Studies

1. Caco-2 cells were grown into 10% fetal bovine serum MEM with penicillin (50 units/mL), streptomycin (50 units/ml) are grown on coverslips in 6-well plates.
2. Before the experiment, seed Caco-2 cells into 6-well culture plates at a density of 50,000 cells per well and incubate at 37°C, under 5% CO2 for 96h.
3. 15 min before transfection, wash the cells with Transfer buffer.
4. Add 1 ml of meidum containing liposomes onto each well in tripliquet, and incubate the plates at 37°C for 2h in the presence of 5% CO2,
5. Wash the cells thrice with PBS and treat with 1 ml of a distill water into cells for 30 min.

6. Add 25 μl of the supernatant to a 96-well plate, and incubate at 37°C for 30min. Quantify the protein content with the BCA protein assay KIT(PIERCE) and report to BSA taken as a reference curve.

7. For the calculation, background of the untreated cells, taken as negative controls, was removed from the sample data. The relative counts obtained for luciferase quantification were divided by the protein content in each well to normalize the results per mg of protein. The cationic formulation was taken as the positive reference formulation.

2.5.1 Protein Content Determination

The protein content of the lysates was measured by the DC Protein Assay reagent using bovine serum albumin as the standard.

1. Put in each well of a 96-well plate 10 μl of sample.
2. Add 25 μl of reagent A and 200 μl of reagent B.
3. Wait for 15 min at room temperature until a blue color appears.
4. Measure absorbance at 650–750 nm.

2.6 In Vivo Pharmacokinetic Evaluation

A suitable animal model can be used for in vivo pharmacokinetic assessment of a topically applied liposome formulation. Rats is most common but tend to provide an estimate compared to human absorb is more permeable. A generalised protocol is outlined in the following section but there can be considerable variation depending on the complexity of information sought, if the determination of distribution into tissues is required in addition to absorption into the circulation:

1. Animals are anaesthetised and liposome suspension applied to a pre-marked test site without occlusion.
2. At a predetermined time, the animal is sacrificed and a blood sample is collected.
3. Extract analytical solutions from all samples using suitable pre-validated solvent

extraction procedures. Drug content in all samples should be analysed by a validated HPLC assay or where possible, by scintillation counting if a radiolabelled active compound is available.

4. Suitable control formulations such as plain drug solution and possibly conventional liposome suspension should be applied to additional animals and processed with the same protocol.

5. Drug in plasma verses time post application is plotted and pharmacokinetic parameters of AUC_{0-24h} (area under curve), C_{max} (peak plasma level), T_{max} (time to peak plasma evel) and $T_{1/2}$ (plasma half-life) are determined.

3 Characteristics of Nanoclay Preparation and Evaluation Intercalation and Exfoliation of Clays

3.1 General Characteristics

Nanoclays are nanoparticles of layered mineral silicates. Depending on chemical composition and nanoparticle morphology, nanoclays are organized into several classes such as montmorillonite, bentonite, kaolinite, hectorite, and halloysite. Organically-modified nanoclays (organoclays) are an attractive class of hybrid organic-inorganic nanomaterials with potential uses in polymer nanocomposites, as rheological modifiers, gas absorbents and drug delivery carriers. Clays originate from the hydrothermal alteration of alkaline volcanic ash and rocks of the Cretaceous period (85-125 million years ago). The airborne ash carried by winds formed deposits characterised by high volume bedding of ash, deposited in seas and alkaline lakes. Different opinions have been expressed regarding the mechanism of the ash to clay transformation. Probably the change began in marine water in reactions involving sufficient amounts of Mg^{+2} and Na^{+}. Several geological processes may have lead to the formation of clays during millions of years[39]. Clays are distinctive from rocks in several aspects:

1. Wet clays can be formed by application of light force and after release of the pressure they retain the imposed shape.
2. Clays are composed of extremely fine crystals, usually plate-shaped, less than 2μm in diameter and less that 10 nm thick.

They are mostly phyllosilicates, i.e., hydrous silicates of Al, Mg, Fe, and other elements. Having at least one small dimension and large aspect ratio they have large specific surface areas. This in turn makes clays physically sorptive and chemically surface active. Several clay types carry an excess negative electric charge owing to internal substitution by lower valency cations, *viz.* Mg^{2+} substituted for Al^{3+},which makes clay slightly acidic. A clay deposit usually contains non-clay minerals as impurities, *viz.* quartz, sand, silt, feldspar, mica, chlorite, opal, volcanic dust, fossil fragments, heavy minerals, sulfates, sulfides, carbonate minerals, zeolites, and many other rock and mineral particles ranging in size from colloidal to pebbles. Clays are classified on the basis of their crystal structure and the amount and locations of charge (deficit or excess) per basic cell. In the context of PNCs, the amorphous clays are a great nuisance as they are difficult to remove from the crystalline ones. The crystalline clays range from kaolins, which are relatively uniform in chemical composition, to smectites, which widely vary in their composition, cation exchange properties, and the ability to expand. The ease of separation of the individual layers is related to the interlamellar charge, x. The latter parameter changes from zero (talc) to x = 0.2 to 0.6 for smectites, to x = 0.6 to 0.9 for vermiculites, and to x = 1 to 2 for micas. Clay particles are usually plate-shaped, less often tubular or scroll-like. Individual clay particles are nanometre-sized at least in one dimension. Aqueous suspensions of clays are thixotropic and sensitive to ion concentration.

Crystalline Clays

Most clays are crystalline, composed of fine, usually plate-shaped crystals about 1 nm thick with high aspect ratio, and have large specific surface areas. They absorb up to a 30-fold amount of water, and when wet, can be easily shaped – pottery is as old as human civilisation.

Kaolins

These include kaolinite, dickite, nacrite and halloysite-endellite. The structural formulae for kaolinite and endellite are $A1_4Si_4O_{l0}(OH)_8$ and $A1_4Si_4O_{l0}(OH)_8 \cdot 4H_20$, respectively. The kaolinitel attice consists of one sheet of tetrahedrally coordinated Si (with O) and one sheet of octahedrally coordinated Al (with O and OH), hence a 1:1, or a two-layer structure. A layer of OH completes the charge requirements of the octahedral sheet. Adjacent cells are spaced about 0.71 nm across the plane. When solvated in ethylene glycol, endellite expands to 1.0 nm in the c-direction. Halloysites are usually tubular or scroll-shaped; they may be differentiated from kaolinite and dickite by treatment with potassium acetate and ethylene glycol.

Serpentines

Substituting Mg for Al in the kaolin structure results in the serpentine, $Mg_3Si_2O_5(OH)_4$. Here all three possible octahedral cation sites are filled, yielding a tri-octahedral group carrying a charge of +6. In kaolinite only 2/3 of the sites are occupied by Al, yielding a di-octahedral group, also with a charge of +6. Most serpentines are tubular or fibrous. Chrysotile occurs in both clino- and ortho-structures.

Illite Group (Micas)

'Mica' is a generic term applied to a group of complex aluminosilicates having a sheet or plate like structure with a wide range of chemical compositions and physical properties. All micas form flat six-sided monoclinic crystals with a remarkable cleavage in the direction of the large surfaces, which permits them to split easily into optically flat films, as thin as one micron. When split into thin films, they remain tough and elastic even at high temperature. The dictionary defines mica as 'a class of silicates having a prismatic angle 120^o, eminentlyperfect basal cleavage, affording thin tough laminae or scales, colorless to jet black, transparent to translucent, of widely varying chemical composition, and crystallising in the monoclinic system'.

Illites or micas are not pure minerals. The mica structure consists of a pair of tetrahedral sheets enclosing an octahedral sheet. Between each such sandwich there are

interlayer sites, which can contain large cations. Considerable variation exists in the composition and polymorphism of the illites. A basal spacing exhibited in XRD, $d_{001} \fallingdotseq 1.0$ nm, is somewhat broad and skewed toward wider spacings. Muscovite derivatives are typically dioctahedral; phlogopite derivatives are trioctahedral. The cation-exchange capacity of illite is CEC = 0.2- 0.3 meq/g of dry clay. The interlayer potassium exerts a strong bond between adjacent clay structures. Thus, mica possess a 2:1 sheet structure, similar to MMT, except that the maximum charge deficit in mica is typically in the tetrahedral layers and contains potassium held tenaciously in the interlayer space. As a result, micas are difficult to exfoliate. However, once exfoliated they form dispersions of platelets with the highest aspect ratio, thus they are particularly useful for the control of gas or liquid permeability. The coordination of the octahedral sheet is completed by OH anions. The general formula of mica group minerals is $XY_{2\text{-}3}Z_4O_{10}(OH)_2$, where X represents the interlayer site, Y the octahedral sites and Z the tetrahedral sites.

The octahedral sheet can be made up in two ways: either dominantly of divalent cations such as Mg^{2+}or Fe^{2+},in which case all three sites are filled (trioctahedralmica), orelse dominantly trivalent cations such as Al^{3+}, in which case one of the three sites is left vacant (dioctahedral mica). If solely Si occupies the tetrahedra, the sandwich is charge-balanced and there is no need for interlayer cations – the resulting minerals are talc (trioctahedral) or pyrophyllite (dioctahedral). In true micas Al substitutes for Si in the tetrahedra, and charge balance is maintained by K, Na or Ca, in the interlayer site.

Chlorites and Vermiculites

Chlorite was identified as a mineral yielding a 1.4 nm basal spacing in clays. Chlorite is a three-layer phyllosilicate separated by a $Mg(OH)_2$ interlayer. Chloritelike structures have been synthesised by precipitating Mg and Al between MMT sheets.

The interlayer sheet in vermiculite is octahedrally coordinated, $6H_2O$about Mg^{2+}. The basal spacing of vermiculite varies from1.4-1.5nm with the nature of the interlayer cation and its hydration. The cation-exchange capacity of vermiculite is relatively high and it may even exceed that of MMT. Vermiculites are known to have high aspect ratio ($p \leq 2{,}500$),

exceeding that of MMT by nearly one order of magnitude.

3.2 Clay Preparation

3.2.1 Intercalation of Clay

The first step in the preparation of clays for use in PNC is purification of the mineral. Depending on the ultimate use of the resulting Na- MMT, before intercalation the powder may be subjected to further preparatory steps, either to reduce the particle size and/or to reduce the particle size distribution. Since the time (t) that intercalant needs to diffuse a distance (l) is given by the proportionality: $t \propto l2$, a decrease of clay particle diameter by 30% results in reduction of the intercalation time by half. the inter diffusion of intercalating molecules is facilitated by reduction of the clay particle size – high stresses not only reduce the diameter but may also cleave the stack, reducing the required force to bend the middle layers during intercalation. Earlier patents similarly focused on the reduction of clay particle size either by mechanical grinding, comminuting or by hydrodynamic forces.

Since the exchange reaction of the inorganic cation (such as Na^+) for the organic one proceeds from the clay platelet edge toward the centre as a regular front, reduction of platelet size reduces the time required for the intercalation. Ion exchange strongly depends on pH – the optimum is about one unit below the pK-value of the organic salt.

It is noteworthy that reduction of particle diameter is detrimental for the control of barrier properties, but it may not be essential for the other performance criteria. Intercalation of clay that has a wide distribution of platelet size often results in an uneven degree of intercalation, evidenced by broad XRD diffraction peaks. The peak is much sharper when more uniform size Na- MMT particles are used. The aims of intercalation are to:

1. Expand the interlayer spacing,
2. Reduce solid-solid interaction between the clay platelets.

3. Improve interactions between the clay and the matrix.

The first goal has been traditionally achieved by making use of the anionic charge within the interlamellar galleries. Since the van der Waals interactions between solid surfaces decrease with the square of the separating distance. insertion of organic or inorganic molecules into the interlamellar space greatly helps to achieve the second aim. To reach the third goal, to compatibilise the system, the principles developed for compatibilisation of polymer blends should be used [40].

For successful intercalation the selected clay should have a cation-exchange capacity: CEC = 0.5- 2.0 meq/g, as for CEC < 0.5 the ion exchange is insufficient, while for CEC > 2.0 meq/g, the interlayer bonding is too strong for easy intercalation, thus smectites and vermiculites have the optimum CEC – theoretically 1.39, experimentally 0.8 to 1.2 meq/g. By contrast, kaolin has a cation-exchange capacity < 0.1 meq/g, while mica, illites, attapulgite and sepiolite are about 0.2 meq/g. As a consequence, MMT, saponite and hectorite are the preferred clays for CPNCs, but since MMT is more abundant and it has a fairly large aspect ratio, $p \cong 300$, (natural hectorite has the smallest) it became the main nanofiller for PNC technology. Owing to the large aspect ratio, $p \lesssim 2{,}000$, of synthetic micas, natural vermiculites and natural micas, several attempts have been made to use them in CPNC as barrier material against permeation of gases, vapours and liquids.

Traditionally, the main use of the intercalated clays has been to produce thixotropic effects in aqueous or non-aqueous systems, e.g., to improve paper coating, lubricant thickening or to prevent sedimentation of dispersed solids. During the last 20 years or so additional uses for clay for CPNC technology have emerged. Intercalation and exfoliation for fine chemical delivery systems is the most recent. Thus, intercalated organoclays have had numerous uses:

Intercalation of the clay particles is diffusion controlled. Water is a ‘natural’ intercalant for clays, but it can hardly be considered unique. Its efficiency is most likely related to the good balance between the dipole moment that drives the process and the molecular size that restricts its motion. In aqueous systems, water molecules can easily diffuse in and the

electrostatic double layer can push the individual platelets apart and keep them away from each other – at low clay concentration total exfoliation can be achieved.

On a molecular scale, intercalation can be visualised as inserting peas between each pair of play-cards in a stack. Evidently, to be able to do that the cards must be pre-spaced and there must be a driving force for the peas to enter the narrow space bending the cards from the edges. Thus, the way to intercalate clay is to use progressively larger molecular species. To prevent re-assembly of layers it is desirable that at least some intercalant is bound to the clay surface.

For the application of clays in CPNC technology intercalation should increase the interlamellar spacing to about 3-4 nm and make the clay organophilic. The goal is usually reached in stages.

1. In dry clay the solid-solid interactions keep the interlamellar gallery at a water monolayer level, of about 0.26 nm. The sheets are strongly bound to each other. The traditional method for reducing the solidsolid interactions, hence to reduce the resistance to intercalant diffusion into interlamellar space, is to disperse the clay in water or an aqueous solution of water-soluble organic solvents, e.g., alcohol or glycol.

2. The second step usually involves exchange of Na^+ for an organic cation. Since the *pK* of onium salts increases with the degree of substitution, in most cases the quaternary onium is used. However, for the use of organoclay as a reactive component (e.g., in thermosets) a primary or secondary onium salt may be preferred. Furthermore, depending on the expected application the onium salt may have a functional group (e.g., a vinyl functionality).

3. In the third step the organoclay may be further treated with reactive compound to compatibilise the clay/polymer systems. Three classes of reactive compounds have been used: known glass-fibre sizing agents (e.g., silanes, titanates, zirconates), known reactive compatibilisers (e.g., oligomeric or polymeric compounds with glycidyl, maleic, isocyanate and other reactive groups), and organometallic compounds. This third step may be a part of the last step in the preparation of CPNC, the exfoliation of organoclay and dispersion of

individual platelets in the polymeric matrix. Several routes have been used to intercalate clay particles. They can be classified as follows:

1. Use of solvents or low *MW* solutions, such as water, alcohols, glycols, crown ether or monomer solutions.
2. Use of organic cations, *viz.* ammonium, phosphonium or sulfonium.
3. Silylation of clay platelets.
4. Incorporation of inorganic compounds that form interlamellar pillars.
5. Use of organic liquids, *viz.* monomers, macromers, oligomers, polymers (PEG, PVAl, PDMS, PVP), copolymers, and their solutions.
6. Melt intercalation.

3.2.2 Exfoliation of Clays

The high surface-to-volume ratio of nanoparticles leads to a high reinforcement efficiency. Thus, CPNCs with well dispersed platelets at a low clay loading of 2 to 5 wt% show highly increased modulus, yield strength, DTUL as well as reduced flame propagation and permeability. In the crystallisable polymer matrix, the clay platelets promote faster crystallisation and higher levels of crystallinity, which results in improved solvent and moisture resistance, but reduced impact strength. The presence of clay may result in modification of the crystalline structure of the matrix polymer, which may promote enhancement of the performance characteristics.

Owing to the nature of the nanoscale reinforcement, the CPNC may be treated as an improved grade of a homopolymer, hence it may be used as a replacement for its matrix polymer in diverse multicomponent polymeric systems, *viz.* blends, composites or foams. For example, Akkapeddi[41] reported using CPNC for making either short or long glass fibre (GF) reinforced composites, getting good processability (e.g., fast moulding cycle), low density, further improvements of modulus, strength, moisture resistance, permeation barrier, etc. The materials were aimed at automotive parts (*viz.* fuel system components, fuel tanks, door and rear quarter panels, consoles, door panels, pillars, under hood components),

packaging (containers, films for food and electronics packaging), appliances, building & construction, electrical & electronic, lawn & garden, power tool applications, etc.

There are four basic structures for polymer/clay mixtures:

1. Conventional clay-filled composite with micron-sized aggregates of clay particles.
2. Nanocomposites with intercalated clay.
3. Exfoliated nanocomposites with locally ordered structure, where the ordering is imposed by flow and concentration, $\phi > \phi_{max}$.
4. Exfoliated nanocomposites with disordered structure, $\phi < \phi_{max}$ *max*.

Exfoliation is the last step in the preparation of CPNC. The methods for achieving it can be discussed under three titles:

1. Polymerisation in the presence of organoclay.
2. Melt compounding a polymer with a suitable organoclay complex.
3. Other exfoliation methods:

• Combining the organoclays with latex.
• Ultrasonic exfoliating of organoclay particles in a low MW polar liquid.
• Others, *viz.* sol-gel templating, co-precipitation, etc.

3.3 Characterisation of Evaluation Nanoclay

3.3.1 X-Ray Diffraction (XRD)

The key to nanoclay performance is the extent of intercalation and exfoliation, XRD is the principal method that has been used to examine this. Their positions and shapes provide information on the structure of the diffracting species, the organoclay. The presence of multiple peaks in XRD spectra is quite common - it often originates from different organoclay structures and its incomplete change during incorporation in a polymeric matrix.

The instruments that measure X-ray scattering are divided into the more common wide angle and newer small-angle X-ray scattering machines, WAXS and SAXS, respectively. It is common to consider the scattering angle $2\theta = 2°$ as a boundary between these two, but newer WAXS instruments frequently are able to provide reliable scattering profile down to $2\theta = 1°$. The interlayer spacing, d_{001}, is commonly determined from the XRD spectrum as arbitrary intensity versus 2θ. The spacing is then calculated from Bragg's law:

$D_{00n}=n/(2sin)$ (2)

where n is an integer is the angle of incidence (or reflection) of the X-ray beam, and λ is the X-ray wavelength – most X-ray machines use Cu-Kąl radiation with $\lambda = 0.1540562$ nm. For the principal reflection, $n = 1$, the dependence given by Equation 2. It is worth noting that, within the range of interest for CPNC ($2\theta = 1\text{-}12°$), there is a straight-line relation between $d_{001}$and $1/(2\theta)$:

$1/2 = -0.00012773 + 0.11331 d_{001}$ or: $d_{001} = 0.0011273 + 8.8253/2$; $R = 1.0000$ (3)

where R is the correlation coefficient. The peak position and the interlayer spacing related to it is one part of the information provided by XRD measurements. The intensity of the diffraction peak and its dependence on the concentration of scattering particles yields another. Cullity and Stock in their monograph on X-ray diffraction derived the following relation for the intensity (I) of the diffraction peak of α-substance mixed with β-substance:

$I\alpha = K\Phi a/[\Phi a\ (\mu\alpha - \mu\beta) + \mu\beta]$ (4)

where Φą . is the volume fraction of the diffracting substance α, and μ . is the mass absorption coefficient. Depending on the relative magnitude of $\mu\alpha$. and $\mu\beta$ within the full range of concentration Equation 4 predicts additivity, as well as positive or negative deviation from it. However, within the limited range of clay concentrations used in CPNC, the relation may be simplified to read:

$I\alpha = K' w\alpha I\text{neat}\alpha$ (5)

where $w\alpha$. is the weight fraction of substance.

It has been frequently observed that during exfoliation (especially during the mechanical exfoliation of intercalated clay in a POmatrix)thepositionofthe XRD peak remains at the same angular position 2θ, but it broadens and its intensity decreases. Parallel with these changes there is an enhancement of the CPNC performance. It can be postulated that in this case the exfoliation process involves breakage of intercalated stacks and/or peeling of individual platelets or short stacks. XRD to calculate the degree of exfoliation *XE*:

$XE = 100\times[1 - A/A_0]$ (6)

where *A* and $A_0$are the area under the XRD peak for the PNC and for the mixture with intercalated clay, respectively. Replacing in Equation 6 the intensity ratio of Equation 5 by the area under the peak ratio, is motivated by an additional assumption that during the progressive dispersion process many stacks slightly change the interlayer spacing hence the observed broadened peak is an envelope over a family of peaks having similar interlayer spacings. However, there are several possible sources for the XRD peak broadening in a CPNC – one being the assumed above existence of a variety of clay stacks with a range of similar d_{001}spacing. Another mechanism of peak broadening is based on the imperfections in the crystalline lattice of *m*-layers of clay platelets forming a stack $t = (m - 1)\times$. d_{001}thick. Another mechanism of peak broadening is based on the imperfections in the crystalline lattice of *m*-layers of clay platelets forming a stack $t = (m - 1)\times d_{001}$ thick and scattering the X-rays at angles θ_1 and θ_2. Because of the small angle difference between θ_1 and θ_2 the destructive interference of reflected beams:

$t = k/(B_1/_2\cos\theta);\ k \leqq 0.9$ (7)

where $\theta \cong (B_1 + B_2)/2$ is the angle of X-ray beam incidence corresponding to the peak position, λ is the X-ray wavelength, and $B_{1/2} \cong \theta_1 - \theta_2$ is peak width (in radians) at half peak height ($I_{max}/2$). From Equation 7 the number of clay platelets per average stack with the interlayer spacing $d_{001}$is:

$m = 1 + t/d_{001}$ (8)

Note that in this interpretation the peak broadening is caused by crystalline defects in individual platelets within the stack having about constant interlayer spacing, and not by overlapping peaks that correspond to stacks with different interlayer spacing.

The development of technology often requires more precise information on the interlayer spacing than that provided by WAXS. With growing frequency SAXS and small angle neutron scattering (SANS) are being used within the effective scattering angle down to 2 θ= 0.05 or the characteristic diffracting distance of about 180 nm. Thus, for example, SAXS and WAXS to study the effects of addition of maleated polyethylene (PE-MA) on PE/MMT structural parameters. By performing scattering experiments on specimens oriented in three orthogonal directions, the authors managed to determine not only the interlayer spacing, but three-dimensional (3D) orientations of six structural features, *viz*. size of tactoids (ca. 120 nm), organoclay ($d_{002} \cong$2.4 to 3.1 nm), spacing in undispersed clay ($d_{002} \cong$1.3 nm), clay (110) and (020) planes, thickness of PE crystalline lamellae ($d_{00l} \cong$19 to 26 nm), and polymer unit cell (110) and (200) planes.

3.3.2 Transmission and Atomic Force Electron Microscopy (TEM and AFM)

At limiting low scattering angle, $2\theta \cong 2^\circ$, the XRD/WAXS scattering intensity and resolution decrease, i.e., the method is not useful for spacing: d > 8.8 nm. Within this range TEM may be used to determine the extent of intercalation/exfoliation. However, TEM also offers a direct method for confirming the XRD data and with growing frequency it is being used at low magnification to check on the uniformity (or lack) of clay stack dispersion in polymeric matrix. The low magnifications are also useful to check the purity

of clay, e.g., the presence of non-layered particles such as quartz. Micrographs with magnification of 130,500 were cover with a mask in which twelve squares of 1×1 inch (2.5cm×2.5 cm) were cut out. The degree of dispersion was expressed as the number of clay platelets per square inch. This dispersion measure was found to correlate well with the tensile modulus. Atomic force microscopy (AFM) has been used mainly in a tapping mode at the cantilever's frequency of 300 kHz and amplitude of 50-100 nm. The difference between the clay modulus and that of a polymer results in good image resolution. Starting in 1990, high resolution TEM (HRTEM) became the preferred tool for the determination of structure, in particular of crystalline nanoparticles, *viz*. carbon (CNT) or boron nitride nanotubes (BN-NT). The magnification in HRTEM is x106 or better, with resolution of 0.1 nm (JEOL 4000EX, 400 kV, Cs = 1mm, focus spread = 8nm, divergence angle=0.7mrad).

3.3.3 Fourier Transform Infrared Spectroscopy (FTIR)

Since 1964 FTIR has been used to study the hydration of bentonite, and the formation of an electrical double layer between the platelets. Significant differences in the silicate stretching region, $\nu_{Si\text{-}O}$ = 1150 to 950cm^{-1}, are related to water (H_2O or D_2O) and hydrated cation (Na^+,K^+,Ca^{+2},etc.) content, which in turn is related to the interlayer spacing between the clay platelets. Yan and co-workershave shown that in hydrated MMT $\nu_{Si\text{-}O}$ exponentially decreases with the clay-to-water ratio, all the way to exfoliation. Oxidation or reduction of the metallic ions within the octahedral clay layers introduces changes to CEC clay hydration and swellability, hence the FTIR spectrum. The use of FTIR for characterisation of CPNCs is more recent. Initially, it has been used in studies of the polymer matrix morphology, e.g., conformation and crystallisation behaviour of sPS .However, the $\nu_{Si\text{-}O}$ stretching vibration has been found to be very sensitive to long range interactions caused either by imposed stress, or expansion of the interlayer spacing. The advantage of the spectroscopic methods, FTIR and Raman, is that along with XRD they are applicable to the intercalated system, and stretch to exfoliated CPNC that do not scatter X-rays. To

examine the interactions between the clay platelets, the intercalating agent and polymer, FTIR provides important information. By comparing the experimental and calculated spectra the type and intensity of interactions can be identified. The method has also been used to analyse the thermal decomposition of ammonium intercalants during the melt compounding method of CPNC preparation.

3.3.4 Nuclear Magnetic Resonance Spectroscopy (NMR)

Solid-state ^{1}H,^{13}C,^{15}N and Simagicanglespinning(MAS) NMR spectroscopy at frequencies 100.40, 30.41 and 79.30 MHz, respectively has been used. The tensile modulus (*E*) was found to be proportional to the chemical shift (*Cs*; in respect to tetramethyl silane) of 15N in ammonium-clay complex with the slope: $dE/d(Cs)$ = 0.1097 (GPa/ppm). The chemical shifts provide information about the degree of clay hydration, the interactions engendered by intercalation and the structure of clay-organic matrix complexes. NMR has also been used to determine PEG chain dynamics within the interlayer spacing of synthetic mica/MMT. According to Aranda and Ruiz-Hitzky the intercalation of MMT by PEG increased the interlayer spacing by $\triangle d_{001}$= 0.8 nm. Thus, the polymer conformation within these interlamellar galleries may be either a 0.8 nm diameter helix, or two chains in a planar zigzag conformation. The former was deemed to be more probable. Measurements of the ^{1}HNMR line width sand relaxation times across a large temperature range were used to determine the effect of bulk thermal transitions. The ^{13}C cross-polarity/magic angles pinning NMR spectra of PEG within the nanocomposite showed that the type of motion being experienced by these chains is the helical jump motion of the -transition, thus the same as within the crystalline phase of neat PEG. The short proton spinlattice relaxation time in the rotating frame, $^{1}HT_{1}$, measured across a wide range of temperatures by ^{1}HNMR provided additional evidence that these chains undergo helical jump motion. Measurements of ^{1}HNMR spectra across a wide temperature range have confirmed that large amplitude motion of the PEG chains within the montmorillonite nanocomposite persist below the *T*g of neat PEG. There was no observed change in the rates of relaxation at the transition

temperatures expected for neat PEG.

Solid-state NMR, both proton and ^{13}C, was used to study CPNC with PA-6as matrix. The nanocomposites with 5 wt% organoclay were generated either by blending or by *in situ* polymerisation. The systems contained mineral MMT having non- stoichiometric amounts of $Mg^{2+}$and Fe^{3+} ions substituted into the octahedral, central layer of the clay platelet. The presence of Fe^{3+} ion contaminants in the MMT induced paramagnetic properties. The paramagnetic contribution to the proton longitudinal relaxation time (T_1 H) is a function of the field and Fe^{3+} concentration in the clay. These paramagnetic properties can be used to determine the hard-to-get information on CPNCs, *viz.* the degree of dispersion, the stability of intercalant, etc. Evidently, NMR can also provide information on the preponderance of α- and γ-crystalline phases of PA-6 in CPNCs. The α-crystallites are characteristic of thene at PA-6, while γ-crystallites are formed in the presence of clay platelets. The Fe^{3+} induced paramagnetism of MMT and there sultingspin-diffusion moderated reduction in longitudinal proton relaxation time, T_1 H, may be used to rank the degree of clay dispersion in CPNCs, and to investigate morphological stratification of the PA-6 α- and γ-crystallites with respect to the clay surface. It was found that variations in T_1 H correlate well with TEM measurements of the clay dispersion. The chemical stability of dimethyl dihydrogenated tallow ammonium ion (2M2HTA) used as MMT intercalant was also investigated. During the organoclay compounding with PA-6 at 240 ℃ most of the intercalant decomposed, releasing a free amine with one methyl and two hydrogenated tallow substituents. According to the authors, the combination of temperature and shear stress in blending caused decomposition. However, judging by T_1H, the CPNCs with the best dispersion of clay also had the most extensively degraded intercalant. The polarity of PA-6 macromolecules well compensated for the loss of the 2M2HTA intercalant. Solid state NMR has also been used to quantitatively determine the degree of clay dispersion in PS/MMT nanocomposites. A new method, similar to the one described above, was developed. In both, paramagnetic Fe^{3+} with in the octahedral layer of MMT has been used. There sultscor relate with XRD and TEM data. The new method is significantly faster than

TEM, but with the difference that the information pertains to the bulk of the specimen, not to its surface. Evidently, both these methods are applicable only to clays containing paramagnetic Fe^{3+}.

3.4 Encapsulation Efficiency

Encapsulation efficiency is commonly measured by encapsulating a hydrophilic marker (i.e. radioactive sugar, ion, fluorescent dye), sometimes using single-molecule detection. The techniques used for this quantification depend on the nature of the entrapped material and include spectrophotometry, fluorescence spectroscopy, enzymebased methods, and electrochemical techniques [32, 34].

If a separation technique such as HPLC or FFF (Field Flow Fractionation) is applied, the percent entrapment can be expressed as the ratio of the unencapsulated peak area to that of a reference standard of the same initial concentration. This method can be applied if the nanoclays do not undergo any purification (e.g. size exclusion chromatography, dialysis, centrifugation, etc.) following the preparation. Any of the purification technique serves to separate nanoclay encapsulated materials from those that remain in the suspension medium. By using the symetic method to make nanoclay for interaction with drugs, and washing it with methanol for three times. The pure nanoclay will be soluted of various disruptive conditions.

Drug entrapment efficiency is calculated as follows:

Entrapment Efficiency (%) = (Total amount drug- Amount of free drug)/ Total amount drug ×100

3.5 In Vitro Drug Release

The experimental setup for the release study comprises a dialysis membrane tube and a glass vessel with diameter just larger than the membrane tube. This is placed in a water bath that is maintained at 37°C.

1. Place buffered saline (pH 2.0/7.4/10.0)/ serum/medium solution in the glass vessel and allow to stand in the water bath until equilibrated to 37°C.
2. Tie one end of the dialysis membrane tube tightly to ensure no leakage.
3. Place the liposome suspension in PBS in the dialysis tube and seal the other end.
4. Suspend the dialysis tube within the glass vessel.
5. Remove samples of the buffer solution at time intervals up to 24 h, replacing each sample with fresh pre-warmed PBS.
6. At 24 h, remove the liposome suspension and lyse the liposomes, as previously described, to liberate the estradiol remaining in the liposomes.
7. Measure the estradiol content in all samples by HPLC using a validated assay.

3.6 In Vitro Cell Culture Studies

1. Caco-2 cells were grown into 10% fetal bovine serum MEM with penicillin (50 units/ml), streptomycin (50 units/ml) are grown on coverslips in 6-well plates.
2. Before the experiment, seed Caco-2 cells into 6-well culture plates at a density of 50,000 cells per well and incubate at 37°C, under 5% CO_2 for 96h.
3. 15 min before transfection, wash the cells with Transfer buffer.
4. Add 1 ml of meidum containing liposomes onto each well in tripliquet, and incubate the plates at 37°C for 2h in the presence of 5% CO_2,
5. Wash the cells thrice with PBS and treat with 1 mL of a distill water into cells for 30 min.
6. Add 25 μl of the supernatant to a 96-well plate, and incubate at 37°C for 30min.

Quantify the protein content with the BCA protein assay KIT(PIERCE) andreport to BSA taken as a reference curve.

7. For the calculation, background of the untreated cells, taken as negative controls, was removed from the sample data. The relative counts obtained for luciferase quantification were divided by the protein content in each well to normalize the results per mg of protein. The cationic formulation was taken as the positive reference formulation.

3.6.1 Protein Content Determination

The protein content of the lysates was measured by the DC Protein Assay reagent using bovine serum albumin as the standard.

1. Put in each well of a 96-well plate 10 μl of sample.
2. Add 25 μl of reagent A and 200 μl of reagent B.
3. Wait for 15 min at room temperature until a blue color appears.
4. Measure absorbance at 650–750 nm.

3.7 In Vivo Pharmacokinetic Evaluation

A suitable animal model can be used for in vivo pharmacokinetic assessment of a topically applied liposome formulation. Rats is most common but tend to provide an estimate compared to human absorb is more permeable. A generalised protocol is outlined in the following section but there can be considerable variation depending on the complexity of information sought, if the determination of distribution into tissues is required in addition to absorption into the circulation:

1. Animals are anaesthetised and liposome suspension applied to a pre-marked test site without occlusion.
2. At a predetermined time, the animal is sacrificed and a blood sample is collected.
3. Extract analytical solutions from all samples using suitable pre-validated solvent extraction procedures. Drug content in all samples should be analysed by a validated HPLC

assay or where possible, by scintillation counting if a radiolabelled active compound is available.

4. Suitable control formulations such as plain drug solution and possibly conventional liposome suspension should be applied to additional animals and processed with the same protocol.

5. Drug in plasma verses time post application is plotted and pharmacokinetic parameters of AUC_{0-24} h (area under curve), C_{max}(peak plasma level), T_{max}(time to peak plasma level) and $T_{1/2}$(plasma half-life) are determined.

4. Reference

1. Scott E. McNeil. (2011). Characterization of Nanoparticles Intended for Drug Delivery. 1-15.

2. Harris, J.M., Chess, R.B. (2003). Effect of pegylation on pharmaceuticals. *Nat Rev Drug Discov* 2, 214–21.

3. Fang, J., Sawa, T., Maeda, H. (2003) Factors and mechanism of "EPR" effect and the enhanced antitumor effects of macromolecular drugs including SMANCS. *Adv Exp Med Biol* 519, 29–49.

4. Maeda, H., Wu, J., Sawa, T., Matsumura, Y., Hori, K. (2000) Tumor vascular permeability and the EPR effect in macromolecular therapeutics: a review. *J Control Release* 65, 271–84.

5. Sahoo, S.K., Labhasetwar, V. (2003) Nanotech approaches to drug delivery and imaging. *Drug Discov Today* 8, 1112–20.

6. RaviKumar,M., Hellermann,G., Lockey,R.F.,Mohapatra, S.S. (2004) Nanoparticle mediated gene delivery: tateoftheart. *Expert Opin Biol Ther* 4, 1213–24.

7. Paciotti, G.F., Myer, L., Weinreich, D., Goia, D., Pavel, N., McLaughlin, R.E., Tamarkin, L. (2004) Colloidal gold: a novel nanoparticle vector for tumor directed drug delivery. *Drug Deliv* 11, 169–83.

8. Desai, N., Trieu, V., Yao, Z., , Dykes, D., Noker, P., Yao, R., Labao, E., Hawkins, M., Soon-Shiong, P. (2006) Increased antitumor activity, intratumor paclitaxel concentrations,

and endothelial cell transport of cremophor-free, albumin-bound paclitaxel, ABI-007, compared with cremophor-based paclitaxel. *Clin Cancer Res* 12, 1317–24.

9. Green, M.R., Manikhasm, G.M., Orlovm, S., Afanasyev, B., Makhson, A.M., Bhar, P., Hawkins, M.J. (2006) Abraxane, a novel Cremophor-free, albumin-bound particle form of paclitaxel for the treatment of advanced non-small-cell lung cancer. *Ann Oncol* 17, 1263–8.

10. Patri, A.K., Kukowska-Latallo, J.F., Baker, J.R. Jr. (2005) Targeted drug delivery with dendrimers: comparison of the release kinetics of covalently conjugated drug and non-covalent drug inclusion complex. *Adv Drug Deliv Rev* 57, 2203–14.

11. Mozafari MR, Mortazavi SM (eds) (2005) Nanoliposomes: from fundamentals to recent developments. Trafford Publishing Ltd,Oxford,UK

12. Volkmar Weissig, (2009). Liposomes Methods and Protocols Volume 1: Pharmaceutical Nanocarriers. 29-63.

13. Khosravi-Darani K, Pardakhty A, Honarpisheh H, Rao VSM, Mozafari MR (2007) The role of high-resolution imaging in the evaluation of nanosystems for bioactive encapsulation and targeted nanotherapy. Micron 38:804–818

14. Nomura SM, Yoshikawa Y, Yoshikawa K, Dannenmuller O, Chasserot-Golaz S, Ourisson G, Nakatani Y .(2001). Towards proto-cells: primitive lipid vesicles encapsulating giant DNA and its histone complex. ChemBioChem 2:457–459

15. Pozzi G, Birault V, Werner B, Dannenmuller O, Nakatani Y, Ourisson G, Terakawa S. (1996). Single-chain polyterpenyl phosphates form primitive membranes. Angew Chem Int Ed Engl 35:177–180

16. Bangham AD, Standish MM, Watkins JC .(1965). Diffusion of univalent ions across the lamellae of swollen phospholipids. *J Mol Biol* 13:238–252

17. Mozafari MR .(2005). Liposomes: an overview of manufacturing techniques. *Cell Mol Biol Lett* 10:711–719

18. Mozafari MR (ed) .(2006). Nanocarrier technologies: frontiers of nanotherapy. Springer, The Netherlands

19. Zhai GX, Chen GG, Zhao Y, Lou HX, Zhang JS .(2002). Study on preparation of low molecular weight heparin nanoliposomes and their oral absorption in rat. *J China Pharm Univ* 33:200–202

20. Bowtle W .(2000). Lipid formulations for oral drug delivery. *Pharm Tech Eur* 12:20–30

21. New RRC (ed) .(1990). Liposomes a practical approach. IRL/Oxford University Press, Oxford, UK

22. Reineccius G .(1995). Liposomes for controlled release in the food industry. In: Risch S, Reineccius G (eds) Encapsulation and controlled release of food ingredients. American *Chemical Society, Washington DC*,pp113–131

23. Mozafari MR, Hasirci V .(1998). Mechanism of calcium ion induced multilamellar vesicle- DNA interaction. *J Microencapsul* 15:55–65

24. Barenholz Y, Lasic D (eds) .(1996). Handbook of nonmedical applications of liposomes, vol III. CRC, BocaRaton,FL

25. Szoka F, Papahadjopoulos D .(1980). Comparative properties and methods of preparation of lipid vesicles (liposomes). *Annu Rev Biophys Bioeng* 9:467–508

26. Gabizon AA, Barenholz Y, Bialer M .(1993). Prolongation of the circulation time of doxorubicin encapsulated in liposomes containing a polyethylene glycol-derivatized phospholipid: pharmacokinetic studies in rodents and dogs. *Pharm Res* 10:703–708

27. Leserman L, Machy P, Zelphati O .(1994). Immunoliposome-mediated delivery of nucleic acids: a review of our laboratory's experience. J Liposome Res 4:107–119

28. Jurima-Romet M, Barber RF, Demeester J, Shek PN (1990) Distribution studies of liposome- encapsulated glutathione administered to the lung. *Int J Pharm* 63:227–235

29. Jurima-Romet M, Barber RF, Shek PN .(1992). Liposomes and bronchoalveolar lavage fluid: release of vesicle-entrapped glutathione. *Int J Pharm* 88:201–210

30. Pegg RB, Shahidi F .(1999). Encapsulation and controlled release in food preservation. In: Shafiur Rahman M (ed) Handbook of food preservation. CRC, *BocaRaton,FL,* pp 611–665

31. Woodbury DJ, Richardson ES, Grigg AW, Welling RD, Knudson BH .(2006). Reducing liposome size with ultrasound: bimodal size distributions. *J Liposome Res*16:57–80

32. Jesorka A, Orwar O .(2008). Liposomes: technologies and analytical applications. *Annu Rev Anal Chem* 1:801–832

33. Szoka FC, Papahadjopoulos D .(1981). Liposomes: preparation and characterization. In: Knight CG (ed) Liposomes: from physical structure to therapeutic application. Elsevier,

Amsterdam, pp51–82

34. Chatterjee S, Banerjee DK .(2002). Preparation, isolation, and characterization of liposomes containing natural and synthetic lipids. *Methods Mol Biol* 199:3–16

35. Hope MJ, Bally MB, Webb G, Cullis PR .(1985). Production of large unilamellar vesicles by a rapid extrusion procedure. Characterization of size distribution, trapped volume and ability to maintain a membrane potential. *Biochim Biophys Acta* 812:55–65

36. El Maghraby GM, Williams AC, Barry BW .(2004). Interactions of surfactants (edge activators) and skin penetration enhancers with liposomes. *Int J Pharm* 276(1–2):143–161

37. Berger N, Sachse A, Bender J, Schubert R, Brandl M .(2001). Filter extrusion of liposomes using different devices: comparison of liposome size, encapsulation efficiency, and process characteristics. *Int J Pharm* 223:55–68

38. Mozafari MR, Reed CJ, Rostron C .(2007). Prospects of anionic nanolipoplexes in nanotherapy: transmission electron microscopy and light scattering studies. *Micron* 38: 787–795

39. L.A. Utracki, (2004). Clay-Containing Polymeric Nanocomposites,Volume 1, 35-345.

40. Kim K,Utracki LA,Kamal MR.(2004). Numerical simulation of polymer nanocomposites using self-consistent mean-field model. *J Chem Phys*.1;121(21):10766-77.

41. M. K. Akkapeddi. (2000) Glass fiber reinforced polyamide-6 nanocomposites. *Polymer Composites Volume 21*, 8.576–585.

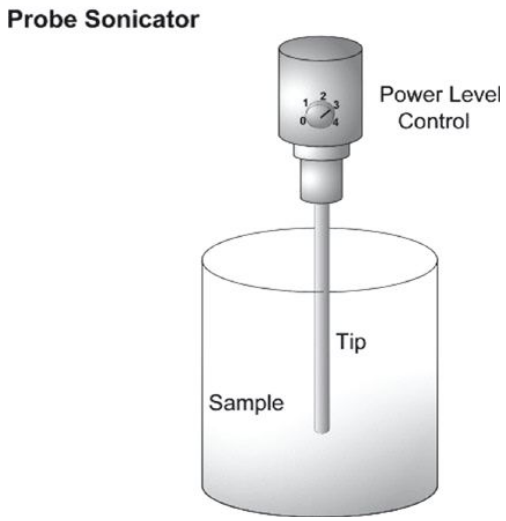

Fig. 1. Schematic representation of a probe-type sonicator

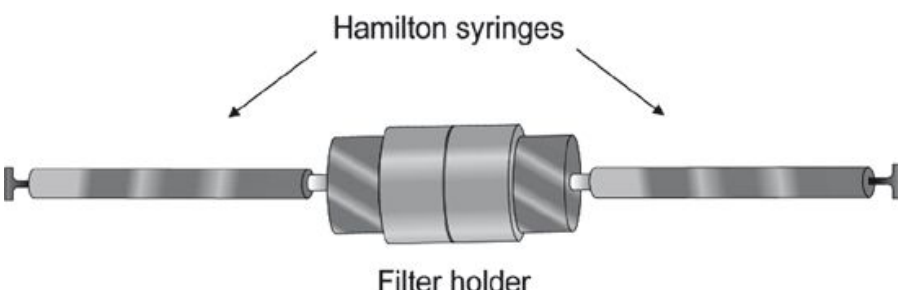

Fig. 2 small, hand-held, extruder used in the manufacture of nanoliposomes

Chapter 2

Fexofenadine nanoliposomes for the enhanced intranasal systemic delivery: development and pharmacokinetic evaluation

Abstract

The purpose of this work was to develop of prolonged release nanoliposome for intranasal delivery and to improve the bioavailability of poorly absorbable fexofenadine. Nanoliposome were designed by using DPPC, DPPG and cholesterol as lipid core materials and chitosnan as accelerator stabilizer. nanoliposome system composed of nanoliposome (Lip) and co-chitosan nanoliposome (CS-Lip) was developed for intranasal delivery, which were characterised by their particle size, zeta potential, entrapment efficiency, solid-state studies, in vitro drug release, cell uptake, mucin adsorption and storage stability at 4 /30°C for 6 months. Pharmacokinetic studies were also performed in SD rat. In vitro study, it was observed that Lip and CS-Lip had better drug entrapment near 66%, desired release and mucin adsorption characteristics, spherical shape and maximum storage stability. Compared to the untreated powder, the CS-Lip could achieve a prolonged retention though its positive charge. It's more explore that Lip and CS-Lip can control the drug release rate in cellar uptake study and avoid to release rapid in shot time. Furthermore, nasal pharmacokinetic study indicated that CS-Lip significantly ($p < 0.05$) enhanced the system exposure of fexofenadine in rats compared to the untreated powder formulation. The CS-Lip was found as a optimal formulation to be controlling fexofenadine release in nasal route. $T_{1/2}$ was prolonged to 6.8 hour after intranasal administration at 2.0 mg/kg dose, and the absolute bioavailability was about 35% compared to the intravenous administration in rats. Our results suggested that these CS-Lip formulations could be used as an effective intranasal dosage form for the control drug release delivery of fexofenadine.

국문초록

두 번째 섹션은 nanoliposome의 특성은 비강 전달 속성과 효과를 관련 설명한다. 이 작품의 목적은 비강 전달을 위해 nanoliposome의 개발과 저조한 흡수성 fexofenadine의 생체 이용률을 높이는 것이었다. Nanoliposome는 액셀러레이터 안정제와 같은 지질 핵심 소재 및 chitosnan로 DPPC, DPPG과 콜레스테롤을 사용하여 설계되었다. nanoliposome (Lip)와 공동 키토산 nanoliposome (CS - Lip)로 구성된 nanoliposome 시스템은 체외 마약 릴리스 셀 이해에서 입자 크기, 제타 전위, entrapment efficiency, 고체 연구에 의해 특징되었고, 비강 전달을 위해 개발되었다. mucin 흡착 및 저장 안정성. Pharmacokinetic 연구는 또한 SD rats 에서 수행되었다. 체외 연구에서, 그것은 Lip 및 CS - Lip 이 66% 근처에 좋은 약물 entrapment, 원하는 릴리스 및 mucin 흡착 특성, 구형 형상과 최대 저장 안정성이 있다고 관찰했다. 치료 분말에 비해 CS - Lip 은 긍정적인 결과에도 불구하고 장기 보존을 달성할 수 있다. 그 Lip 을 연구하고, CS - Lip 을 저장하고 이해 연구함으로써 약물 방출 속도를 제어하고 촬영 시간에 따른 릴리스 피할 수 있다. 또한, 비강 pharmacokinetic 연구는 CS - Lip ($P < 0.05$)은 치료 분말 제제에 비해 rats 에 대한 fexofenadine의 시스템 노출을 강화 시킨 것을 지적했다. CS - Lip 은 비강 경로에서 fexofenadine 버전을 제어하는 최적의 배합으로 발견되었다. 비강으로 2.0 mg / kg 용량으로 투여시 $T_{1/2}$ 는 6.8시간으로 연장되었고, 절대 생체이용율은 정맥 투여에 대비해 약 35%였다. 우리의 결과는 다음과 CS - Lip 공법은 fexofenadine 의 제어 약물 릴리스 전달을위한 효과적인 비강 투여 형태로 사용될 수 있다고 제안했다.

1. Introduction

Allergic rhinitis (AR) are common diseases with classical symptoms such as sneezing, nasal pruritus, congestion and rhinorrhoea, it is now recognised that AR has a significant impact on quality of life [1]. Antihistamine remains the principal one in the clinical treatment of AR. Especially, the second-generation antihistamines of fexofenadine are recommended first-line treatment for AR[2], Fexofenadine hydrochloride (Fex) is a selective histamine H1 receptor antagonist and is clinically effective in the treatment of seasonal allergic rhinitis as a first-line agent for adults and children 6 years of age and older[3]. Although Fex has few adverse effect compare for the first- generation antihistamines such as terfenadine and astemizole etc.[4-6], but the most common adverse event observed with Fex was headache, which occurred with similar frequency in patients treated with placebo[7-11], This rare adverse event has been associated with greatly elevated blood levels of these agents, resulting from drug overdose, hepatic insufficiency (dysfunction), or interactions with other drugs or food that inhibit their metabolism. Although Fex is appear to be only minimally metabolized in the liver, but Fex pharmacokinetics depends on the activity of P-glycoprotein(P-gp) [12-14] and organic aniontransporting polypeptide (OATP) family transporters [15,16]as uptake transporters, In addition, drug-drug and drug-food interaction reports relevant to Fex have shown that fruit juice, and verapamil affected systemic exposure dose of Fex with therapeutic implications [17,18]. So in order to avoid the drug-drug, drug-food interaction and transporters effect, we need to seek for a stability effective route and vehicle to decrease the adverse effects and improved bioavailability to the systemic pathway of Fex.

Intranasal administration offers a noninvasive alternative as a direct delivery of therapeutics to the AR. Over the last several years, there have been a sharp increase in the amount of research focused on the nasal pathway for AR drug delivery [19]. It was shown that nasal musous as the systemic pathway, in which the drug is absorbed across the nasal cavity into the systemic circulation. However, the nasal cavity presents several barriers like physical removal of formulation by mucocilliary clearance, enzymatic degradation, and low

permeability of the nasal epithelium. Several methods have been developed such as using mucoadhesive polymer, absorption enhancer and lipid emulsions, etc., to prolong the contact time of drugs with the nasal mucosa and enhance its permeation into the nasal mucosa [19-22]. Currently, Fex have low solubility and low permeability, thus effort to increase the absorption and increasing the drug residence time in the nasal cavity of the drug is needed.

Compared with liquid nasal formulations or powder dosage forms, Nanoliposomes (Lip) has high permeability stability vesicles, which can entrap both hydrophobic and hydrophilic compounds within their structure, protect entrapped compounds from degradation and release the entrapped compounds at designated targets[23,24]. So it cannot only prolong the contact time between the drug and the absorptive sites in the nasal cavity, but also release drug slowly and continuously [25,26], hence it is especially useful for those drugs used chronically and in small doses. The aim of the present study is a strategy to formulate the chitosan –coated nanoliposomes (CS-Lip) system of Fex for nasal drug administration to achieving improved delivery to the systemic pathway and avoidance of hepatic first-pass elimination for therapeutics to AR. achieving balanced of action and higher bioavailability with less toxicity and adverse effect.

2. Materials and methods

2.1 Materials

Fexofinadine, piroxicam, DPPC (1, 2- ditetradecanoyl- sn- lycero- 3- phosphocholine), cholesterol (Cho), chitosan (CS), DPPG (1,2-dipa;mitoyl-sn- glycero -s-phospho -rac-glycerol, sodium salt) and mucin were obtained from Sigma Chemical Co. (St. Louis, MO, USA). Triethylamine, HBS, mannital, sucrose, D-glucose and lactose was obtained from Junsei Chemical Co. (Tokyo, Japan). Acetonitrile, methanol, ethanol and acetic acid were obtained from Merck Co. (Darmstadt, Germany). All other chemicals were of analytical grade and all solvents were of HPLC grade.

Caco-2 (human colon carcinoma cell) was obtained form Korea cell line bank (Seoul, Korea). MEM medium, Trypsin 0.25% (1×) solution, Penicillin- streptomycin solution (10,000 units/ml penicillin 10,000 μg/ml streptomycin) and Fetal Bovine Serum (FBS) were obtain from thermo scientific company. 4% capric sulfate and BCA solution were obtain from novagen company.

2.2 Preparation of liposomes

Lip were prepared by hydration of lipid film which was modified from Takeeuchi et al[27] and described previously by Siamornsak er al.[28]. Briefly, the mixture of DPPC, DPPG, Cho and Fex in molar ratio of 8: 1: 2.25: 0.45 was dissolved in a small amount of chloroform and placed in a rotary evaporator at 45℃ until a thin film was obtained, allowed to stand in a vacuum chamber for 4 hours to ensure complete solvent removal, 1 ml of HBS butter (pH=7.4) was used to hydrate the thin film, the hydrated thin film was melted in water bath at 45℃ for 2 hours and blended to obtain Lip. In order to reduce particle size, the Lip were then passed through an extruder (Lipo Fast-Pneumatic, Avestin, Canada) using 0.4 μm polycarbonate membrane filters to generate submicron- sized Lip.

For the preparation of CS-Lip, Lip suspension in HBS buffer was added drop wise into the CS solution (0.1% (w/v) in acetic acid 0.1M and the pH was adjusted to 5.5 by dilute NaOH, under stirring (600 rpm at room temperature) in a volume ratio of 1: 4 for 1 hour. The suspension was left overnight at 4℃. CS-Lip were harvested from the mixture by centrifugation at 15,000×*g* for 30min at 4 ◦C and resuspended in HBS (pH 7.4). This washing procedure was performed twice [29]. Optical microscope.

2.3 Determination of particle size and surface charge

The average particle size and the change in surface properties (zeta potential value) of the Lip and CS-Lip were evaluated by a particle size anglyzer (Zetasizer, model 3000HS_A, Malvern Instrument, UK). The average particle size was calculated from 10 measurements and displayed with a polydispersity index. The 20μl sample was diluted with 5 ml of filtered deionized water prior to the determination of surface properties the average zeta potential value was calculated.

2.4 Transmission electron microscopy

Lip and CS-Lip were analyzed via field emission transmission electron microscope (FE-TEM). A 2μl of each liposomal susupension was applied to copper coated with a carbon grid. The excess was drawn off with filter paper, after drying overnight at room temperate, the sample were examined under the transmission electron microscope (Tecnai G2F30, Philips, USA). The particle size was measured by the software (Gatan program) accompanying the transmission electron microscope.

2.5 Determination of entrapment efficiency

The entrapment efficiency (EE,%) of Fex in the Lip or CS-Lip was determined by centrifuging the liposomal suspension at a speed of 25000× g for 45 min at 4℃ and and assaying the free Fex in supernatant portion A, the Lip were washed twice by HBS and added to 1 ml ethanol to broken out of the Lip and assaying the Fex B by HPLC (Perkin Elmer Series 200; Waltham, MA, USA) at the 195 nm, The octadecylsilane column (Gemini C18, 4.6mm×150mm, 5μm; Phenomenex, Torrance, CA, USA) was eluted with the mobile phase consisting of 0.1M triethylamine: acetonitrile: methanol (50: 25: 25, v/v/v%, pH 3.3 adjusted with phosphoric acid) at a flow rate of 1.0 ml/min. The EE,% was then calculated using Eq.(1). Experiments were performed in triplicate.

$$EE\% = [B/(A+B)\times 100] \quad (1)$$

2.6 In vitro drug release studies and stability studies for long-term storage

The release experiments were run immediately after the separation of the free Fex from that encapsulated in Lip and CS-Lip. To avoid erroneous results due to sudden temperature changes, the purified liposome preparations were gradually warmed to 37℃. Both Lip and CS-Lip samples were diluted 4 times in different buffers (pH = 4.0; 7.4; 10) and cellar medium, blank plasma, which were incubated at 37℃ in water bath. The samples were

absorbed at 0, 0.5, 1, 15, 2, 4,8, 12, 24 hour and centrifuged at a speed of 25000× g for 45 min at 4℃and assaying the free Fex in supernatant portion by HPLC

Samples were made of freeze- dried power of Lip and CS-Lip with optimal stuffing of lactose 10%. Samples were stored at 4℃ and 25℃ for 6 months and collected at 0, 0.03, 0.1, 0.23, 0.5, 1, 3, 6 months. The sample added 0.2 ml D.W to measure the entrapment efficiency and size. Briefy, 20μl suspension was diluted to 5ml by water to measure for size and zeta potential, the other liposomal suspension was centrifuged for 45 min at 25000g. The deposit was washed with water for twice and dissolved with 200μl ethanol. The drug concentration of each sample was determined by HPLC.

2.7 Mucin adsorption studies

Adsorption of mucin (extracted from porcine stomach mucosa) in the surface of Lip and CS-Lip were measured to evaluated the mucoadhesive properties [37]. Briefy, 1 ml of mucin solution (1mg/ml) A was stirred with 1 ml of Lip and CS-Lip for a concentration 1.45mg/ml. which were incubated for 1 hour in water bath at 37℃. Then, the suspension was centrifuged at 25000g for 30 min at 4℃. The free mucin B was collected by Bradford colorimetric method[38], which added Bradford reagent to mucin solution and incubated for 10min at 37℃. Above solution were transferred to 96-well plate and detected at UV 595 nm. Amount of mucin absorbed on Lip and CS-Lip was determined from the calibration curve. The adsorption % was then calculated using Eq.(2).

$$\text{Adsorption } \% = [(A - B)/A] \times 100 \quad (2)$$

2.8 Cell uptake study in Caco-2 cells

Caco-2 cell is comely used for the evaluation of drug transport across the nasal membrane, Furthermore, muscin synthesis was proved in Caco-2 cells [30,31]. Cell were seeded into 6-well plate at a density of 5×10^5 cells per well. At one week post-seeding,

cells were incubated with drug solution, Lip and CS-Lip at 50μM, At the end of 2 hour incubation, drug solution was removed and the cells were washed three times with ice-cold phosphate- buffered saline. After the cell lysis, cells were harvested and sonicated for 5 min. Acetonitrile was added to the cell lysate, vortexed vigorously and centrifuged for 10 min at 20000g. the supernatant was collected and the drug concentration of each sample was determined by HPLC, The protein amount of each sample was also determined by Bradford protein assay.

2.9 In vivo pharmacokineticsstudies

2.9.1 Experimental procedure

Male Sprague–Dawley rats (250–260g) were purchased from Samtako Bio Co. (Osan,Korea). All animal studies were performed in accordance with the "Guiding Principles in the Use of Animals in Toxicology" adopted by the Society of Toxicology (USA). Rats were divided into five groups (n = 6 per each group). Groups 1–3: 2mg/kg of Fex (nasal), 2mg/kg of Fex in Lip (nasal), 2mg/kg of Fex in CS-Lip (nasal); Group 4:10 mg/kg of Fex (p.o.) Group 5: 5mg/kg of Fex (i.v.) A single dose of approximately10 mg/kg Fex is comparable to the clinical dose of 120 mg in humans [33,34]. Also, For the intranasal administration groups, the dose and 25μl of the formulation was administered onto the nostrils of 250g rat used in the present study were selected based on the previous report [35,36] as well as assay sensitivity. Fex dissolved in and water for oral administration and in saline (0.9%) for i.v. administration. Blood samples were collected from the femoral artery at 0, 0.05, 0.16, 0.25, 0.5, 1, 2, 4, 8, 12, 24 h following an intravenous administration. Blood samples were also collected from the femoral artery at 0, 0.25, 0.5, 0.75, 1, 1.5, 2, 4, 8, 12, 24 h following an oral and intranasal administration. Blood samples were centrifuged and the obtained plasma was stored at −70 ◦C until analyzed.

2.9.2 Plasma treatment and analysis

Plasma concentration of Fex was determined by the HPLC method described as follows. In brief, 10μl of piroxicam (10μg/ml) as an internal standard was added to 90μl of each plasma sample and then the mixture was deproteinized by adding 200μl of acetonitrile. After centrifugation of the samples at 20,000×*g* for 10min, the supernatant was evaporated and the residue was reconstituted with 120μl of the mobile phase, and then 50μl of aliquots were injected directly into the HPLC system (Perkin Elmer Series 200; Waltham, MA, USA). The octadecyl silane column(Gemini C18, 4.6mm×150mm, 5μm; Phenomenex, Torrance, CA, USA) was eluted with the mobile phase consisting of 0.1M triethylamine: acetonitrile: methanol (61: 19.5: 19.5, v/v/v%, pH 4.4 adjusted with phosphoric acid) at a flow rate of 1.0 ml/min. The UV detector set at 195 nm. The calibration curve from the standard samples was linear over the concentration range of 0.01–0.5μg/ml. The detection limit of Fex was 0.01μg/ml.

2.10 Statistical analysis

All mean values were presented with their standard deviation (mean ± S.D.). Statistical analysis was conducted using a one-way ANOVA followed by a posteriori testing with Dunnett correction. A p value less than 0.05 was considered statistically significant.

3. Results and discussion

3.1 Preparation and characterization of Lip and CS-Lip

The physicochemical properties of the drug, especially solubility, permeability and partition coefficient, can be important determinants for the extent of its liposomal incorporation. Therefore, considering the Fex as a lipophilic nature of the drug and its low aqueous solubility and its high solubility in chloroform [39], a first series of liposomal formulations was prepared by dissolving Fex in this organic solvent, together with Cho, DPPC and DPPG in differ race were evaluated. The obtained liposomal dispersions were characterized for EE,%, particle size, polydispersity index and Zeta-potential Tab.1.and Fig.1(A). The results indicate that, as expected, the total amount of drug entrapped in the vesicles progressively increased with increasing DPPC concentration initially dissolved in the lipophilic phase during vesicle preparation. These findings could be explained by considering that, when the drug is dissolved together with the phospholipids mixture, it will be located within the liposomal bilayer, where the acyl chains of phospholipids provide a favourable environment for the lipophilic Fex molecules. However, the intercalating incorporation of the drug into the bilayer could alter the microstructure of the vesicular membrane, thus giving rise to a re-arrangement of the membrane structure and a decrease in ordering and stability of the system, and hindering an effective drug entrapment. This hypothesis is supported by the reduction of the liposomal membrane organization order [40,41]. Moreover, the vesicles were characterized by a higher homogeneity, as demonstrated by the polydispersity index that dropped from 0.35 to 0.1. Fig.2. On the other hand, measurements of Zeta-potential values indicated that it was scarcely influenced by three races of phospholipids during the preparation. Therefore, a contribution of the phospholipids to the liposomal charge can be excluded. In this regard, the negative charge of the vesicles, which in all cases was in the range between −107 and−109 mV, could be attributable to the ionisation of the phosphate groups of DPPC and DDPG molecules.

Lip was coated with 0.1% of CS [42], and its effects on liposome physicochemical properties were evaluated, as shown in Tab.1 and Fig.1(B). In the liposome formulation, DPPC and DPPG were added as a negatively charged lipid which provided the binding force to the positively charged CS. The Lip was negatively charged, and with the CS coated Lip which zeta potential increased from −109 to +11.8 mV, a condensed coating layer was formed on the particle surface and transferred the zeta potential into positive.

3.2 In vitro drug release studies and stability studies for long time

The drug release of Lip and CS-Lip in the simulated nasal circumstances (35 ◦C, pH 7.4) was studied. Furthermore, evaluate the possible effect on pH, cell medium and plasma. The results of drug release studies in different pH circumstances, cell medium and blank plasma. The corresponding drug permeation profiles are shown in Fig.3. It can be observed that all liposomal formulations Fig. 3(A) showed an initial fast release phase followed, after 6–8 h, by a plateau phase. Meanwhile, the drug release rate affected by pH =4.0 in Lip and CS-Lip, which was significantly lower than others solution. But the drug release rate in pH=10.0 little higher pH=7.4. The CS-Lip was not significantly higher than Lip in the simulated nasal circumstances or cell medium and blank plasma. The drug release profile was prominently prolonged by the Lip encapsulation and further release by CS coating. Otherwise, the drug was completely entrapped in the Lip without any drug free in solution or absorbed on the liposome surface, and therefore there was no burst release at the beginning. In this case, the drug release rate depends on the membrane permeability which is affected by the fluidity of lipid bilayer[43].

Lip and CS-Lip stability studies were measured until 6 month storage in freeze-dry power formulation at 4℃ and 25℃. Select to a stability stuffing of lactose 10% to protect for Lip in freeze-dry process Fig. 4,5. The result showed that lactose 10% scarcely any effect on EE,% and size of Lip and CS-Lip. Although of mannitol, D-Glucose and sucrose weren't effect on the size. But they decrease EE,% from 60- 20 percent. Especially, HBS exceeding effect on the stability of Lip and CS-Lip in freeze-dry process. After 6 month-

storage, the EE,% significantly decreased at 25℃ compare for store in 4℃, although the size of Lip or CS-Lip were slight changed at 25℃ than 4℃ Fig.6, 7 and Tab.2, Implying that the freeze-dry power formulation at 4℃ as a stability store condition to Lip and CS-Lip in long time.

3.3 Mucin adsorption studies

The results of mucodahesive adsorption studied across nasal mucin of Fex from the different Lip and CS-Lip formulations, while the corresponding mucin adsorption profiles shown in Fig.8. The amount of mucin adsorbed on the surface of CS-Lip was approximately 7-fold higher than Lip. The amount of mucin adsorbed increased follow with CS dose. Adsorption rate of Lip was almost 10%, implying that Lip have affinity to mucin to a certain extent. Compared for CS-Lip has higher affinity with mucin, which was 70 precent of mucin was adsorbed into CS-Lip. Because of the positively charged of CS has electronic interaction with negatively charged mucin secreted from nasal epithelial cells.[27,29] Therefore, a contribution of CS-Lip can improve the mucodahesive.

3.4 Cellular uptake study

The Lip and CS-Lip effect of Fex on the cellular accumulation was examined in Caco-2 cells. As illustrated in Fig. 9, the cellular accumulation of Fex was significantly higher than Lip and CS-Lip to the cellular uptake of Fex. Furthermore, the cellular accumulation of Fex in Lip was significantly lower than CS-Lip. A similar result of cellular accumulation of Fex in free drug and drug with blank Lip, implying that blank Lip have not effect on the cellular uptake of Fex. But the Lip significantly prolong to the cellular uptake of Fex. Moreover, the interactive adsorbability between CS-Lip with cellular membrane by electronic interaction. Thus, the positively charged CS coating layer can provide a binding force to the cellular surface. Nevertheless, the bioadhesion of CS is not exclusively determined by the positive charge. It could also be promoted by the presence

of free amine and hydroxyl groups of CS molecules which form hydrogen bonds to the cellar membrane surface. This might explain that the CS could achieve a prolonged retention though its positive charge was limited at neutral pH. It's more explore that Lip and CS-Lip can control the drug release rate in cellar uptake study and avoid to release of high drug concentration in shot time.

3.5 In vivo pharmacokinetics studies

The vivo studies were performed in SD rats that were determined in order to evaluate the Fex absorption in nasal cavity and nasal mucous membrane retention of CS, compared with Lip in aqueous solution Fig.12. Two representative chromatograms including an intact blank plasma (A), and a plasma sample supplemented with lower range of fexofenadine and the internal standard piroxican (B) in Fig.11. A standard curve of Fex in PK study Fig.10. The plasma concentration profiles of Fex after oral and intravenous administration are shown in Fig.12(A). The mean plasma concentration profile of Fex from the intranasal delivery of Fex in Lip and CS-Lip formulations and Fex powder is displayed in Fig.12(B). The corresponding bioavailability and pharmacokinetic parameters are shown in Tab. 3. Compared for oral administration of Fex at 10mg/ml dose in rat that its bioavailability is 6.2%, the nasal delivery of Fex at 2.0 mg/kg dose in power and Lip formulation showed similar bioavailability of 24-25% relative to intravenous administration, the Fex at 2.0 mg/kg dose of bioavailability is 34.7% in CS-Lip formulation are shown in Fig.13. In this case, nasal administration of Fex, the bioavailability increased 4-5 fold higher than oral administration. Furthermore, compared for the power and Lip formulation of Fex, the bioavailability of Fex in CS-Lip formulation significantly increased 10%. The mean maximum concentration (C_{max}) of Fex into Lip and CS-Lip are significantly lower than power formulation in nasal and oral administration. This might be due to the rapid absorption of drug in the intranasal administration route[33]. Otherwise, the drug steady release depends on the lecithoid membrane permeability which is affected by the fluidity of

lipid bilayer[43]. On account of some reports that most common adverse event observed with headache after Fex orally, which occurred rate increase follow with the dose of Fex in similar frequency in patients treated with placebo[7-11], the C_{max} as a impotent parameter to evaluate drug concentration in blood levers. So that, control to a lower C_{max} of Fex at the rapeutical dose that will be benefit to reduce the adverse event in clinical application. T_{max} and $T_{1/2}$ of Fex in Lip and CS-Lip are higher than in power formulation. The AUC of Fex in CS-Lip is significantly higher than in Lip and power formulation in nasal administration. Implying that Lip and CS-Lip have a favorable membrane permeability of the fluidity of lipid bilayer, which is significant prolong to the release race of Fex compare for drug release quickly in nasal administration. Moreover, the CS-Lip increased the systemic exposure dose of Fex than Lip and power formulation. The enhanced absorption may be explained that the drugs absorption will be effect on the generally rapid clearance of the nasal cavity in nasal administration [32]. CS belong to bioadhesive property can decrease the rapid clearance of the nasal vibrissa and enhance the drug resort time in nasal cavity[26]. Moreover, the nasal mucosae retention was significantly prolonged by CS, compared with either Lip or drug power. CS also demonstrated an improved nasal mucosae drug penetration rate, which was attributed to the penetration enhancing effect of CS. The results adapt to foregoing studies in mucin adsorption and cellular uptake.

4. Conclusions

The Lip system comprising DPPC, DPPG and Cho showed high stability and steady permeability capacity of Fex. The optimized formulations of Lip contained with CS layer that has brought a significant modification of its nasal drug delivery behaviors. Following intranasal administration in rats, compared to the powder formulation, CS-Lip and Lip showed significantly lower C_{max} and prolong to $T_{1/2}$, meanwhile, CS-Lip significantly increased the systemic expose ddose of Fex. So that, control to a lower concentration of drug in blood levels and elevated the bioavailability of Fex in therapeutical dose scope. It will be benefit to reduce the adverse event and provide a new therapeutical method in clinical application.

5. References

1. Bachert C,Maurer M. (2010). Safety and efficacy of desloratadine in subjects with seasonal allergic rhinitis or chronic urticaria: results of four postmarketing surveillance studies. *Clin Drug Investig*.30(2):109-22.

2. Hay JW, Kaliner MA. Curr Med Res Opin.,(2009). Costs of second-generation antihistamines in the treatment of allergic rhinitis: US perspective. Curr *Med Res Opin*. 25(6):1421-31.

3. Simpson K and Jarvis B.,(2000). Fexofenadine: a review of its use in the management of seasonal allergic rhinitis and chronic idiopathic urticaria. *Drugs* 59:301–321

4. Yap YG,Camm AJ.,(2002). Potential cardiac toxicity of H1-antihistamines. *Clin Allergy Immunol*.17:389-419.

5. Bernstein DI, Schoenwetter WF, Nathan RA, Storms W, Ahlbrandt R, Mason J.（1997）. Efficacy and safety of fexofenadine hydrochloride for treatment of seasonal allergic rhinitis. *Ann Allergy Asthma Immunol* 79: 443–448.

6. Meeves SG, Appajosyula S.,(2003). Efficacy and safety profile of fexofenadine HCl: a unique therapeutic option inH1-receptor antagonist treatment. *J Allergy Clin Immunol*. 112(4 Suppl): S69–S77.

7. Meltzer EO,Scheinmann P,Rosado Pinto JE.,(2004). Safety and efficacy of oral fexofenadine in children with seasonal allergic rhinitis--a pooled analysis of three studies. *Pediatr Allergy Immunol*. 15(3):253-60.

8. Simpson K,Jarvis B.,(2000). Fexofenadine: a review of its use in the management of seasonal allergic rhinitis and chronic idiopathic urticaria. *Durgs*. 59(2):301-21.

9. Kulthanan K,Gritiyarangsan P,Sitakalin C.,(2001).Multicenter study of the efficacy and safety of fexofenadine 60 mg. twice daily in 108 Thai patients with chronic idiopathic urticaria. *J Med Assoc Thai*. 84(2):153-9.

10. Graft DF,Bernstein DI,Goldsobel A.,(2001).Safety of fexofenadine in children treated for seasonal allergic rhinitis. *Ann Allergy Asthma Immunol*. 87(1):22-6.

11. Dhar S, Basu D, Mistri G, Hazra PK, Malakar S, Dutta AK.,(2002). Evaluation of the efficacy and safety of fexofenadine in the management of chronic idiopathic urticaria: A prospective study with 512 patients Indian. *J Dermatol Venereol Leprol*. 68(2):73-6.

12. Cvetkovic M, Leake B, Fromm MF, Wilkinson GR, and Kim RB.,(1999). OATP and Pglycoprotein transporters mediate the cellular uptake and excretion of fexofenadine. *Drug Metab Dispos* 27:866–871.

13. Perloff MD, von Moltke LL, and Greenblatt DJ. (2002). Fexofenadine transport in Caco-2 cells: inhibition with verapamil and ritonavir. *J Clin Pharmacol.* 42:1269–1274.

14. Putnam WS, Ramanathan S, Pan L, Takahashi LH, and Benet LZ. (2002). Functional characterization of monocarboxylic acid, large neutral amino acid, bile acid and peptide transporters, and P-glycoprotein in MDCK and Caco-2 cells. *J Pharm Sci* 91:2622–2635.

15. Nozawa T, Imai K, Nezu J, Tsuji A, and Tamai I.,(2004). Functional characterization of pH- sensitive organic anion transporting polypeptide OATP-B in human. *J Pharmacol Exp Ther* 308:438–445.

16. Niemi M, Kivisto KT, Hofmann U, Schwab M, Eichelbaum M, and Fromm MF.(2005) . Fexofenadine pharmacokinetics are associated with a polymorphism of the SLCO1B1 gene (encoding OATP1B1). *Br J Clin Pharmacol* 59:602–604.

17. Dresser GK, Bailey DG, Leake BF, Schwarz UI, Dawson PA, Freeman DJ, and Kim RB., (2002). Fruit juices inhibit organic anion transporting polypeptide-mediated drug uptake to decrease the oral availability of fexofenadine. *Clin Pharmacol Ther* 71:11–20.

18. Lemma GL, Wang Z, Hamman MA, Zaheer NA, Gorski JC, and Hall SD. (2006). The effect of short- and long-term administration of verapamil on the disposition of cytochrome P450 3A and P-glycoprotein substrates. *Clin Pharmacol Ther* 79:218–230.

19. Callens C, Remon JP., (2000). Evaluation of starch-maltodextrin-Carbopol 974 P mixtures for the nasal delivery of insulin in rabbits. *J Control Release*, 66: 215–220.

20. Callens C, Pringels E, Remon JP. ,(2003). Influence of multiple nasal administrations of bioadhesive powders on the insulin bioavailability. *Int J Pharm,* 250: 415–422.

21. Mitra R, Pezron I, ChuWA,MitraAK.,(2000).Lipid emulsions as vehicles for enhanced nasal delivery of insulin. *Int J Pharm*, 205: 127–134.

22. Merkus FW, Verhoef JC, Marttin E, Romeijn SG, van der Kuy PH, Hermens WA, Schipper NG., (1999). Cyclodextrins in nasal drug delivery. *Adv Drug Deliv Rev,* 36: 41–57.

23.Benech, r.o .,(2002). Inhibiton of Listeria innocua in cheddar cheese by assition of nisin Z in liposoems or by in stu production I mixed culture. *Appl. Environ.Microbiol*, 68, 3683-3690.

24. Shehata,t ,(2008).Prolongation of residence time of liposome by surface- modification with mixture of hydrophilic polumers. *Int. J .Phram*. 359, 279-279.

25. Aliasgar Shahiwala.,(2004). Nasal delivery of levonorgestrel forcontraception: an experimental study in rats. Fertility and sterility. vol. 81.

26. Wu-Xiao Ding ,Xian-Rong Qi. (2007). Pharmacokinetics and Pharmacodynamics of Sterylglucoside-Modified Liposomes for Levonorgestrel Delivery via Nasal Route. *Drug Delivery*, 14:101–104.

27. H.Takeuchi,Y. (2003). Mucoadhesive properties of carbopol or chitosan-coated liposomes and their effectiveness in the oral administration of calcitonin to rats, *J.Control. Release* 86, 235-242.

28. P. Sriamornsak, N.Thirawang, J.Nunthanid, S.,(2007). Atomic force microscopy imaging of novel self-assembling pectin-liposome nanocomplexes, *Carbohydr. Polym*.71,324-329.

29. R. Galovic Rengel, K. Barisic, Z. Pavelic, T. Zanic Grubisic, I.Cepelak,J. Filipovic-Grcic.,(2002).High efficiency entrapment of superoxide dismutase into mucoadhesive chitosan-coated liposomes. *Eur.J. Pharm. Sci*. 15,441.

30. Niv Y,Byrd Jc,Ho SB.,(1992). Mucin synthesis and secretion in relation to spontaneous differentiation of colon cancer cells in vitro. *Int J Cancer,* 50.10:147-152.

31. Li, L., Nandi, I.,Kim,K.H.,(2002). Development of an ethyl laurate-based microemulsion for rapid-onset intranasal delivery of diazepam. *Int. J. Pharm*. 237,77–85.

32. Illum, L.,(2003). Nasal drug delivery-possibilities, problems and solutions. *J. Control. Rel.* 87:187–198.

33. Dresser, G.K., Bailey, D.G., Leake, B.F., Schwarz, U.I., Dawson, P.A.,Freeman, D.J.,Kim, R.B.,(2002). Fruit juices inhibit organic anion transporting polypeptidemediated drug uptake to decrease the oral availability of fexofenadine. *Clin. Pharmacol. Ther.* 71, 11–20.

34. Kamath, A.V., Yao,M.,Zhang,Y.,Chong,S.,(2005). Effect of fruit juices on the oral bioavailability of fexofenadine in rats. *J. Pharm. Sci.*9 4, 233–239.

35. Illum, L., Watts, P.J., Cheng, Y.-H., (2001). Novel formulations of fexofenadine. United States West Pharmaceutical Services Drug Delivery & Clinical Research Centre, Ltd. 20010051613.

36. Hong-Mei Piao, Dae-Duk Kim.,(2010). Preparation and evaluation of fexofenadine microemulsions for intranasal Delivery. *International Journal of Pharmaceutics* 395, 309–316

37. Filipovic-Grcic J , Skalko-Basnet N.,(2001). Mucoadhesive chitosan-coated liposomes: characteristics and stability .*J Microencapsul,*18(1):3-12.

38. Bradford MM.,(1976). A rapid and sensitive method for the quantitation of microgram quantities of protein utilizing the principle of protein-dye binding. *Anal Biochem.* 72:248-254.

39. Sapkal NP,Kilor VA,Shewale BD,Bhusari KP,Daud AS,(2010). Study of the Complexation Behaviour of Fexofenadine with β-Cyclodextrin. *Indian J Pharm Sci*. 72(3):318-23.

40. E. de Paula, S.Schreier.,(1995). Use of a novel method for determination of partition coefficient to compare the effect of local anaesthetics on membrane structure, *Biochim. Biophys.* Acta1240.25–33.

41. C.M. Saia Cereda, D. Riberio de Araujo, G. Bruschini Brunetto, E. de Paula, (2004). Liposomal prilocaine preparation, characterization and in vivo evaluation, *J. Pharm. Pharmaceut. Sci*. 235–240.

42. Nan Liu, Hyun-Jin Park.,(2010). Factors effect on the loading efficiency of Vitamin C loaded chitosan-coated nanoliposomes. *Colloids Surf B Biointerfaces*.76(1):16-9.

43. Volodkin, D., Mohwald, H., Voegel, J.C., Ball, V., (2007). Coating of negatively charged liposomes by polylysine: drug release study. *J. Control. Release* 117, 111–120.

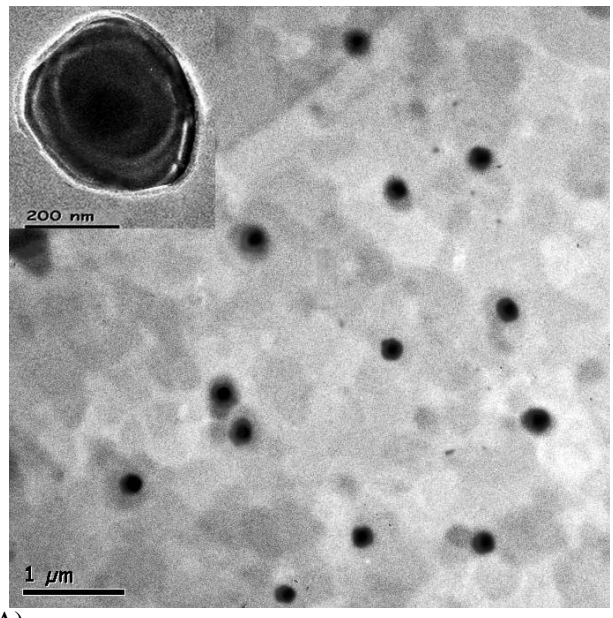

(A)

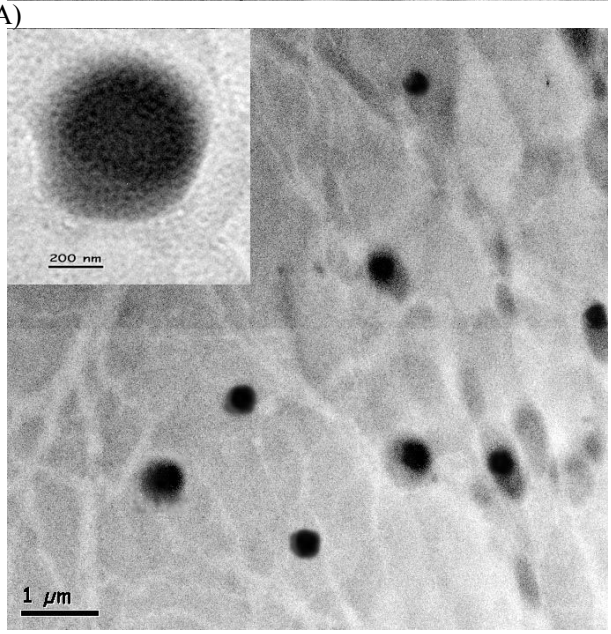

(B)

Fig.1 Transelectron microscopy (TEM) of (A) Lip and (B) CS-Lip.

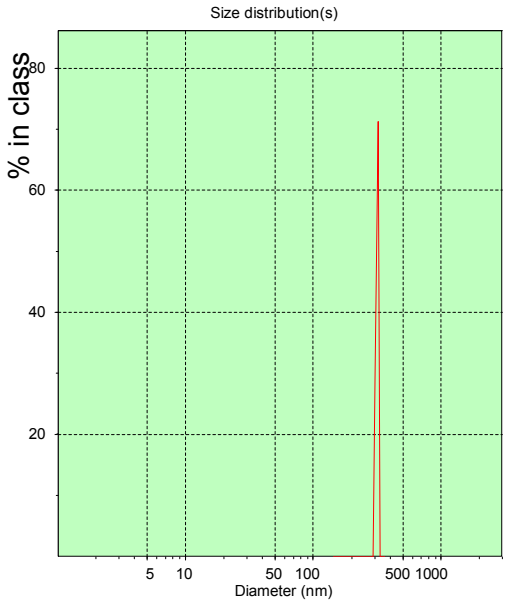

(A)

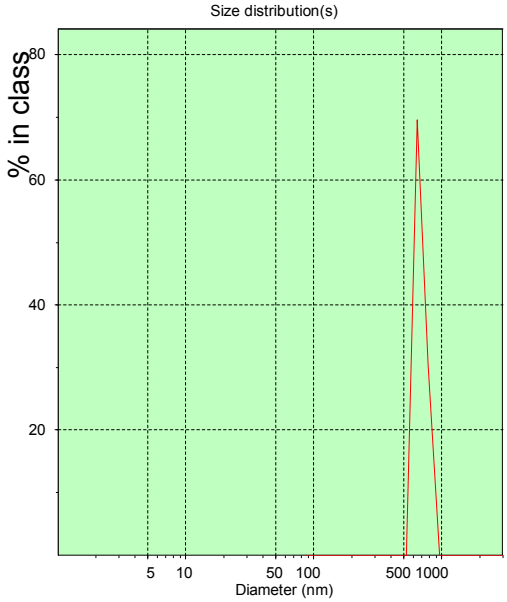

(B)

Fig.2. Polydispersity index of (A) Lip and (B) CS-Lip.

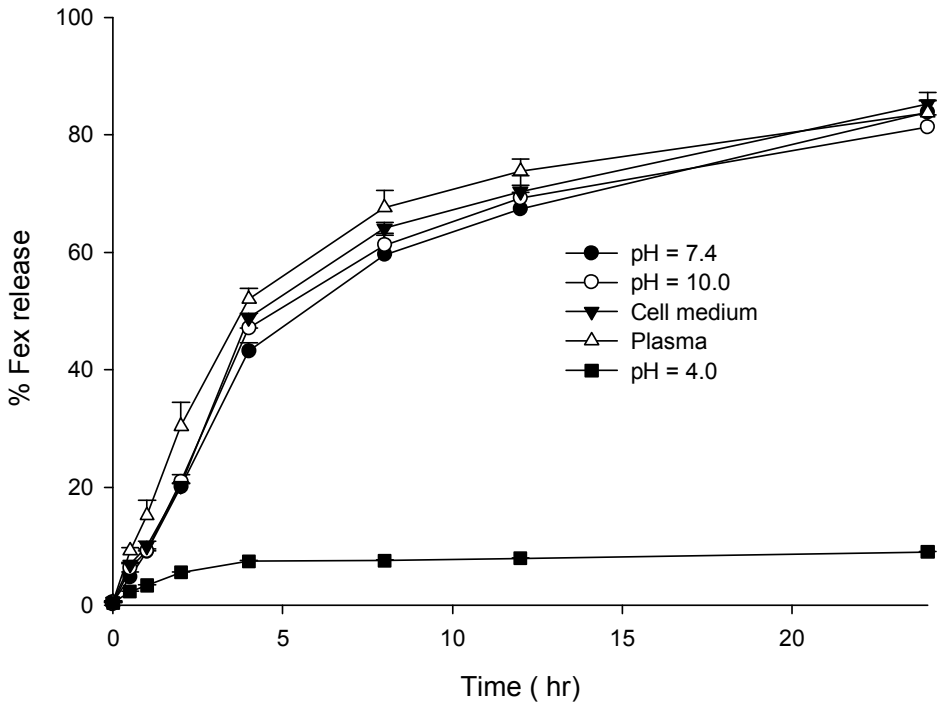

Fig.3(a) In vitro drug release profiles of Lip in different buffer, cell medium and plasma.

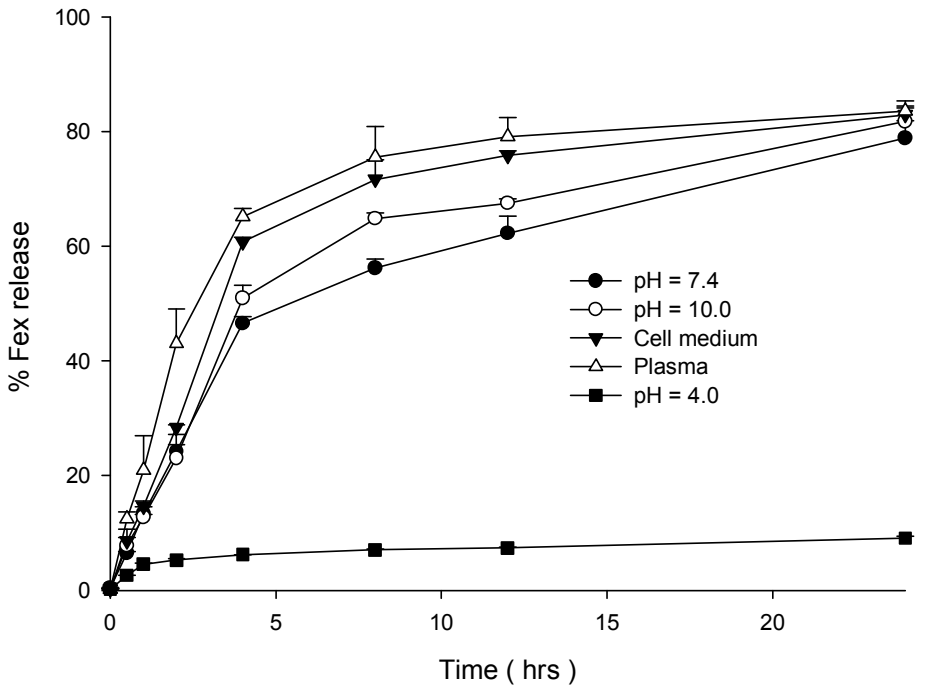

Fig.3(b) In vitro drug release profiles of CS-Lip in different buffer, cell medium and plasma.

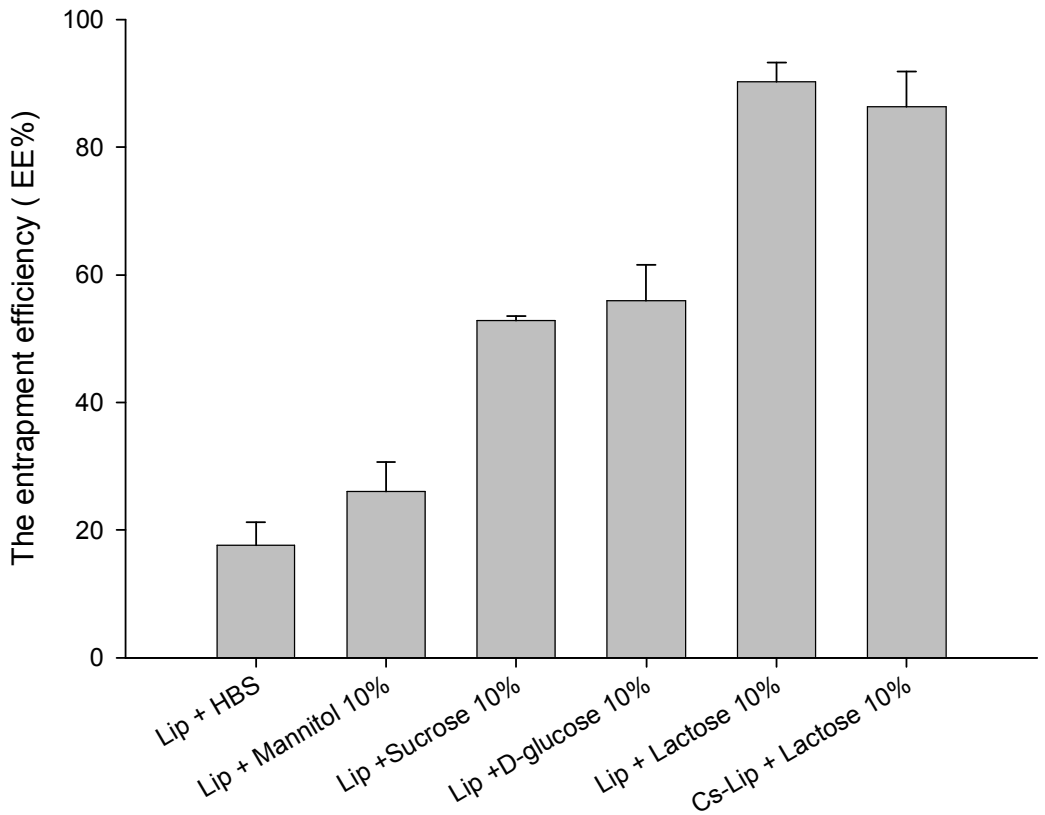

Fig.4 Drug entrapment efficiency Lip and CS-Lip with different stuffing in freeze- dried power.

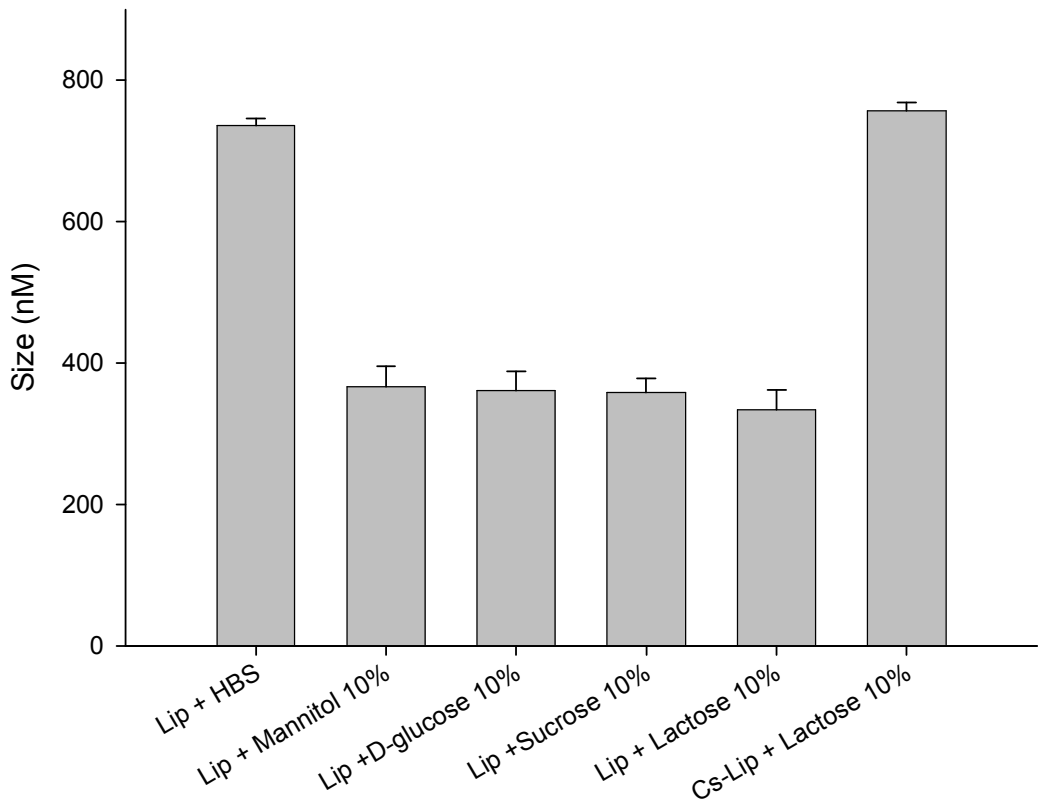

Fig.5 The size of Lip and CS-Lip with different stuffing in freeze- dried power.

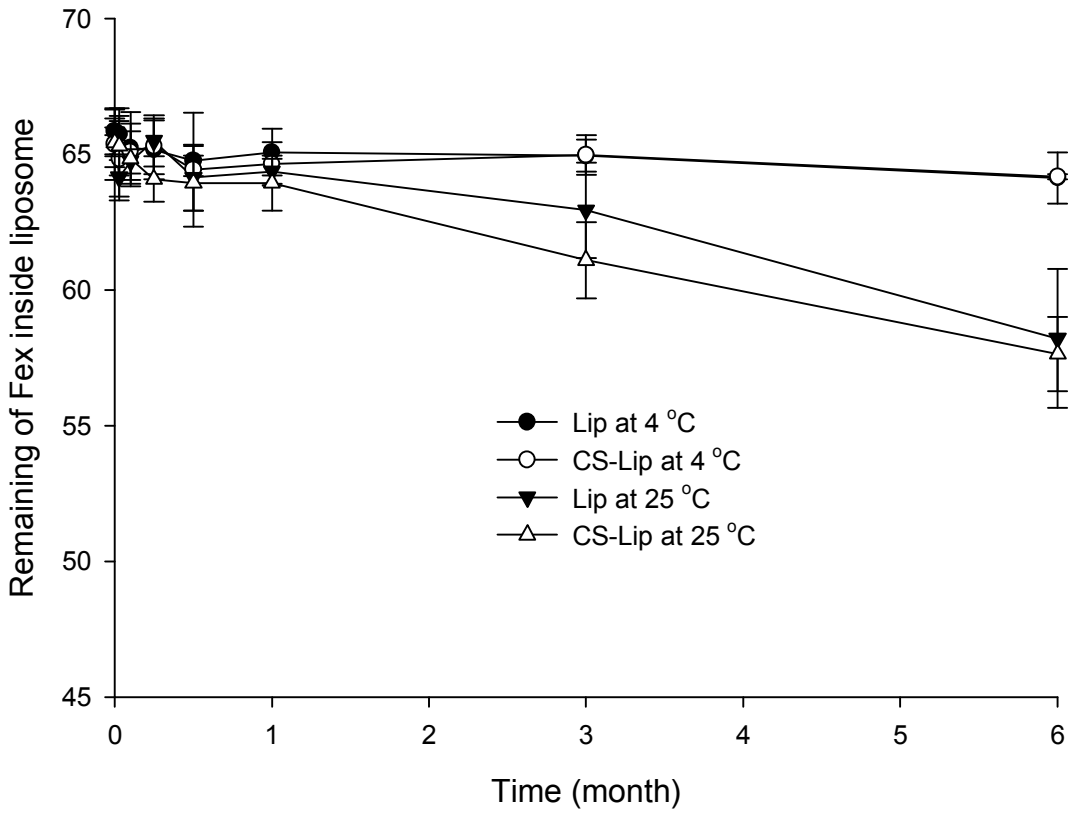

Fig.6 Remaining drug of inside liposome of Fex in Lip and CS-Lip at 4/25℃ in six month stability study.

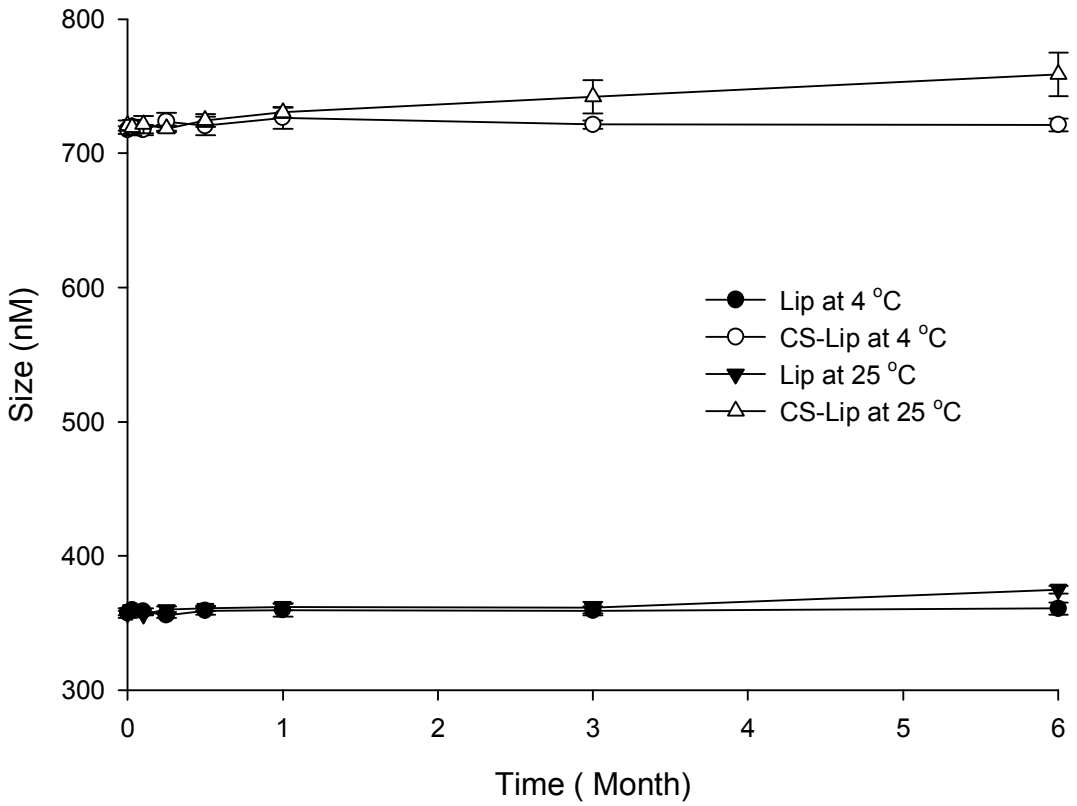

Fig.7 Size of Lip and CS-Lip at 4/25℃ in six month stability study.

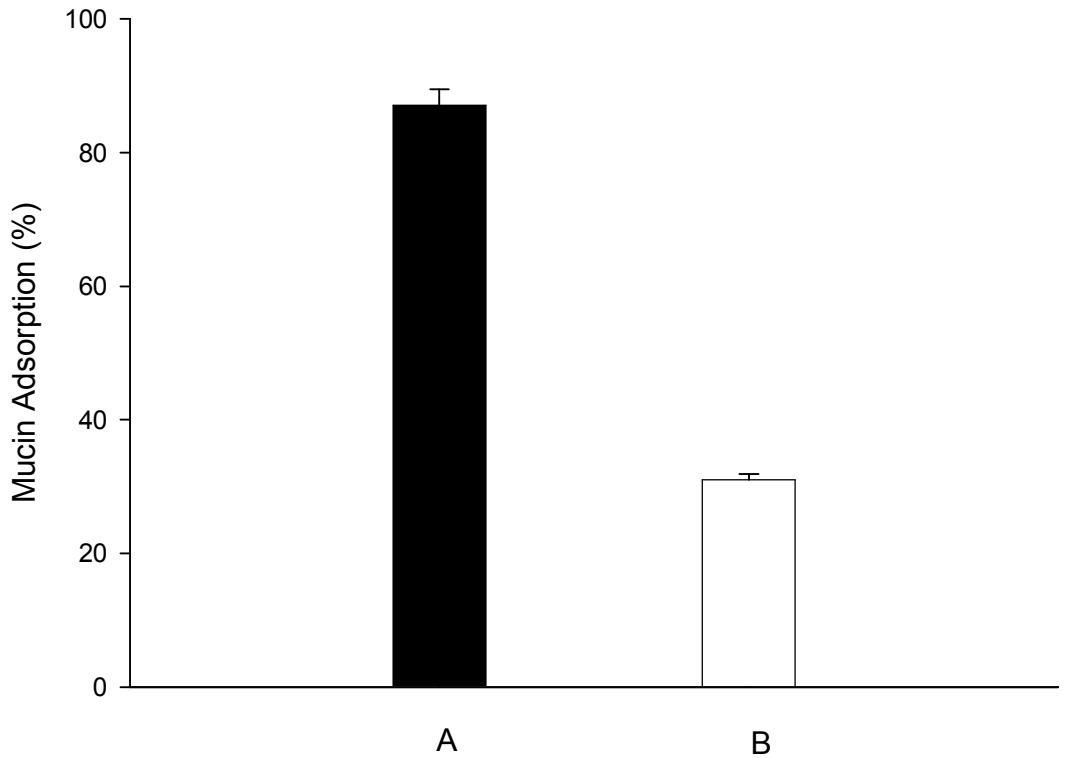

Fig.8 Mucoadhesives of CS-Lip and Lip. A = Mucin (2 mg/ml): CS-Lip (1.45 mg/ml) = 1: 1; B = Mucin (2 mg/ml): Lip (1.45 mg/ml) = 1: 1.

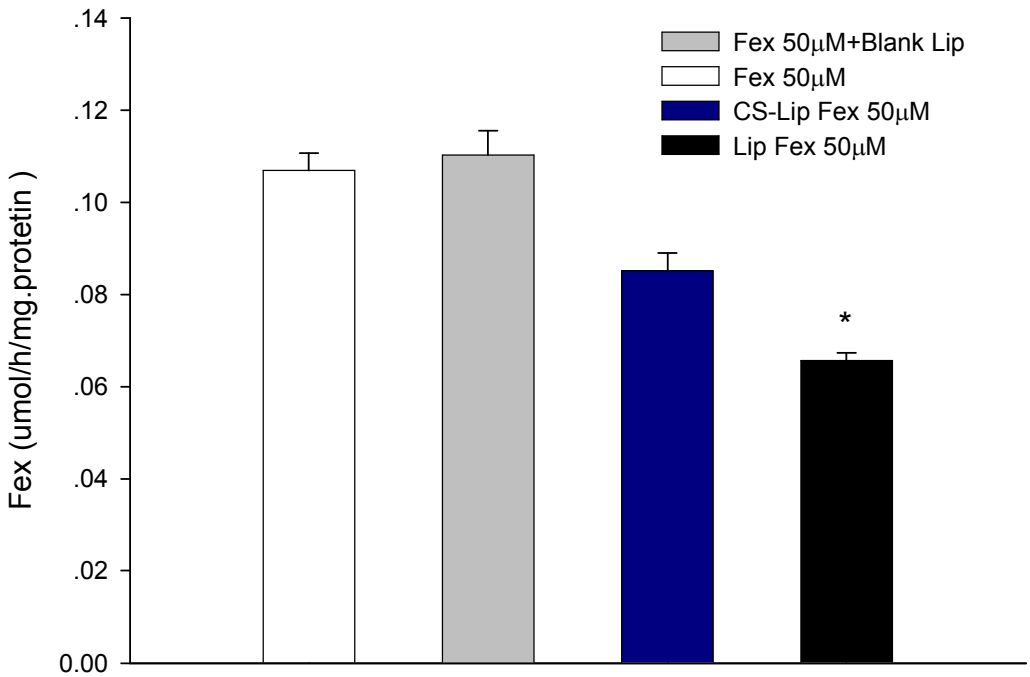

Fig.9 Cellular accumulation of Fex, blank Lip, Lip and CS-Lip in Caco2 cells (mean ± S.D., n = 6). *p < 0.01, compared with the control given Fex alone.

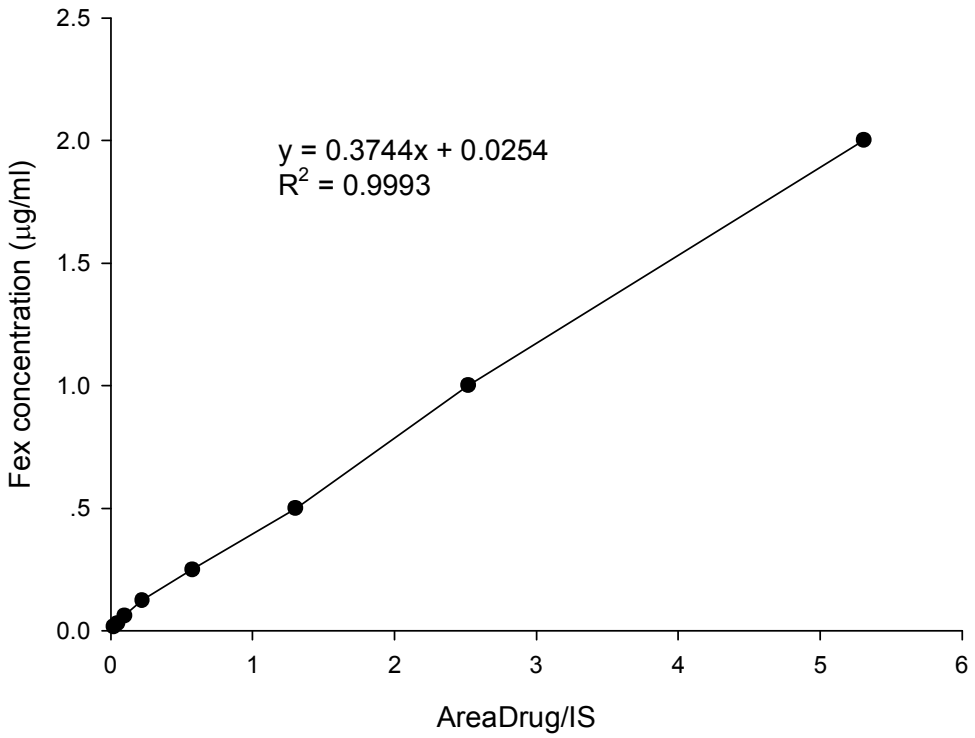

Fig.10 The standard curve of fexofenadine in pharmacokinetics study.

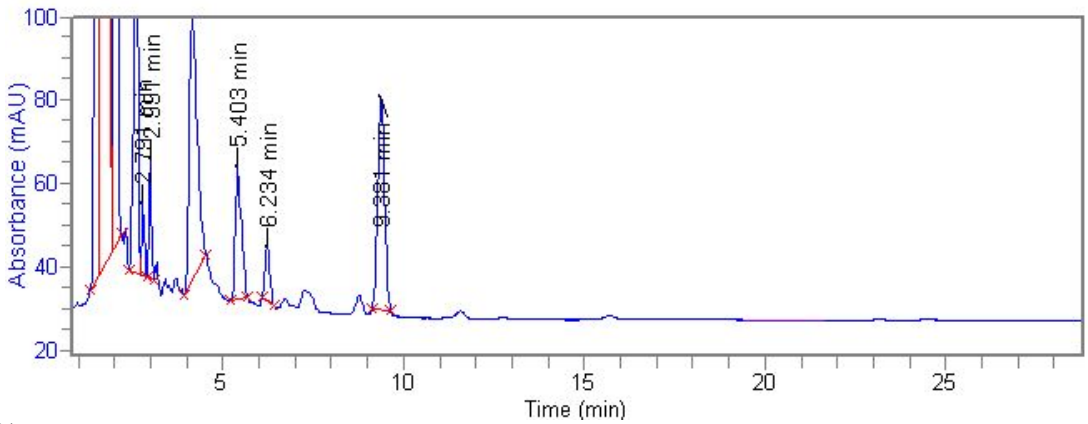

(A)

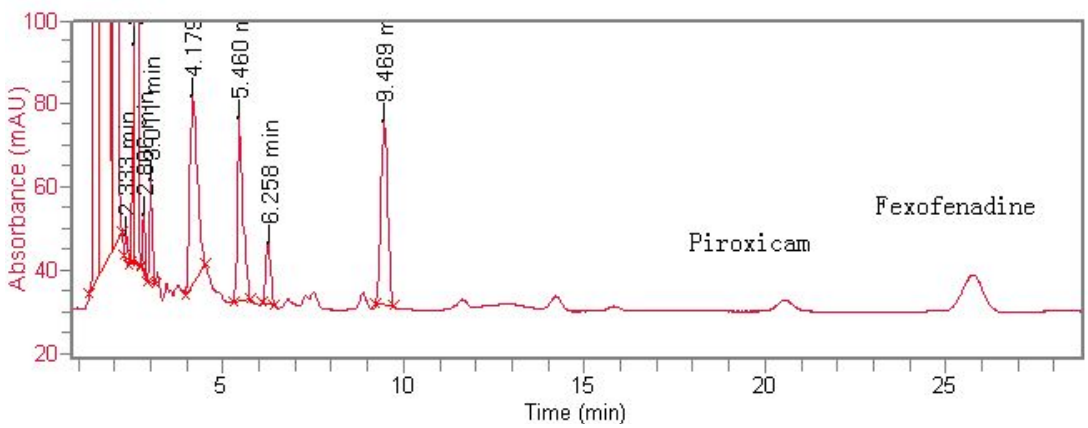

(B)

Fig.11 Two representative chromatograms including an intact blank plasma (A), and a plasma sample supplemented with lower range of fexofenadine and the internal standard piroxican (B).

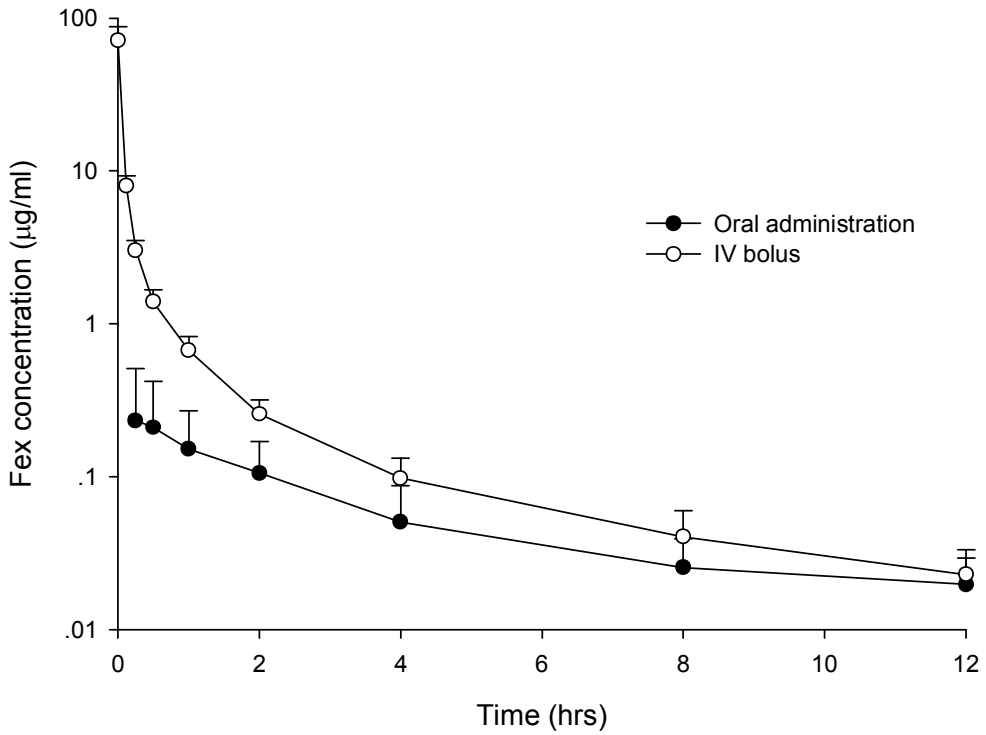

Fig.12(A) The mean plasma concentration–time profiles of Fex after intravenous administration (2.0mg/kg) and oral (10mg/kg).

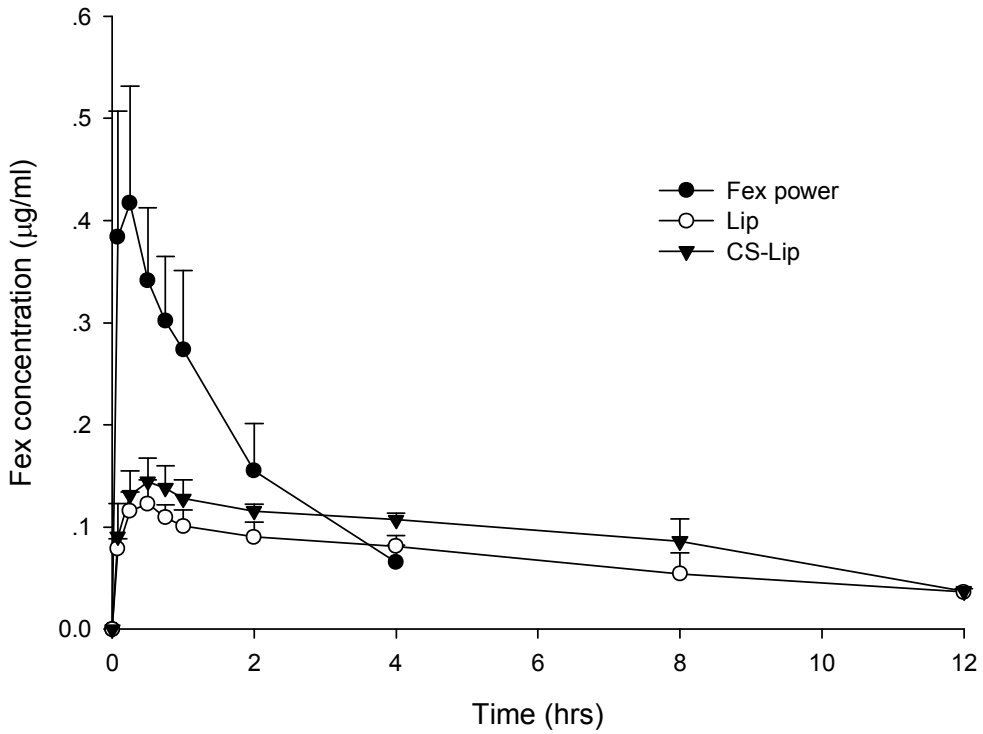

Fig.12 (B) The mean plasma concentration–time profiles of Fex in intranasal delivery of Lip, CS-Lip and Fex power (2.0 mg/kg).

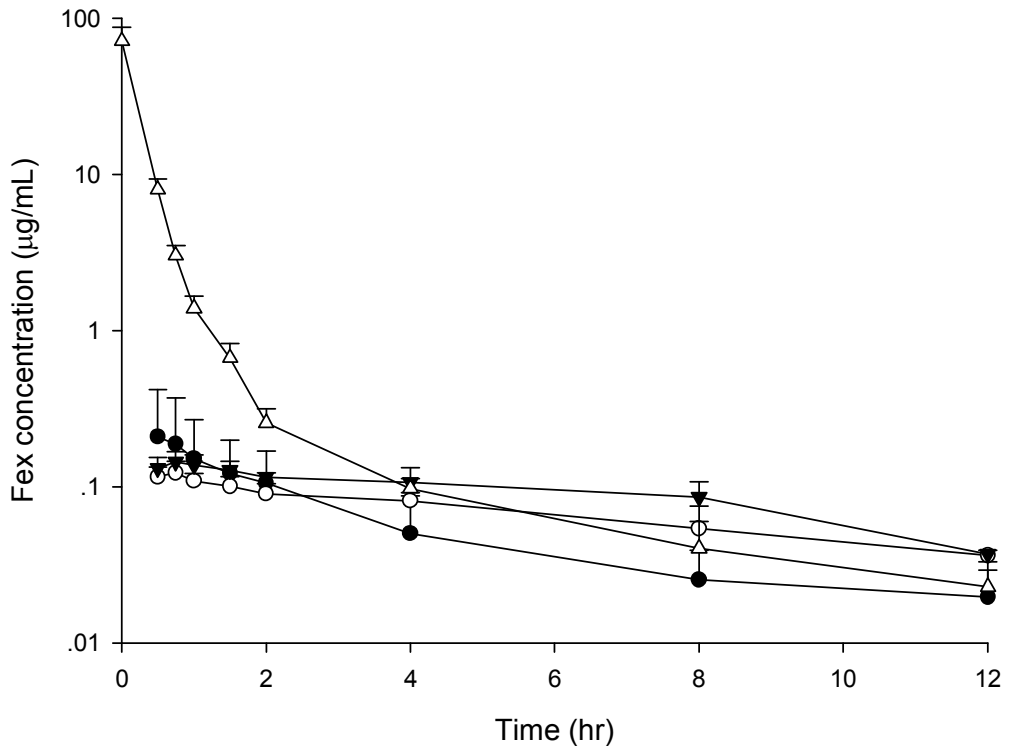

Fig.13 The mean plasma concentration–time profiles of Fex after intravenous administration (5.0mg/kg) -△- , oral administration (10mg/kg) -●-, intranasaladministrationofLip (2.0 mg/kg) -○- and intranasal administration of CS-Lip (2.0 mg/kg) -▼-.

Table 1

Effect of phospholipids race and CS on the encapsulation efficiency (EE%), particle size, polydispersity index (P.I.) and Zeta-potential (ζ) of Lip, each value represents the mean±S.D. (n = 3).

No.	phospholipids race	size (nm)	(mV)	(P.I.)	(EE%)
DPPC:DPPG:cholesterol	(2:1:0.75)	378.6±11.5	-109.7±3.5	0.068±0.015	20.7±1.2
DPPC:DPPG:cholesterol	(4:1:1.56)	371.2±6.7	-108.8±2.1	0.051±0.008	30.5±1.5
DPPC:DPPG:cholesterol	(8:1:2.25)	358.9±5.5	-109.7±5.4	0.035±0.007	65.9±1.4
CS(0.1%)+DPPC:DPPG:Cho	(8:1:2.25)	715.7±14.2	11.83±1.5	0.103±0.016	66.1±1.0

Table 2
Size and remaining drug of inside liposome of Fex in Lip and CS-Lip at 4/25℃ in six month stability study

Storage type	Lip		CS-Lip		Lip		CS-Lip	
Storage condition	4℃				25℃			
Time (Month)	Size(μM)	EE %	Size(μM)	EE %	Size (μM)	EE %	Size (μM)	EE %
0	357.4±1.6	65.8±0.1	717.4±2.8	65.4±1.3	357.6±3.5	65.8±0.9	720.7±3.9	65.4±0.9
0.03	360.1±2.4	65.7±1.0	719.7±5.1	64.8±1.4	359.8±3.8	64.2±0.9	719.3±5.8	65.3±1.1
0.1	359.0±2.4	65.2±1.3	717.4±4.0	65.1±1.0	357±1.3	64.7±0.5	721.4±6.5	64.8±1.0
0.25	356.1±2.2	65.2±1.1	723.4±6.7	65.3±1.0	360.1±2.7	65.5±1.0	718.7±2.5	64.1±0.8
0.5	359.3±2.9	64.7±0.6	720.5±7.1	64.4±2.1	361.1±1.9	64.1±1.2	724.5±4.7	63.9±1.0
1	359.8±5.1	65.1±0.9	726.4±7.9	64.6±0.8	362.1±2.4	64.4±0.5	730.6±4.0	63.9±1.0
3	359.2±3.4	64.9±0.6	721.5±3.1	65.0±0.7	361.5±4.4	62.9±1.8	742.2±12.4	61.1±1.4
6	360.8±4.4	64.1±0.9	721.3±4.8	64.2±0.1	375.0±3.0	58.2±2.6	758.9±16.2	57.6±1.4

Table 3

Pharmacokinetic parameters of fexofenadine after administration in intranasal routes in rats.

	Dose(mg/kg)	C_{max} (ng/mL)	T_{max} (hour)	$T_{1/2}$ (hour)	AUC (ug.h/mL)	BA(%)
IV	5			11.3±6.3	7.97±0.90	
PO	10	0.34±0.29	0.9±0.8	5.3±1.7	0.92±0.28	6.2±2.0
fexofenadine	2	0.42±0.12	0.17±0.1	1.47±0.11	0.75±0.19	25.0±8.0
liposome	2	0.12±0.02*	0.5*	6.61±1.29*	0.71±0.23	24.5±7.5
coating-liposome	2	0.22±0.03*	0.5*	6.84±1.51*	1.04±0.12†	34.7±6.3

All data are expressed the means±standard deviation (n = 4).

* $p < 0.05$ compared with intranasal delivery of fexofenadine power.

† $p < 0.05$ compared with intranasal delivery of nanoliposomes and fexofenadine power.

Chapter 3

Enhanced dissolution and bioavailability of rebamipide via the preparation of organo-clay based drug delivery system

Abstract

This study aimed to improve the dissolution and bioavailability of rebamipide via the oral delivery system using clay-based organic-inorganic hybrid materials. Aminopropyl functionalized magnesium phyllosilicate was prepared by protonation of the interlayer aminopropyl groups of a synthesized organo-functionalized and trioctahedral magnesium phyllosilicate was used to prepare exfoliated cationic organoclay dispersions(AMP-clay) that were subsequently re-assembled in the presence of rebamipide was incorporated into an intercalated layered nanocomposites (Reb-AMPclay). The Reb-AMPclay was synthesized with drug loading efficiency of 55% and its structural characteristics were confirmed by ^{1}H-NMR, FT-IR, XRD, and TEM. Solubility and drug release characteristics of rebamipide from organo-clay was evaluated over the pH range of 2.0 ~ 10.0 and also in the simulated gastric or intestinal fluids. The systemic exposure of rebamipide following an oral administration of Reb-AMPclay was also investigated in rats.. Compared to the untreated powder, the Reb-AMPclay significantly improved the solubility as well as the extent of drug release of rebamipide at low pH, leading to the pH-independent drug release of rebamipide. Particularly, Reb-AMPclay increased the dissolution of rebamipide by approximately 1000 folds in simulated gastric juice, compared to the untreated powder. Furthermore, oral pharmacokinetic study indicated that Reb-AMPclay significantly ($p < 0.05$) enhanced the oral exposure of rebamipide in rats compared to the untreated powder

formulation and a physicalmixture of rebamipide with AMP-clay (Reb-mix-AMPclay). Following an oral administration of Reb-AMPclay (equivalent to 20 mg/kg of rebamipide), the C_{max} and AUC of rebamipide increased by 2.1 and 1.8 folds, T_{max} decrease to 3.0 folds, respectively while there was no significant change in $T_{1/2}$. Rebamipide intercalated organo-clay appeared to be effective to improve the pH-independent dissolution and the bioavailability of rebamipide in rats.

국문초록

세 번째 섹션은 약물 전달에서 nanoparticles의 소설 AMP - Clay 를 제공한다. 이 연구는 점토 기반의 유기-무기 하이브리드 재료를 사용하여 경구 전달 시스템을 통해 rebamipide 의 해산과 생체 이용률을 향상시키기 위해 목표로 하고 있다. Aminopropyl 기능화 마그네슘 phyllosilicate가 phyllosilicate가 이후 rebamipide의 존재에 다시 모였다. 피부 박피를 양이온 organoclay의 분산 (AMP - Clay)를 준비하는 데 사용된 합성 organo 기능화 및 trioctahedral 마그네슘의 층간 aminopropyl 그룹의 protonation에 의해 준비되었고 통합되었다. intercalated nanocomposites 계층 (Reb - AMPclay). Reb - AMPclay 55 %의 약물 로딩 효율 합성되었으며, 그 구조 특성은 ^{1}H - NMR, FT - IR, XRD 및 TEM에 의해 확인되었다. organo - Clay 에서 rebamipide의 용해도 및 약물 릴리스의 특징은 2.0 ~ 10.0의 산도 범위 또한 시뮬레이션 위장이나 창자 체액에서 평가되었다. Reb - AMPclay의 경구투여에 의한 rebamipide의 전신 노출도 rats에서 조사되었다. 치료 분말에 비해 Reb - AMPclay rebamipide는 독립적인 약물 릴리스로 이어지는 용해도뿐만 아니라, 낮은 산도에서의 rebamipide의 약물 릴리스의 범위를 향상시켰다. 특히, Reb - AMPclay는 치료 가루에 비해, 가상 위액에 약 1000 폴드에 의해 rebamipide의 용해를 증가시켰다. 또한, 구두 pharmacokinetic 연구 Reb - AMPclay 은 크게 ($P < 0.05$) 치료 분말 제제 및 AMP - clay (Reb - mix - AMPclay)과 rebamipide의 physicalmixture에 비해 rats에서 rebamipide의 구두 노출 향상된 것을 지적했다. $T_{1/2}$에 상당한 변화가 없는 반면 Reb - AMPclay의 경구투여 (20 mg/kg rebamipide) 이후 rebamipide의 C_{max}와 AUC는 각각, 2.1, 1.8배 증가하였고 T_{max} 가 3.0로 감소했을 때 $t_{1/2}$는 변화가 없었다. Organo -Clay 와 결합한Reb는 산도에 독립적인 용해와 rats에서 rebamipide의 생체 이용률을 향상시키는데 효과적인 것으로 보였다.

1. Introduction

Organo-clays are nanoparticles of layered mineral silicates and in recent years they have attracted much research interest. Silicate clay has been extensively applied for developing high performance materials due to its unique combination of mechanical and thermal properties.[1-7] It is composed of individual microscopic sheets and has a highly layered sandwichlike structure. Each sheet has a thickness of about 1 nm and lateral dimension between 100 to 1000 nm.[8,9] Excess negative charges usually exists on the surface of each sheet since a part of Al^{3+} and Si^{4+} in aluminum-oxygen octahedron and silicon-oxygen tetrahedron of clay crystal cell were replaced by Mg^{2+}. As a matter of fact, hydrated sodium ions and other ions were adsorbed in the gallery space between the sheets through electrostatic adsorption to keep an electrostatic balance. These hydrated ions have the ability easily to exchange with other organic and inorganic ions through cationic exchange process.[10-12]

Organo-clays and polymer-layered nanocomposites have uses in a wide range of applications. Organically modified organoclays, are currently employed in the manufacture of inks, paints, greases and cosmetics to enhance colour retention and rheological properties [13]. Recent studies have also revealed the prospective use of Organo-clays in food packaging products [14,15]. Organo-clay was described the benefits of a grafted as a filler for dental adhesives [16]. Another potential application which is emerging is the controlled release of therapeutic agents [17,18].

Rebamipide, 2-(4-chlorobenzoylamino)-3-[2(1H)- quinolinon-4-yl] propionic acid, is a quinolinonederived gastroprotective agent approved in Korea for the treatment of gastric ulcers, acute gastritis, and exacerbated chronic gastritis.[19–21] The mechanism of its anti-inflammatory and gastroprotective actions involves increased mucus secretion,[22] enhanced generation of endogenous prostaglandin E2 inthegastric mucosa, 3 inhibition of proinflammatory cytokine secretion by immune cells,[23,24] and scavenging of cytokineinduced reactive oxygen species.[25] Although the characteristics of rebamipide in preclinical and clinical area], which is one of key factors to effect on the develop of oral

dosage form at the initial stage. rebamipide is poorly soluble in water and ether and poorly absorbed into the systemic circulation; because of its low solubility and low permeability, it is considered a Class IV agent according to the US Food and Drug Administration (FDA) Biopharmaceutics Classification System. [26]Therefore, rebamipide absence systemic activity at the target organ of the stomach.[27]. In order to develop the safe formulation that can improve the absorption of rebamipide, we have compared the different excipients as an absorption enhancer. We have found that AMP-Clay is a promising absorption enhancer and better than other excipients in terms of the absorption improving ability.

In particular, Organo-clay is being developed as an efficient method to disperse poorly water soluble drugs in polymers for enhanced delivery. we report the synthesis and characterization of a range of host–guest layered nanocomposites based on the intercalation of rebamipide, within the interlayer spaces of an aminopropyl -functionalized magnesium phyllosilicate (approximate unit cell composition, $[H_2N(CH_2)_3]_8Mg_6Si_8O_{16}(OH)_4$). Mg-AMP clay show that these materials exhibit controlled release of the rebamipide molecules under neutral or acidic conditions, and that these vivo profiles can be significantly increased by co-intercalation of anionic macromolecules AMP-clay. Our results suggest that intercalation materials prepared by the reassembly of exfoliated aminopropyl- functionalized magnesium phyllosilicates could have uses in a wide range of health care applications.

2. Materials and method

2.1 Materials

Rebamipide, furosemide and 3-aminopropyltriethoxysilane (APTES, 99%) were obtained from Sigma Chemical Co. (St.Louis, MO, USA). Magnesium chloride hexahydrate (98.0%), isopropanol and triethylamine was obtained from Junsei Chemical Co. (Tokyo, Japan). Acetonitrile, methanol, ethanol, tert-butyl methylether and acetic acidwere obtained from Merck Co. (Darmstadt, Germany). All other chemicals were of analytical gradeand all solvents were of HPLC grade.

Caco-2 (human colon carcinoma cell) and A549 (lung epithelial cancer cell) was obtained form Koreacelllinebank (Seoul, Korea). MEM medium, Trypsin 0.25% (1×) solution, Penicillin- streptomycin solution (10,000 units/ml penicillin 10,000 μg/ml streptomycin) and Fetal Bovine Serum (FBS) were obtain from the rmos cientific company. 4% capric sulfate and BCA solution were obtain from novagen company.

2.2 Formulation Design and Procedures

2.2.1 Screening the excipient as absorption enhancer

Several mucoadhesive polymers have been used as absorption promoters, including the methyl cellulose, lactose, chitosan, carbopol, sodium alginate, HPMC 4000, PEG 6000, AMP-Clay. The effect excipients on the solubility of rebamipide was investigated. 100 mg of rebamipide were added to 10 ml buffer (pH 2.0, 6.8, 10.0), distilled water, SGF and SIF in test tubes, with 0.5% excipients (expect with 1% carbopol) vortexed for 5 min and shaken at 37 °C (Shaking water bath KMC12055 WI) for 72 h. Resultant samples containing undissolved AMP clay suspended in the test medium were centrifuged at 14500 rpm for 30 min and the clear supernatants obtained, suitably diluted with methanol and 10 μl of aliquots were injected directly into the HPLC system (Perkin Elmer Series 200; Waltham, MA, USA). The octadecylsilane column (Gemini C18, 4.6mm×150mm, 5μm; Phenomenex, Torrance, CA, USA) was eluted with the mobile phase consisting of 1.6% aceticacid: acetonitrile (70: 30, v/v%,) at a flow rate of 1.0 ml/min. The UV detector set at 229nm. The calibration curve from the standard samples was linear over the concentration range of 0.01–500 μg/ml. The detection limit of Reb was 0.01μg/ml.

2.2.2 Screening the optimal original clay by cytotoxicity study

Several original clay have been used as screening for optimal clay by cytotoxicity, including Mg^{2+}, Ca^{2+}, Al^{3+}, Co^{2+}, Fe^{3+}, Mn^{2+}, Sn^{2+}, Zn^{2+} (APTES)-Clay. The cells-A549 were seeded into 96-well plates at a density of 5×10^{3}cells· $well^{-1}$. After 24 h incubation at 37°C, various concentrations of differention clay with (0.1~1000μg/ml) were added to the cells and the plates were incubated for 48/72 hours. At the end of incubation, cell viability was determined by a modified colorimetric assay using 3-(4,5-dimethylthiazol-2-yl)-2,5-diphenyl- tetrazolium bromide (MTT).[28] Briefly, medium with the drug was removed and replaced by fresh medium (200 μl· $well^{-1}$) containing 0.1 mg/ml MTT. After 4 h incubation

at 37°C, the medium was aspirated and the cells were extracted with 100μl· well^{-1} of DMSO. The concentration of the extracted formazan metabolite was determined by the measurement of absorbance at 550 nm in a 96-well plate reader. The 50% cytotoxic concentration (CC50) was determined from the nonlinear regression of a dose-response curve using Sigma Plot 9.0 (Systat Software Inc., PointRichmond, CA).

2.3 Preparation of Reb-AMP clay

Aminopropyl-functionalized magnesium phyllosilicate was prepared by Stephen Mann reported methods[29,30]. In brief, magnesium chloride (3.07g,) was dissolved in ethanol (93.2 ml) and 3-aminopropyltriethoxysilane (4.75 ml) added dropwise with rapid stirring. A white precipitate formed almost immediately and was stirred overnight. The resulting product was isolated by centrifugation and washed in ethanol (50 ml), before drying in air at 40℃. ^{1}H-NMR, TEM, XRD, and FT-IR spectroscopy confirmed the characteristic disordered lamellar structure typical of this class of synthetic materials. An aqueous solution of the sodium salt of rebamipide (1 ml, 10 mg/ml) was added slowly to the exfoliated organoclay suspension (1 ml, 10 mg/ml). The product, which precipitated immediately, was left to age overnight and then collected by centrifugation, and dried at room temperature in air.

2.4 Determination of entrapment efficiency

The entrapment efficiency (EE,%) of rebamipide in the AMP-clay was calculated by dissolving AMP-clay equivalent to 20mg Reb-nanoclay (A) in a suitable quantity of methanol. Sonicate for 10 min. the sample was centrifuging at a speed of 25000 × g for 30 min at 4℃.The supernatant liquor was diluted with methanol for ten times and analyzing (B) by HPLC (Perkin Elmer Series 200; Waltham, MA, USA) at the 225 nm, The octadecylsilane column (Gemini C18, 4.6mm×150mm, 5μm; Phenomenex, Torrance, CA, USA) was eluted with the mobile phase consisting of 1.6% acetic acid : acetonitrile (70: 30, v/v%,) at a flow rate of 1.0ml/min. The EE,% was then calculated using Eq.(1).

Experiments were performed in triplicate.

EE%= [B /A×100] Eq.(1)

2.5 Determination of Solubility

Rebamipide, Reb-AMPclay, physicalmixture of Reb-mix-AMPclay equivalent to 10 mg of rebamipide were added to 10mL buffer (pH 2.0, 6.8, 10.0), distilled water, SGF and SIF in test tubes, vortexed for 5 min and shaken at 37°C (Shaking water bath KMC12055 WI) for 72 h. Resultant samples containing undissolved AMP-clay suspended in the test medium were centrifuged at 25000g 30 min and the clear supernatants obtained, suitably diluted with methanol and analyzed by HPLC and 10 μl of aliquots were injected directly into the HPLC system (Perkin Elmer Series 200; Waltham, MA, USA). The octadecylsilane column (Gemini C18, 4.6mm×150mm, 5μm; Phenomenex, Torrance, CA, USA).was eluted with the mobile phase consisting of 1.6% acetic acid :acetonitrile (70: 30, v/v%,) at a flow rate of 1.0mL/min. The UV detector set at 229 nm.

2.6 *In-Vitro* Rebamipide Release

Drug release tests of rebamipide power and Reb-AMPclay (equivalent to 10 mg rebamipide) were performed in 10 ml buffer (pH 2.0, 6.8, 10.0), distilled water, SGF and SIF (37°C). as the dissolution medium using Shaking water bath (Shinseang Instrument Co., SouthKorea). Buffer (pH=2.0) prepare of 50 ml of potassium chloride (0.1M) and 10.6 ml volume of hydrochloric acid (0.1M). Mix and adhust the final volume to 100 ml with deionized water. Buffer (pH=6.8) prepare of 51 ml Solium phosphate monobasic (0.1M) and 49 ml dibasic solutions(0.1M) and final volume to 200 ml with deionized water. Buffer (pH=10.0) prepare of 27.5 ml sodium carbonate (0.1M) and 22.5 ml sodium bicarbonate (0.1M) solutions and final volume to 200 ml with deionized water. Adjust the final pH using a sensitive pH meter. The artificial gastric fluid (pH= 2.0) was prepared by

dissolving 2 grams of NaCl in deionized water (Direct Q3 Water Purification System) and adding 7 ml of HCl (1N) to a volume of 1L using deionized water. The artificial intestinal fluid (pH=7.4) was prepared by adding 6.8 grams KH_2PO_4 and 10 grams pancreatin, 0.2M NaOH adjust pH=7.4 in a volume of 1L. At the specified times on 0, 0.5, 1, 4, 12, 24 hour, 200 μl samples were withdrawn, centrifuged and assayed for rebamipide content by HPLC. Equivalent amount of fresh medium pre-warmed to 37°C was replaced after each sampling. HPLC methodis (Perkin Elmer Series 200; Waltham, MA, USA) at the 229 nm, The octadecylsilane column (Gemini C18, 4.6mm×150mm, 5μm; Phenomenex, Torrance, CA, USA) was eluted with the mobile phase consisting of 1.6% acetic acid : acetonitrile (70:30, v/v%,) at a flow rate of 1.0 ml/min.

2.7 *In-vitro* Stability and long-term storage study

Drug release stability tests of rebamipide power, Reb-mix-AMPclay and Reb-AMPclay (equivalent to 0.8 μg/mL rebamipide in SGF; 20μg/ml rebamipide in SIF and D.W) were performed in 10 ml distilled water, SGF and SIF (37°C) as the dissolution medium using Shaking water bath (Shinseang Instrument Co., SouthKorea). At the specified times on 0, 0.5, 1, 4, 12, 24 hour, 200μl samples were with drawn, centrifuged and assayed for rebamipide content by HPLC. Equivalent amount of fresh medium pre-warmed to 37°C was replaced after each sampling. HPLC methodis (Perkin Elmer Series 200; Waltham, MA, USA) at the 229 nm, The octadecylsilane column (Gemini C18, 4.6mm×150mm, 5μm; Phenomenex, Torrance, CA, USA) was eluted with the mobile phase consisting of 1.6% acetic acid :acetonitrile (70:30, v/v%,) at a flow rate of 1.0 ml/min. Samples were stored at 4℃ and 25℃for 4 months and collected at 0, 0.25, 0.5, 1, 2, 4 months. The sample added 1 ml methanol (pH=10.0) to measuret he entrapment efficiency. Briefy, The sample added in methanol (1mg/ml). Sonicate for 10 min. the sample was centrifuging at a speed of 25000 × g for 30 min at 4℃.The supernatant liquor was diluted with methanol for fifty times and analyzing by HPLC.

2.8 Cell uptake study in Caco-2 cells

Caco-2 cell is comely used for the evaluation of drug transport across the gas-intestinal membrane, Furthermore, muscin synthesis was proved in Caco-2 cells [31,32]. Cell were seeded into 6-well plate at a density of 5×10^5cells per well. At one week post-seeding, cells were incubated with drug solution, rebamipide. Reb-AMPclay and Reb-mix-AMPclay at 20μM, At the end of 2 hour incubation ,drug solution was removed and the cells were washed three times with ice-cold phosphate- buffered saline. After the cell lysis, cells were harvested and sonicated for 5 min. Acetonitrile was added to the cell lysate, vortexed vigorously and centrifuged for 10 min at 20000g. The supernatant was collected and the drug concentration of each sample was determined by HPLC, 10 μl of aliquots were injected directly into the HPLC system (Perkin Elmer Series 200; Waltham, MA, USA). The octadecylsilane column (Gemini C18, 4.6mm×150mm, 5μm; Phenomenex, Torrance, CA, USA) was eluted with the mobile phase consisting of 1.6% acetic acid : acetonitrile (73: 27, v/v%,) at a flow rate of 1.0 ml/min. a fluorescence detector as excitation 330 nm and emission at 370 nm. The protein amount of each sample was also determined by Bradford protein assay.

2.9 Pharmacokinetic Study

2.9.1 Animal

Male Sprague–Dawley rats (245–250g) were purchased from Samtako Bio Co. (Osan,Korea). All animal studies were performed in accordance with the “Guiding Principles in the Use of Animals in Toxicology” adopted by the Society of Toxicology (USA). Rats were divided into two groups (n = 6 per each group). Group1: 20 mg/kg of rebamipide (p.o.), Groups 2: Reb-AMPclay equivalent to 20mg/kg of Reb (p.o.). Groups 3: Reb-mix-AMPclay equivalent to 20mg/kg of rebamipide (p.o.). A single dose of approximately 20 mg/kg rebamipide [33]. rebamipide, Reb-AMPclay and Reb-mix-AMPclay were suspended in methycellulose (0.5 %) oral administration. Blood samples were collected

from the femoral artery at 0, 0.25, 0.5, 0.75, 1, 1.5, 2, 4, 8, 12, 24 h following an oral administration. Blood samples were centrifuged and the obtained plasma was stored at −70 ◦C until analyzed.

2.9.2 HPLC assay

Plasma concentration of rebamipide was determined by the HPLC method described as follows. In brief, 10μL of furosemide (40μg/ml) as an internal standard was added to 90μl of each plasma sample and then the mixture was vortexed for 10 min (Vortex Genie-2, VWR Scientific, West Chester, PA, USA), then the mixture was deproteinized by adding 100μl of acetonitrile. After centrifugation of the samples at 25,000×*g* at 4 ◦C for 10min (MICRO17TR, Micro high speed centrifuge, S Korea), the supernatant was removed, and then 50μl of aliquots were injected directly into the HPLC system (Perkin Elmer Series 200; Waltham, MA, USA). The octadecylsilane column (Gemini C18, 4.6mm× 150mm, 5μm; Phenomenex, Torrance,CA,USA) The octadecylsilane column (Gemini C18, 4.6mm×150mm, 5μm; Phenomenex, Torrance, CA, USA) was eluted with the mobile phase consisting of 5.5 mM NaH_2PO_4 with 1% aceticacid: acetonitrile(73: 27 v/v%,) at a flow rate of 1.0 ml/min. The fluorescence detector set at Ex. 330 nm and Em. 370 nm.. The calibration curve from the standard samples was linear over the concentration range of 15–500 ng/ml. The detection limit of rebamipide was 15 ng/ml.

2.9.3 Pharmacokinetic data analysis

Noncompartmental pharmacokinetic analysis was performed by using Kinetica version 5.0 (Thermo Fisher Scientific Inc., Waltham, MA). The area under the plasma concentration–time curve (AUC) was calculated using the linear trapezoidal method. The maximum plasma concentration (C_{max}) and the time to reach the maximum plasma concentration (T_{max}) were observed values from the experimental data. The elimination rate constant (K_{el}) was estimated by regression analysis from the slope of the line of best fit, and the half-life ($T_{1/2}$) of the drug was obtained by $0.693/K_{el}$. Total plasma clearance (CL)

was calculated by Dose/AUC. Additional estimated parameter using noncompartmental pharmacokinetic analysis was the volume of distribution (V_{dss}). The relative bioavailability (R.B.) of rebamipide was estimated by $AUC_{rebamipide\ -\ AMP\ clay}/AUC_{rebamipide} \times 100$.

2.10 Statistical analysis

All mean values were presented with their standard deviation (mean±S.D.). Statistical analysis was conducted using a one-way ANOVA followed by a posteriori testing with Dunnett correction. A p value less than 0.05 was considered statistically significant.

3. Results and discuss

3.1 Formulation Design and Procedures

3.1.1 Screening the excipient as absorption enhancer

Several polymers have been used as absorption promoters, including the methyl cellulose, lactose, chitosan, carbopol, sodium alginate, HPMC 4000, PEG 6000, AMP-Clay. The effect excipients on the solubility of rebamipide was investigated. 10 mg of rebamipide were added to 10ml buffer (pH 2.0, 6.8, 10.0), distilled water, SGF and SIF in test tubes, with 0.5% excipients (expect with 1% carbopol), Tab.1. introduce that AMP-clay have strong promoter in rebamipide solubility. Furthermore, chitosan and sodium alginate also have significant increase the solubility of rebamipide in SGF or SIF, basic on the solubility of rebamipide with different excipients, we found the AMP-clay as an optimal absorption promoter in rebamipide formulation development.

3.1.2 Screening the optimal original clay by cytotoxicity study

The potential toxicity of synthesized organoclays was evaluated using cultured cancer cells from lung organs at various concentrations in terms of cell viability, membrane damage, and apoptosis. Because organoclays have attracted much attention as drug delivery nanocarriers for biological purposes, the assessment of their potential toxicity should be critical to expanding their application to the development of effective drug delivery systems. Several original clay have been used as screening for optimal clay by cytotoxicity, including Mg^{2+}, Ca^{2+}, Al^{3+}, Co^{2+}, Fe^{3+}, Mn^{2+}, Sn^{2+}, Zn^{2+} (APTES) clay. Origina lclays cytotoxicity was determined in A549 Cells were seeded into 96-well plates at a density of 5× 103 cells · well-1. After 48/72 h incubation at 37°C. As shown in Fig.1a the effects of organoclays on cell viability and proliferation were measured using the MTT assay, which is based on the reduction of the yellow tetrazolium salt MTT by metabolically active cells, resulting in purple formazan crystals. Menadione showed positive toxic control in cell

viability for the entire cell lines tested, over the concentration range of 10-1000 μg/mL. In the case of A549 cells, Compare for the Zn^{2+}, Co^{2+}, Mn^{2+} organo-clays have higher end to block cell viability, the Mg^{2+}, Sn^{2+}, $Fe^{3+}$and Al^{3+} organo-clay display low cytotoxicity. In addition, the cytotoxicity of the organoclays was time-dependent and maintained a high toxicity as the incubation time increased up to 48/72 h (Fig.1b). These results suggested that Mg^{2+}, Sn^{2+}, $Fe^{3+}$and Al^{3+}organo-clays should have little toxicity on the proliferation or viability of cells. Base on the sigmal 9.0 data analysis, we chose Mg^{2+} organo-clay (AMP-clay) as optimal candidate in drug delivery system[34].

3.2 Preparation of Mg-AMP clay, and determination of drug encapture effection

3.2.1 Synthesis of AMP clay

Aminopropyl-functionalized magnesium phyllosilicate was readily prepared by co-condensation in an ethanolic solution containing magnesium chloride and 3-aminopropyltriethoxysilane. The as-synthesized clay consisted of a disordered talclike 2 : 1 trioctahedral smectite structure with a central brucite octahedral sheet overlaid on both sides with a tetrahedral silicate network comprising covalently linked uncharged aminopropyl functionalities. The organoclay was subsequently delaminated in water by protonation of the amino side chains to produce clear suspensions of micrometer-sized exfoliated sheets that could be restacked spontaneously into a bulk phase by addition of anionic guest molecules such as Reb and AMP-clay. Corresponding ^{1}H-NMR measurements were performed to identify the structures of AMP clay and AMP clay modified rebamipide which were dissolved in D_2O at a concentration of 10 mg/ml. The NMR spectra were recorded on a spectrometer (Advance 400 model, Bruker, Germany) at room temperature. FT-IR spectra of the products were obtained on IR-grade potassium bromide (KBr) pellet (NICOLET 6700, Thermoscientific, USA). X-ray diffraction (XRD) patterns were obtained on a X-ray diffractometer (X'Pert PRO, PANalytical B.V.) with Cu Kα radiation at 20mA

and 40 kV. Powder samples were pressed onto glass X-ray sample holder. Diffraction patterns were recorded between 3° and 70° (2θ) with a step size of 0.05° and scanning speed of 2°/min. Transmission electron microscopy (TEM, TECNAI20, EEI, Netherland) imaging were obtained on a bright field emission microscope with Lab 6 electron gun and an accelerating voltage of 200 kV.

3.2.2 Structure of AMP clay modified rebamipide.

The typical IR absorption bands of AMP-clay were depicted in Fig.2.c, which showed NH_2 stretching (3600~3200cm^{-1}), aliphatic CH_2 stretching (2950~2850cm^{-1}), Si-O-Sistretching (1120cm^{-1}), and Mg-O-Sibending (670cm^{-1}) respectively. In the FT-IR spectrum for the AMP-clay modified rebamipide(Fig 2a), the acid carbonyl(C=O) band was disappeared and the two different amide C=O bands were newly appeared on the 1680 and 1640cm^{-1} in solid state (KBrpellet). It means that the carboxyl group of rebamipide crystal dispersed in water reacted with the amine group in the exfoliated AMP clay, as a result, the formation of the AMP modified rebamipide was identified. And IR absorption bands of AMP-clay with NH_2 stretching (3600~3200cm^{-1}) band which might come from the unreacted AMP-clay were also shown in Fig. 2a. In the Fig 2c, microcracks in rebamipide crystal region and the laminated & delaminated AMP-clays were shown, and big rod-like crystals of rebamipide have very thin outer layer (top left inset of Fig. 2c that means the crystal might be wrapped with exfoliated AMP-clay[35,36]. In this aqueous modification process, there are restacking of the exfoliated AMP-clay which results in re-lamination of AMP-clays, and lots of cracks on rebamipide crystals were produced and they were wrapped with delaminated AMP-clays. So exfoliated AMP-clay moiety between cracks in rebamipide crystal were also shown in a TEM image(Fig 3 d). The crystals covered with the small amount of exfoliated AMP-clay increased the solubility of the drug in water up to 510.67 μg/ml from 23.91 μg/ml. So in the Fig.4 b, the ^{1}H-NMR spectrum of rebamipide has lower signal to noise ratio compared to that of the modified drug due to its poor

solubility. Fig 4 b, c, the numbered peaks are associated with aliphatic CH, CH_2 and aromatic CH in the rebamipide structure. The ^{1}H-NMR spectrum of AMP-clay modified rebamipide shows relatively weak peaks for AMP clay(Fig. 4) and strong drug peaks which coincided with the results in TEM analysis in Fig.3. In the XRD patterns(Fig.5), the smectite reflection (d_{060}=1.57Å) of AMP clay was shown in that of the modified drug that means the structural framework of the AMP-clays was retained the during the modification. But the interlayer reflection (d_{001}=14.8Å) was decreased because of the exfoliation of AMP-clay[37]. The (020) reflection of modified drug has same intense as the AMP-clay does.

3.3 In-Vitro Rebamipide Release, Solubility and Stability

In vitro study indicated the co-intercalation of rebamipide and AMP anionic macromolecules resulted in significant changes in the drug release profiles into buffer pH 2.0, 6.8, 10.0, distilled water, SGF and SIF (Fig.6). The rebamipide displayed clear pH dependency with aqueous buffers in the scope of pH from 2.0 to 10.0. Compared to the untreated powder, the Reb-AMPclay significantly improved dissolution as well as the extent of drug release at low pH. Particularly, the dissolution of rebamipide increased ($p < 0.05$) by 1006.3 and 2.3 fold in simulated gastric and intestinal fluid compared to rebamipide. It was observed that the enhancement ($p < 0.05$) in solubility of rebamipide were 21.4, 1097.9, 8.16, 1006.3 and 2.3 fold at distill water, buffer solution (pH=2.0, 6.8,) and simulated gastric or intestinal fluid compared to rebamipide alone(Tab.2). But, compare for the rebamipide power in buffer solution (pH=10.0), Reb-AMPclay solubility decrease 5.2 fold. (Figs.6b-d) represent the drug release profiles of rebamipide at pH 2.0, 6.8 and 10.0 buffer. As it was expected, the pH value of the release medium influenced the kinetic profile of rebamipide dissolution. The fast first order dissolution at pH 6.8 and 10.0 indicates that the drug release is determined by the intrinsic dissolution of rebamipide in neutral, alkaline medium, while at pH 2.0 and SGF the extent and rate of drug release is influenced by acidic medium. Whereas co-intercalation of AMP-clay increased the

dissolution rate of rebamipide in pH 2.0 and SGF, extraction of the drug from organo-clay composite was profile in which the dominant mode of dissolution was from the interlayer spaces rather than Reb power alone. The results suggested that rebamipide molecules remain strongly bound to the interlayer aminopropyl groups in the presence of AMP-clay, and that the dissolution rate is diffusion increased by pH associated with rebamipide is co-intercalated clay polymers. In contrast, rebamipide molecules appear to be low dissolution in acidic medium and distill water. It was displayed clear that the dissolution of rebamipide can be affected by high pH dependency and ions of aqueous buffers.

Compared to the rebamipide power, the solubility of rebamipide significant difference was found on co-intercalation AMP-clay in buffer (pH 2.0, 6.8, 10.0), distilled water, SGF and SIF. However, the difference factors indicating that the solubility of Reb-AMPclay will be decreased in buffer (pH=10.0). Because of the presence factor such as the pH, protein and metal ions can limit the rate of oxidation of Mg-AMPclay and enhance the solubility of rebamipide [38, 39]. Reb-AMPclay basic on the electrostatic interactions between host and guest species may also contribute to the partitioning of H^+/OH^- ions between the rebamipide and AMP-clay matrix, which could further alter the oxidation pathway of intercalated molecules matrix compared to the distill water solution.

Drug release stability tests of rebamipide power Reb-mix-AMPclay and Reb-AMPclay (equivalent to 0.8 μg/ml Reb in SGF; 20 μg/ml rebamipide in SIF and D.W) were performed in 10 ml distilled water, SGF and SIF (37°C).The effects of AMP-clay on rebamipide release stability were measured by HPLC method. As shown in Fig.7 that AMP-clay no change rebamipide release stability in distilled water, SGF and SIF during 24hour. In addition, Reb-AMPclay long-team stability were evaluate at 4℃ and 25℃ for 4 months. Fig.8. The result shown that AMP-clay don't change rebamipide stability in long-team storage. These results suggested that AMP-clay don't effect on the rebamipide stability.

3.4 Cellular uptake study

The Reb-AMPclay and Reb-mix-AMPclay effect of rebamipide on the cellular accumulation was examined in Caco-2 cells. As illustrated in Fig.9, Compared to the rebamipide free, the cellular accumulation of rebamipide was approximately 2.6-fold lower in the cellular uptake of Reb -AMPclay. Furthermore, the cellular accumulation of rebamipide intercalated AMP-clay was significantly higher than Reb-mix-AMPclay. Thus, this result of cellular accumulation of rebamipide increased by intercalated AMP-clay or mix AMPclay, implying that intercalated Reb-AMPclay significantly increased the cellular uptake of rebamipide.

3.5 Pharmacokinetic characteristics of Rebamipide in the presence of AMP-clay

Rebamipide was formulated in three different vehicles such as formulation Ⅰ (Reb-power), formulation Ⅱ (Reb-AMPclay) and formulation Ⅲ(Reb-mix-AMPclay) in aqueous (0.5%) methylcellulose. The dose of rebamipide in each suspension for formulation Ⅰ~ Ⅲ (20 mg/kg), respectively, implying that formulation Ⅱ and Ⅲ should be more effective to dissolve rebamipide.

Mean plasma concentration–time profiles of rebamipide in the presence and the absence of AMP-clay were characterized in rats and illustrated in Fig.12. The mean pharmacokinetic parameters of rebamipide were also summarized in Tab.3. A standard curve of rebamipide and chromatograms in Fig.10,11. As shown in Tab.3, the pretreatment with Reb-AMPclay altered the oral exposure of rebamipide compared to the control group given rebamipide alone. The oral exposure of rebamipide tends to be increased via the concurrent use of AMP-clay although only. Reb-AMPclay indicated statistical significance ($p < 0.05$). Consequently, the relative bioavailability of Reb increased by approximately 1.81 fold under the pretreatment with Mg-AMP clay. There also have significant change in C_{max} and T_{max}. C_{max} increased by 2.1, T_{max} decrease to 3.0 folds, respectively while there was no significant change in $T_{1/2}$. To further explore the potential in vivo increased absorption of rebamipide by the intercalated AMP-clay, which effect on the pharmacokinetics of

rebamipide was evaluated in rats. As summarized in Tab.3, combined use of AMP-clay with rebamipide enhanced the oral exposure of rebamipide significantly ($p < 0.05$) when compared to the control group given rebamipide alone and Reb-mix-AMPclay. This results accord with we previous verification, compared to rebamipide lacking AMP-clay formulation, the dissolution of Reb-AMPclay was dramatically increased in SGF and SIF (Fig.6e,f), indicating the active involvement of AMP-clay in the gastrointestinal environment. Moreover, the solubility of rebamipide no change significantly ($p < 0.05$) in the presence of Reb-mix-AMPclay, implying that the intercalation AMP-Clay formulation that enhance the rebamipide systemic exposure in vivo study. Supporting the role of AMP-Clay as an effective formulation enhanced the oral exposure of rebamipide in pharmacokinetics study.

4. Conclusion

The present study suggests that exfoliated dispersions of an aminopropyl functionalized magnesium phyllosilicate have been used to prepare a intercalated lamellar nanocomposites containing entrapped rebamipide. The rebamipide -intercalated organoclays exhibit controlled release profiles with rates that depend on the electrostatic and steric interactions occurring between host and co-intercalated polymer molecules, this paper indirect that the intercalated lamellar nanocomposites effective to improve the dissolution, solubility of rebamipide and enhance absorption of rebamipide in vivo/vitro study, suggesting that the concomitant use of Mg-AMP clay may provide a therapeutic benefit in the oral delivery of pH-independent and insoluble drug.

5. References

1. Schmidt, D.Shah, D.Giannelis, E. P. (2002*)*. New advances in polymer/layered silicate nanocomposites. 63, 205–212

2. Suter, J. L.; Coveney, P. V.; Greenwell, H. C.; Thyveetil, M.-A. (2007). Large-scale molecular dynamics study of montmorillonite clay: Emergence of undulatory fluctuations and determination of material properties *J.Phys. Chem. C* , 111, 8248–8259.

3. Phillip B. Messersmith, Emmanuel P. Giannelis. (1994). Synthesis and characterization of layered silicate-epoxy nanocomposites. *Chem. Mater.* , *6* (10), pp 1719–1725

4. Giannelis, E. P. (1996). Preparation and characterization of polystyrene/ montmorillonite nanocomposite by melt intercalative compounding *Ad*V. *Mater.* 8, 29–35.

5. Alexandre, M. and Dubois, P. (2000). Polymer-layered Silicate Nanocomposites: Preparation, Properties and Uses of a New Class of Materials , *Mater. Sci. Eng*. Rep. 28: 1-63.

6. Vaia, R. A.; Ishii, H.; Giannelis, E. P. (1993). Synthesis and properties of 2-dimensional nanostructures by direct intercalation of polymer melts in layered silicates *Chem. Mater.* 5, 1694- 1696.

7. Ogata, N.; Jimenez, G.; Kawai, H.; Ogihara, T. (1997). Structure and thermalr mechanical properties of poly_*l*-lactide.–clay blend *J. Polym. Sci., Part B: Polym. Phys. 35*, 389-396.

8. Pavlidou, S.; Papaspyrides, C. D. (2008). A review on polymer–layered silicate

nanocomposites Prog. *Polym. Sci.* 33, 1119–1198.

9. Geoffrey, M.; Bowers, David; Bish, L.; James Kirkpatrick, R. (2008). H2O and cation structure and dynamics in expandable clays: 2H and 39K NMR investigations of hectorite. *J.Phys. Chem. C* , 112, 6430–6438.

10. Kornmann, X.; Lindberg, H.; Berglund, L. A. (2001). Synthesis of epoxy–clay nanocomposites: influence of the nature of the clay on structure. *Polymer*, 42, 1303-1310.

11. Manias, E.; Touny, A.; Wu, L.; Strawhecker, K.; Lu, B.; Chung,T. C. (2001). Polypropylene/ montmorillonite nanocomposites. Review of the synthetic routes and materials properties.*Chem. Mater. 13*, 3516.

12. Jacobs, J. D.; Koerner, H.; Heinz, H.; Farmer, B. L.; Mirau, P.; Garrett, P. H.; Vaia, R. A. (2006). Dynamics of alkyl ammonium intercalants within organically modified montmorillonite: dielectric relaxation and ionic conductivity *J. Phys. Chem. B.*, *110*, 20143–20157.

13. Patel HA, Somani RS, Bajaj HC, Jasra RV. (2006). Nanoclays for polymer nanocomposites, paints, inks, greases and cosmetics formulations, drug delivery vehicle and waste water treatment. *Bull. Mater. Sci*. 29: 133–145;

14. Pereira de Abreu DA, Paseiro Losada P, Angulo I, Cruz JM. (2007). Development of new polyolefin films with nanoclays for application in food packaging. *Eur. Polym. J.* 43: 2229–2243;

15. Sozer N, Kokini JL. (2009). Nanotechnology and its applications in the food sector. *Trends Biotechnol.* 27: 82–89;

16. Atai M, Solhi L, Nodehi A, Mirabedini SM, Kasraei S, Akbari K, Babanzadeh S. (2009). PMMA- grafted nanoclay as novel filler for dental adhesives. *Dent. Mater*. 25: 339–347.

17. Park JK, Choy YB, Oh JM, Kim JY, Hwang SJ, Choy JH. (2008). Controlled release of donepezil intercalated in smectite clays. *Int. J. Pharm.* 359: 198–204.

18. Yuan Q, Shah J, Hein S, Misra RDK. (2010). Controlled and extended drug release behavior of chitosan-based nanoparticle carrier. *Acta Biomater.* 6: 1140–1148.

19. Arakawa T, Kobayashi K, Yoshikawa T, Tarnawski A. (1998). Rebamipide: Overview of its mechanisms of action and efficacy in mucosal protection and ulcer healing. *Dig Dis Sci*. ; 43(Suppl 9):5S–13S.

20. Yamasaki K, Ishiyama H, Imaizumi T, et al. Effect of OPC-12759, (1989). a novel antiulcer agent, on chronic and acute experimental gastric ulcer, and gastric secretion in rats. *Jpn J Pharmacol*. 49:441–448.

21. Yamasaki K, Kanbe T, Chijiwa T, et al. (1987). Gastric mucosal protection by OPC-12759, a novel antiulcer compound, in the rat. *Eur J Pharmacol*. 142:23–29.

22. Ishihara K, Komuro Y, Nishiyama N, et al. (1992). Effect of rebamipide on mucus secretion by endogenous prostaglandin-independent mechanism in rat gastric mucosa. *Arzneimittelforschung*. 42:1462–1466.

23. Aihara M, Imagawa K, Funakoshi Y, et al. (1998). Effects of rebamipide on production of several cytokines by human peripheral blood mononuclear cells. *Dig Dis Sci*. 43(Suppl

9):160S– 166S.

24. Nagano C, Wakebe H, Azuma A, et al. (1998). IFN-gamma-induced iNOS mRNA expression is inhibited by rebamipide in murine macrophage RAW264.7 cells. *Dig Dis Sci*. 43 (Suppl 9):118S–124S.

25. Naito Y, Yoshikawa T, Tanigawa T, et al. (1995). Hydroxyl radical scavenging by rebamipide and related compounds: Electron paramagnetic resonance study. *Free Radic Biol Med*. ;18:117–123.

26. US Food and Drug Administration. Guidance for industry: Waiver of in vivo bioavailability and bioequivalence studies for immediate-release solid oral dosage forms based on a biopharmaceutics classification system.(2009). http:// www.fda.gov /downloads /Drugs/ Guidance Compliance Regulatory Information /Guidances /ucm070246. pdf. Accessed November 3.

27. Naito Y, Yoshikawa T, Iinuma S, et al. (1996). Local gastric and serum concentrations of rebamipide following oral administration to patients with chronic gastritis. *Arzneimittelforschung*. 46:698–700.

28. Carmichael, J.; DeGraff, W. G.; Gazdar, A. F.; Minna, J. D.; Mitchell, J. B. *Cancer Res. (*1987).*47*, 943–946.

29. N. T. Whilton, S. L. Burkett and S.Mann., (1998). Hybrid lamellar nanocomposites based on organically functionalized magnesium phyllosilicate clays with interlayer reactivity *J. Mater. Chem.*, 8, 1927.

30 A. J. Patil, E. Muthusamyand S.Mann,Angew,.(2004). Synthesis and Self-Assembly of

Organoclay-Wrapped Biomolecules *Chem., Int. Ed*. 43, 4928.

31. Niv Y,Byrd Jc,Ho SB.,(1992). Mucin synthesis and secretion in relation to spontaneous differentiation of colon cancer cells in vitro. *Int J Cancer*, 50.10:147-152.

32. Li, L., Nandi, I.,Kim,K.H.,(2002). Development of an ethyl laurate-based microemulsion for rapid-onset intranasal delivery of diazepam. *Int.J.Pharm.* 237,77–85.

33. Masateru Miyake a, Takanori Minami b, Masao Hirota c, Hajime Toguchi a, Masaaki Odomi a, Ken-ichi Ogawara d, Kazutaka Higaki d, Toshikiro Kimura d,* (2006).Novel oral formulation safely improving intestinal absorption of poorly absorbable drugs: Utilization of polyamines and bile acids. *Journal of Controlled Release* 111, 27 – 34.

34. Hyo-Kyung Han,† Young-Chul Lee,‡ Moo-Yeol Lee,† Avinash J. Patil,§ and Hyun-Jae Shin*,‡ (2011). magnesium and calcium organo phyllosilicates: synthesis and In vitro cytotoxicity study. *ACS Appl Mater Interfaces.*3(7): 2564-72

35. A. J. Patil, E. Muthussamy, and S. Mann, *Angew. Chem. Int. Ed., (*2004), 43, 4928.

36. S. L. Burkett, A. Press, and S. Mann, *Chem. Mater.,* (1997), 9, 1071

37. S.C. Holmström, A. J. Patil, M. Butler, S. Mann, *J. Mater. Chem.,* (2007), 17, 3894

38. Gunckel S,Santander P,Cordano G,(1998). Antioxidant activity of gallates: an electrochemical study in aqueous media. *Chem Biol Interact.* 3;114(1-2):45-59.

39. Kumamoto M,Sonda T,Nagayama K,Tabata M.(2001). Effects of pH and metal ions on antioxidative activities of catechins. *Biosci Biotechnol Biochem.*1;65(1):126-32.

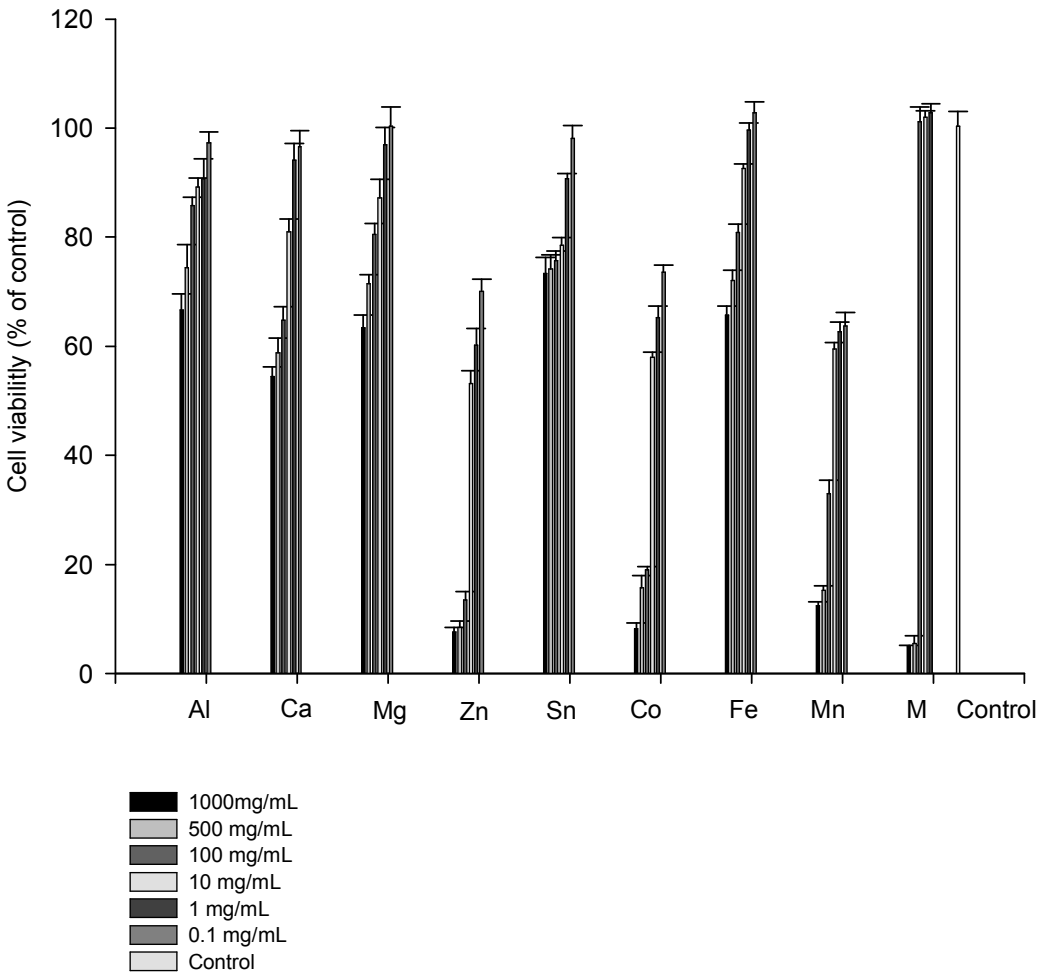

Fig. 1(a) Effects of organoclays on cell viability. Concentration-dependent cytotoxic effects of organoclays were evaluated after a 48/72 h incubation.. Cytotoxicity is expressed relative to nontreated control cells. M (menadione 0.1~100μM). Data are represented as means SD (n = 6). * $p < 0.05$ compared to the control group.

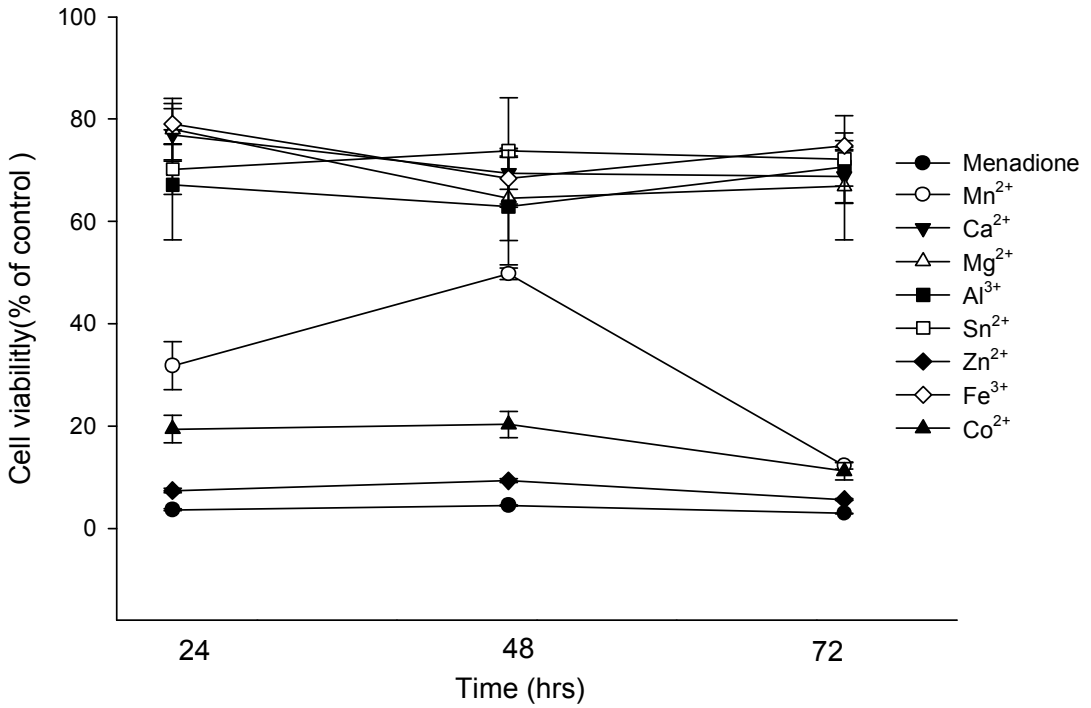

Fig. 1(b) Time-dependent cytotoxicity of origao-clay was assessed at a concentration of 1000 μg/ml

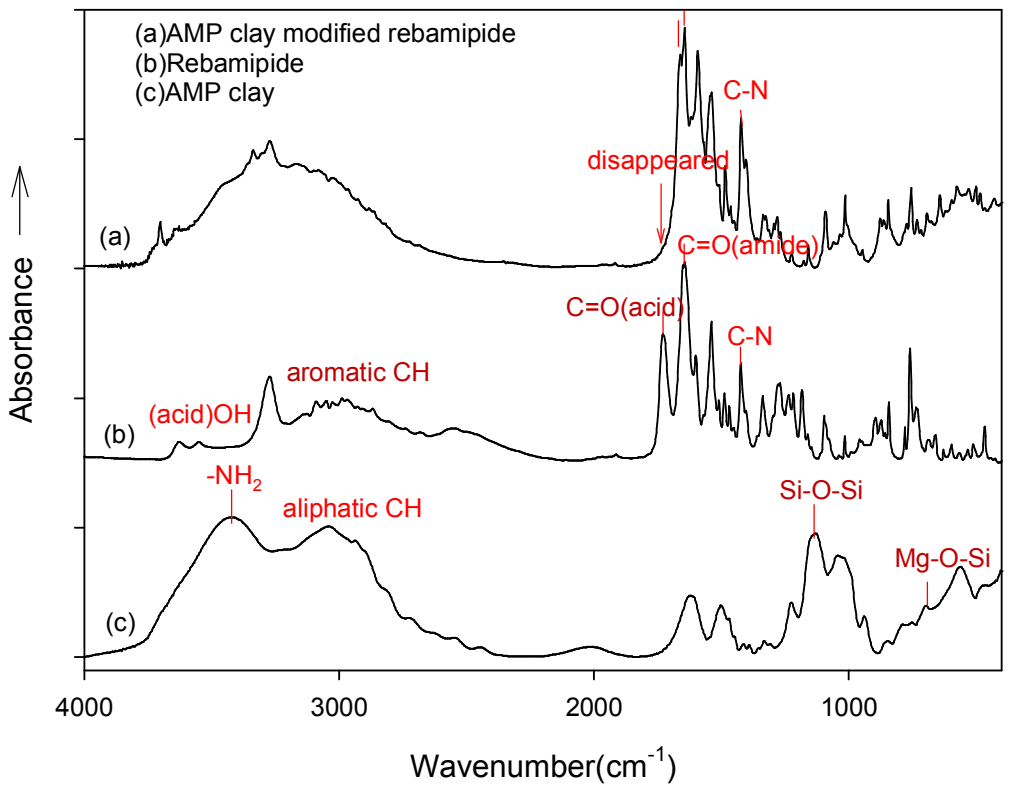

Fig.2 FT-IR spectra of AMP-clay modified rebamipide(a), rebamipide(b), and AMP-clay(c) (KBr pellet)

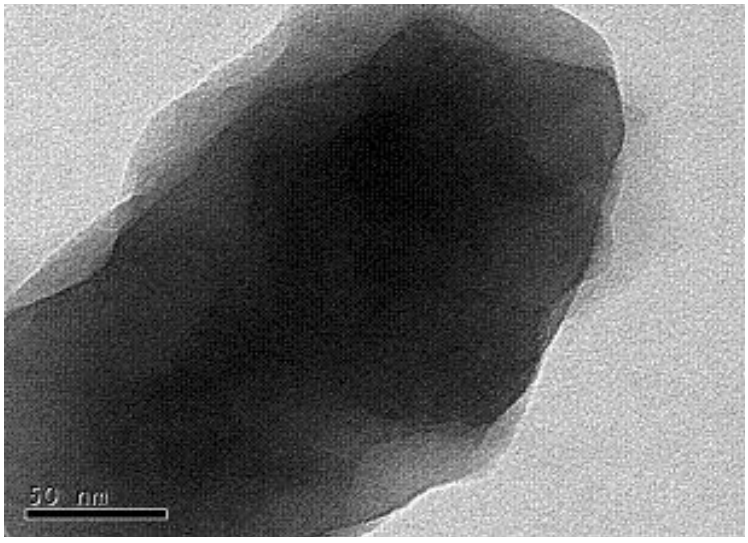

(a) Layered structure of AMP-clay

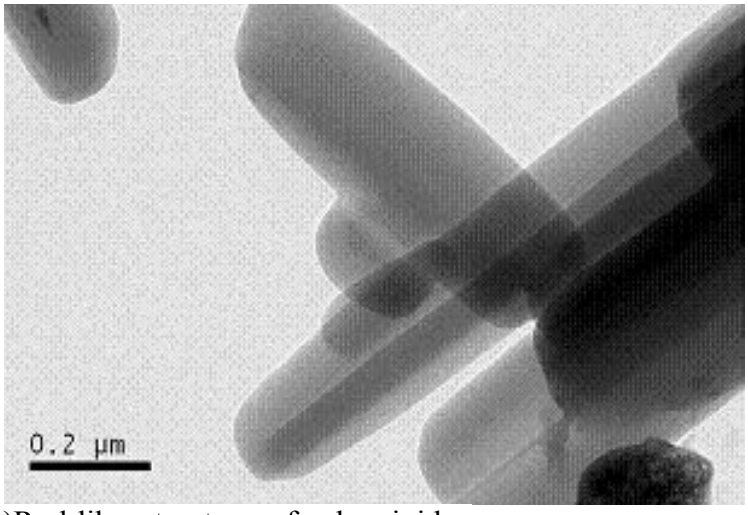

(b)Rod-like structure of rebamipide

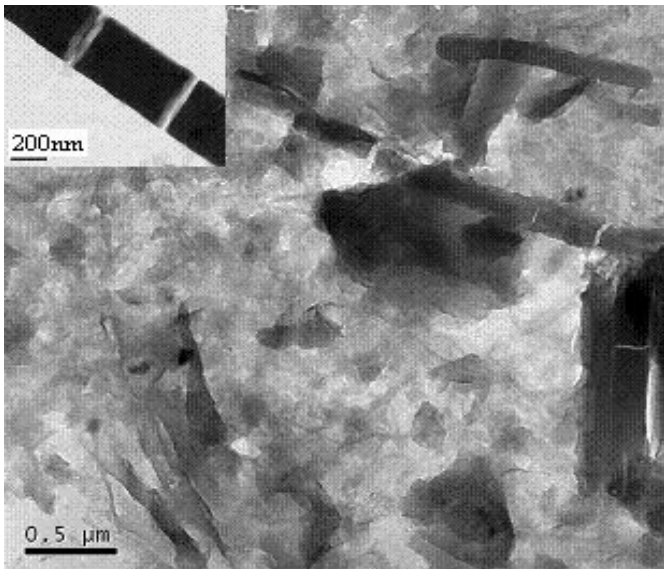

(c) Rebamipide wrapped with AMP-clay.

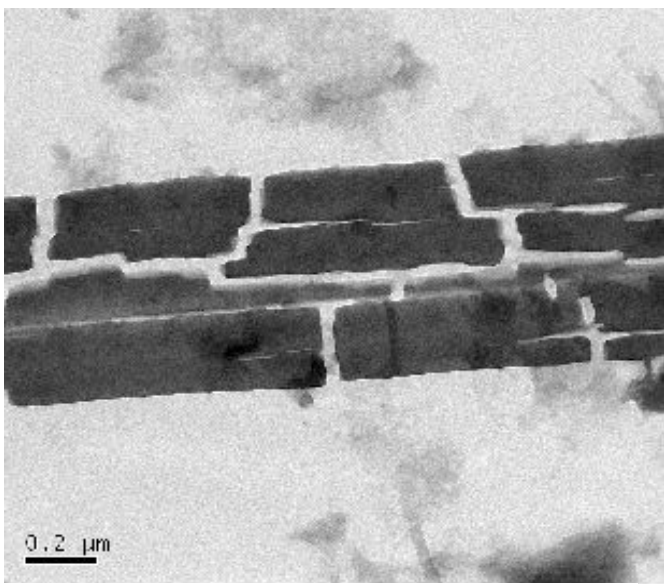

(d) Exfoliated AMP clay between rebamipide cracks

Fig.3 TEM images of AMP clay(a), rebamipide (b), and AMP clay modified rebamipide (c, d)

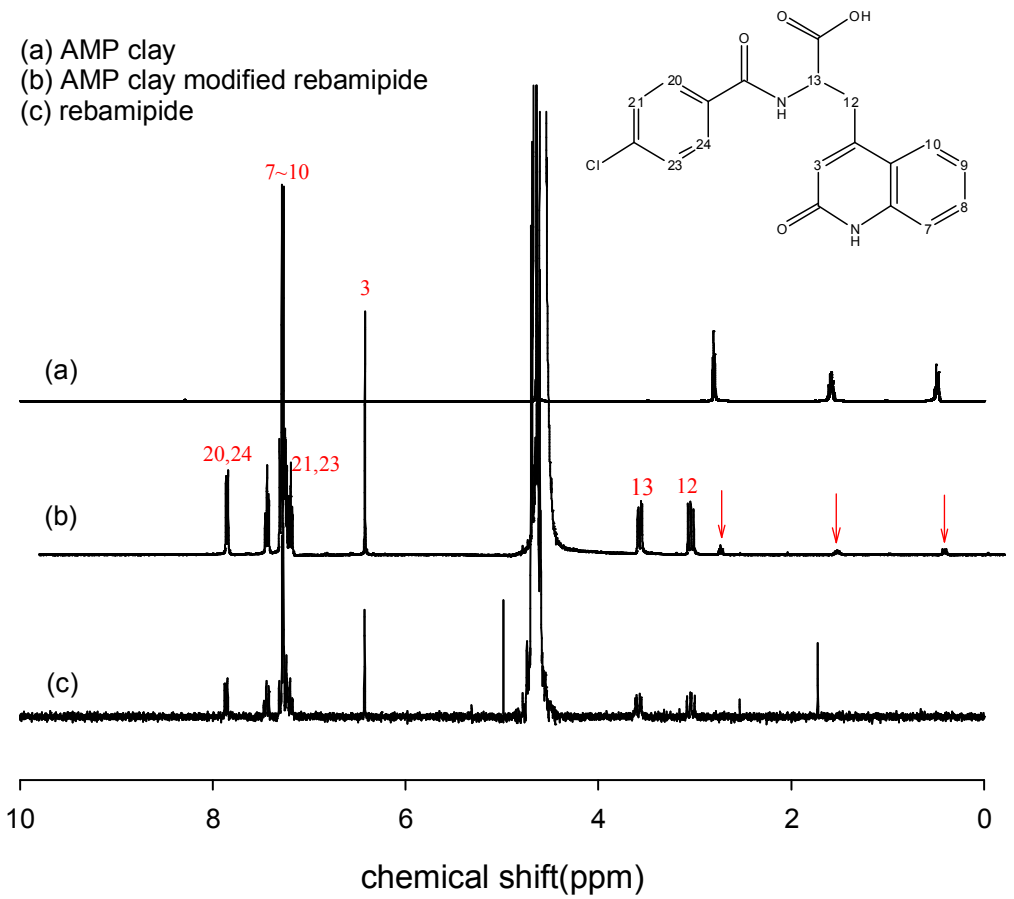

Fig.4 ^{1}H-NMR spectra of AMP-clay (a), AMP clay modified rebamipide (b), and rebamipide (c) (D_2O)

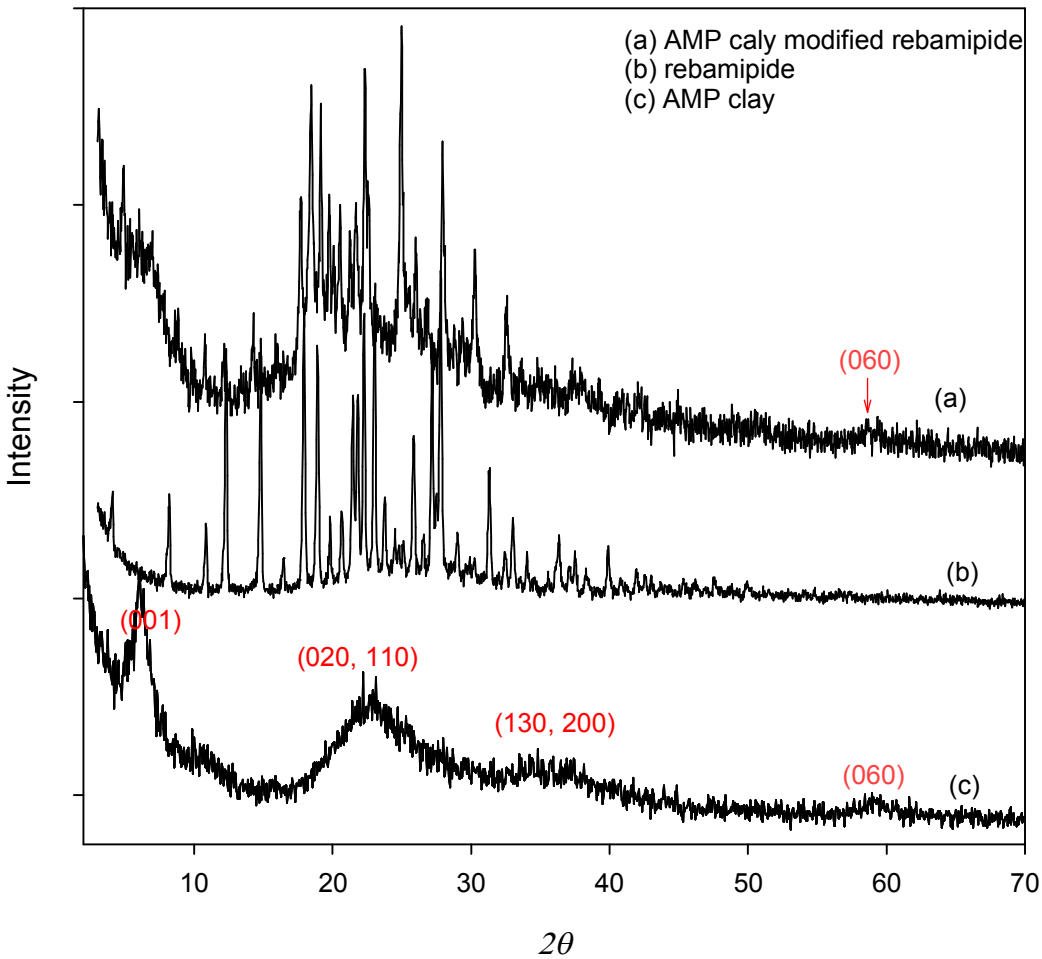

Fig.5 X-ray diffraction patterns of AMP-clay modified rebamipide(a), and rebamipide(b) and AMP-clay(c).

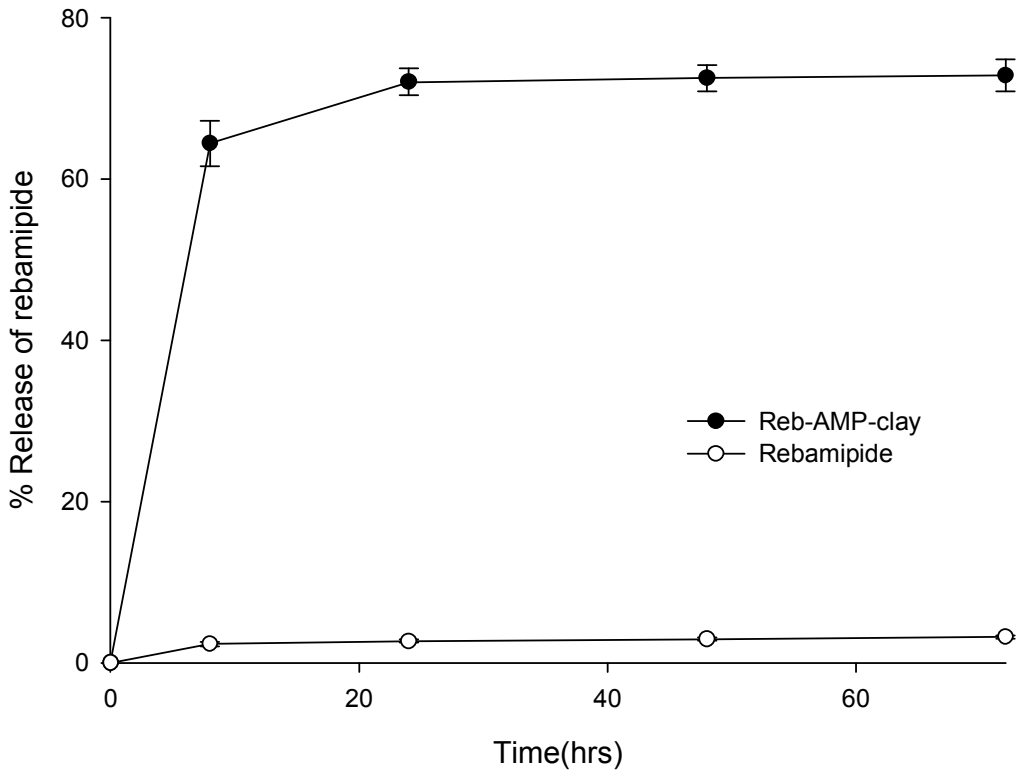

Fig. 6(a) Rebamipide and Reb-AMPcaly release in D.W (n=3).

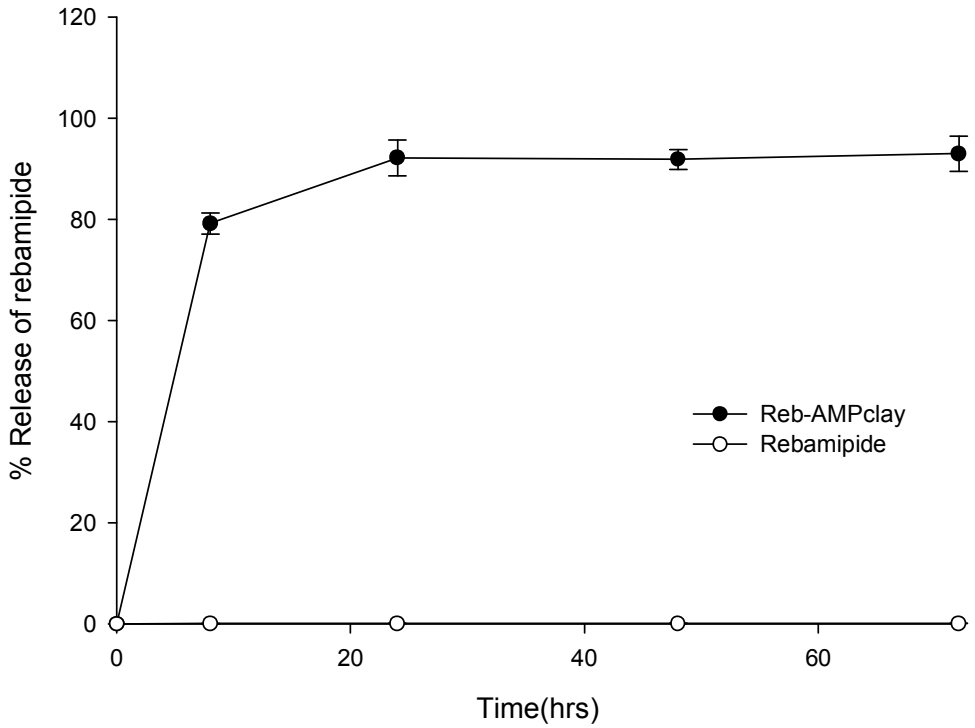

Fig. 6(b) Rebamipide and Reb-AMPcaly release in buffer (pH = 2.0) (n=3).

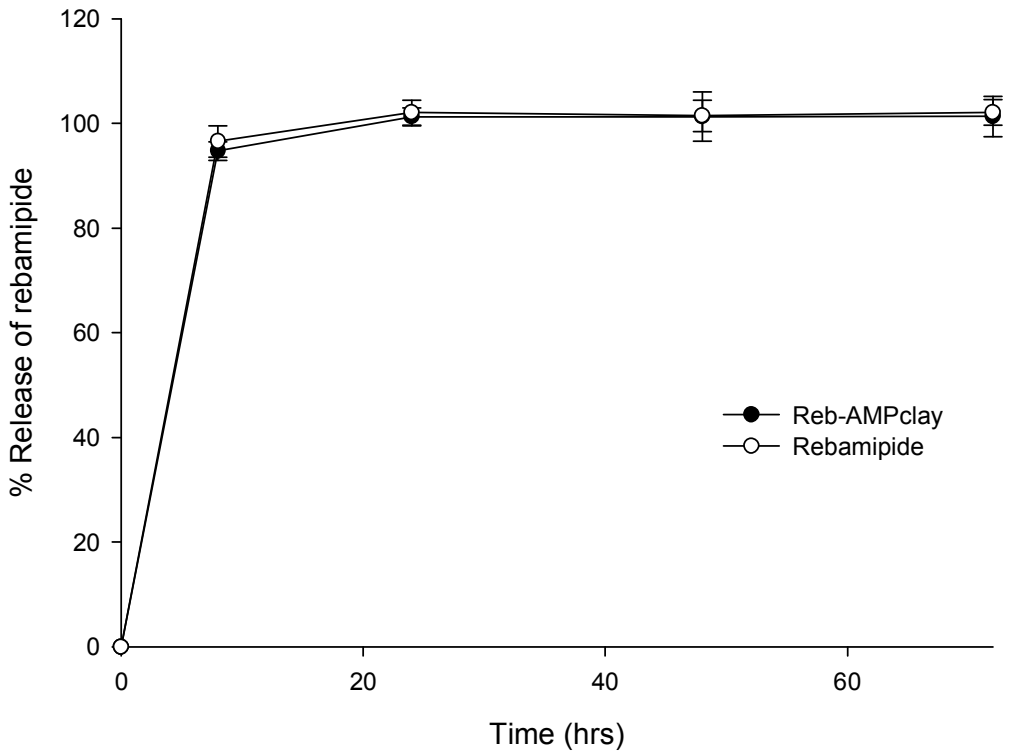

Fig. 6(c) Rebamipide and Reb-AMPcaly release in buffer (pH = 6.8) (n=3).

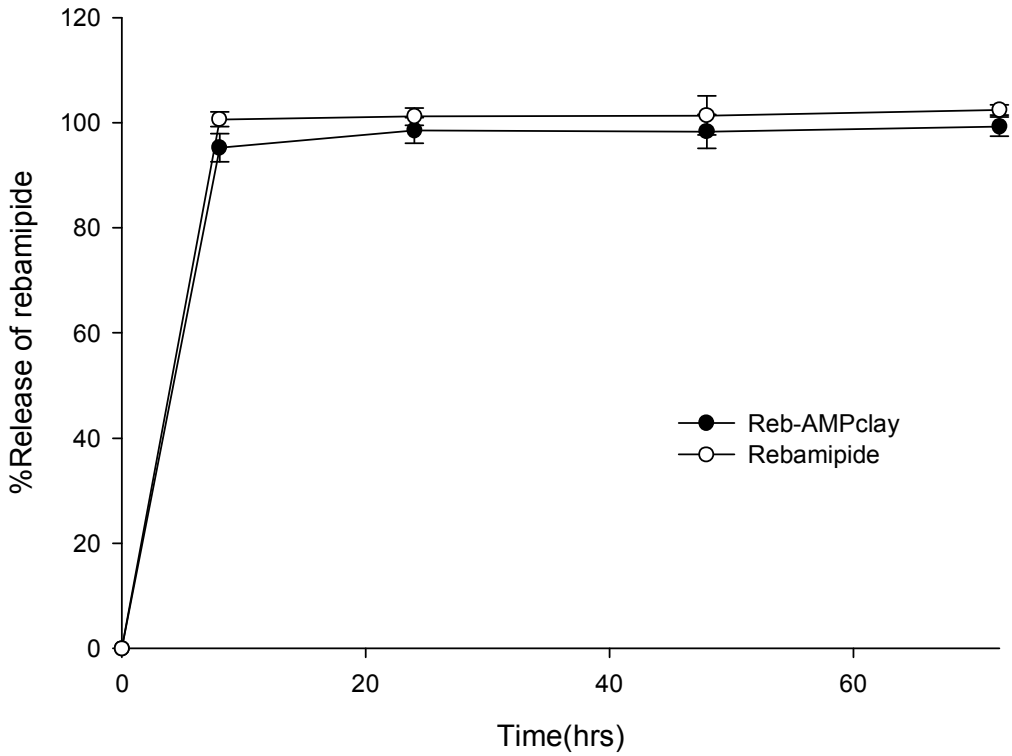

Fig. 6(d) Rebamipide and Reb-AMPcaly release in buffer (pH = 10.0) (n=3).

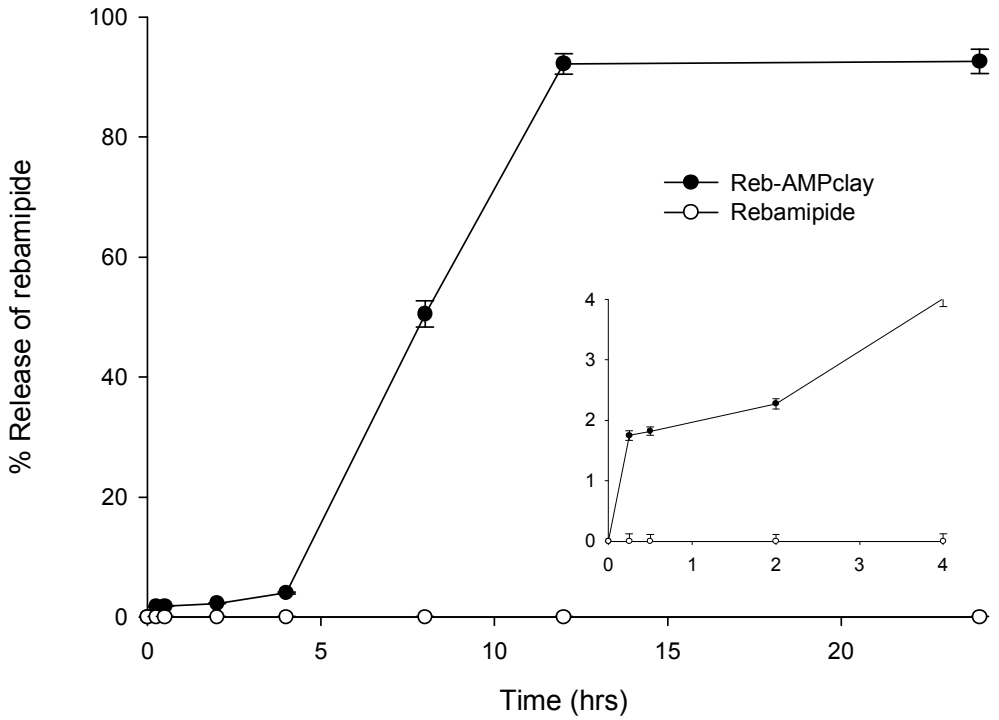

Fig. 6(e) Rebamipide and Reb-AMPcaly release in SGF (n=3).

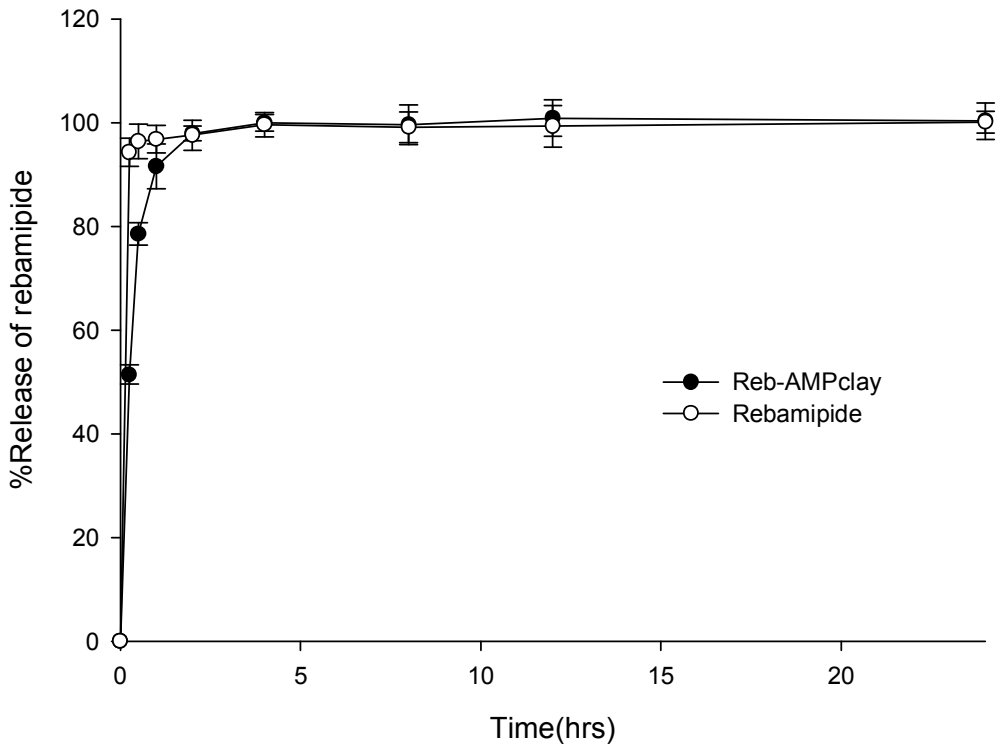

Fig. 6(f) Rebamipide and Reb-AMPcaly release in SIF (n=3).

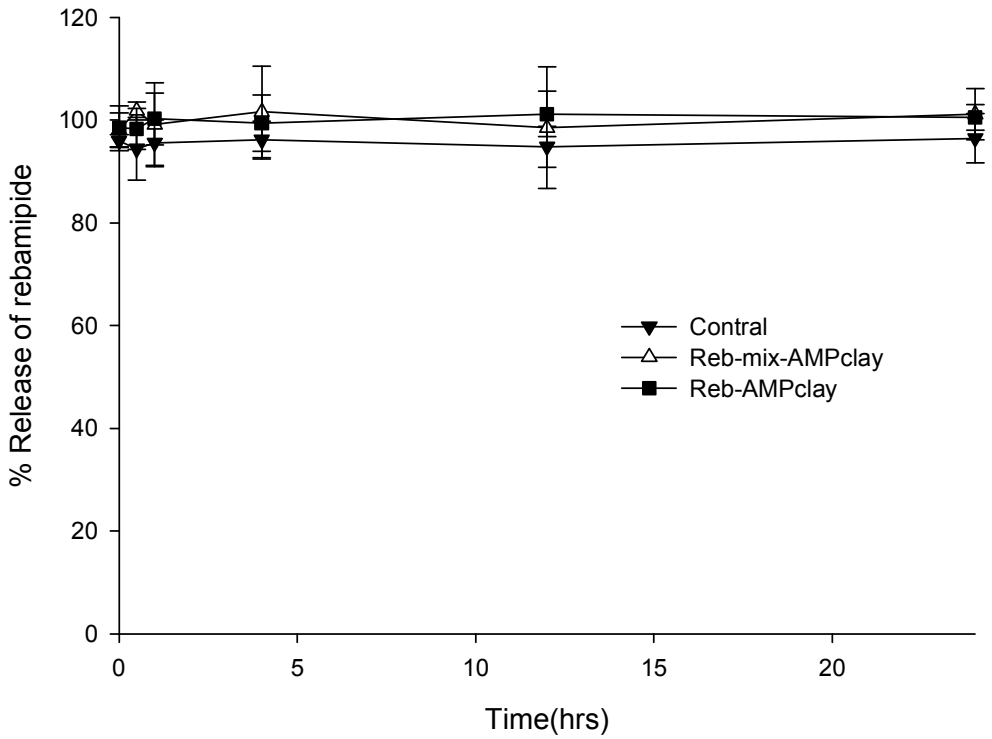

Fig. 7(a) The release stability of rebamipide in D.W.(n=3)

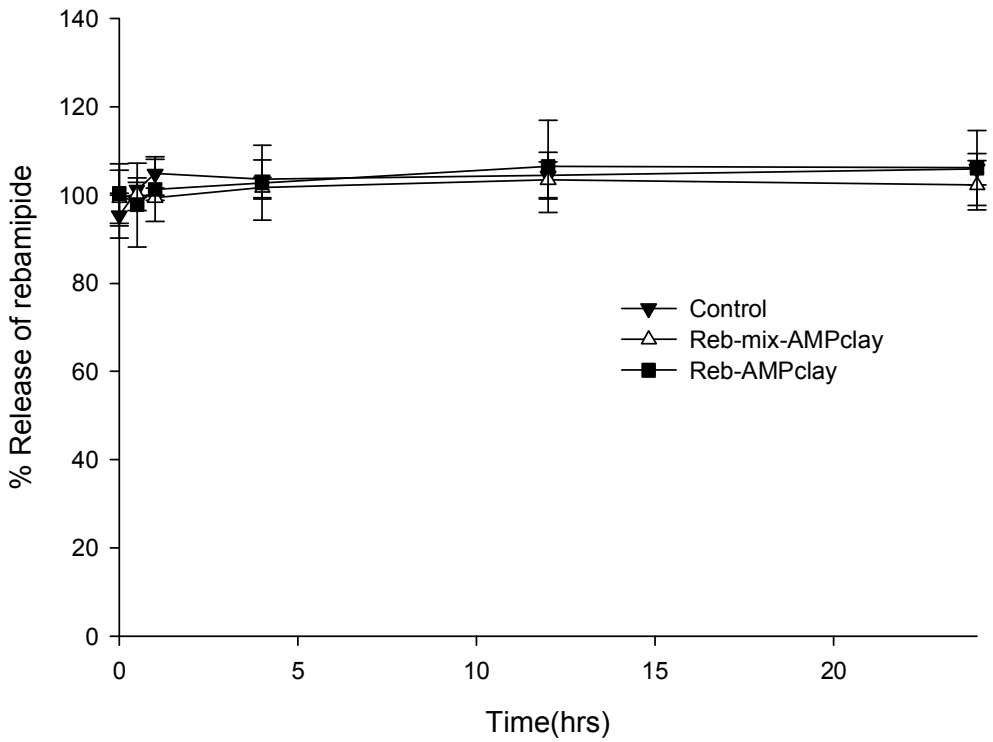

Fig. 7(b) The release stability of rebamipide in SGF.(n=3)

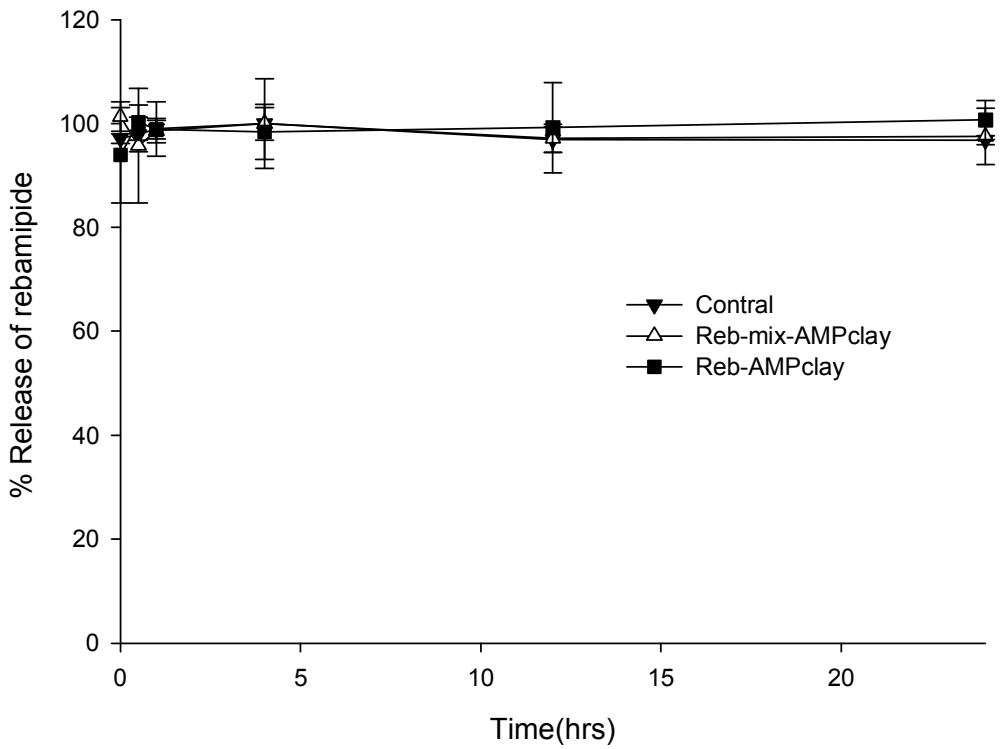

Fig. 7(c) The release stability of rebamipide in SIF.(n=3)

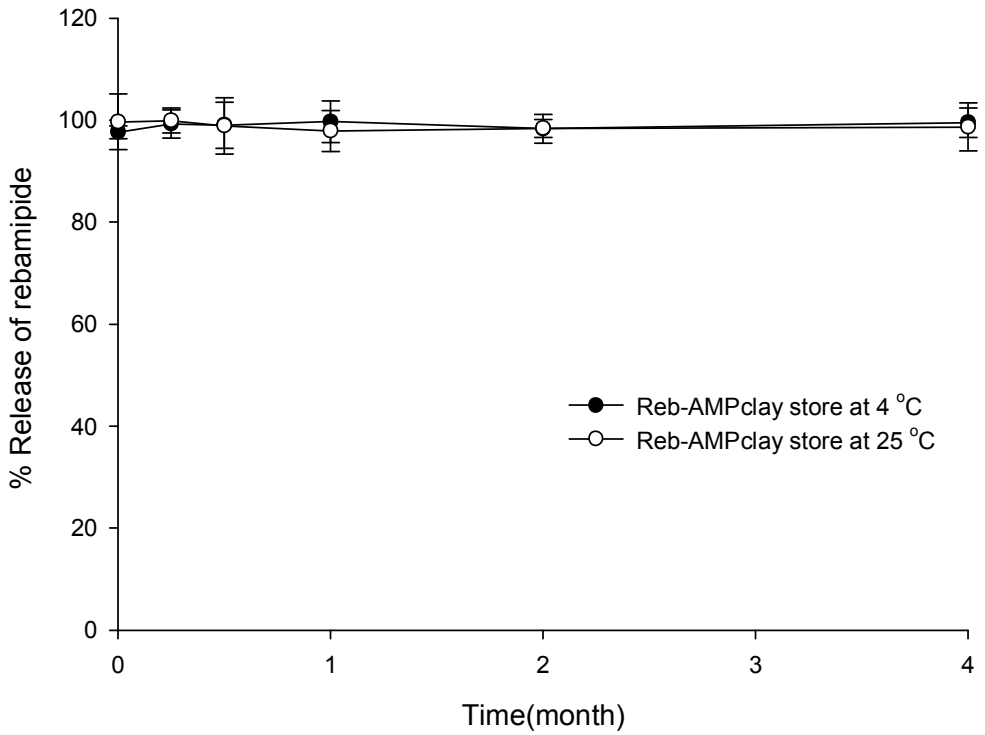

Fig.8 The stability of Reb-AMPclay in long-team storage.(n =3)

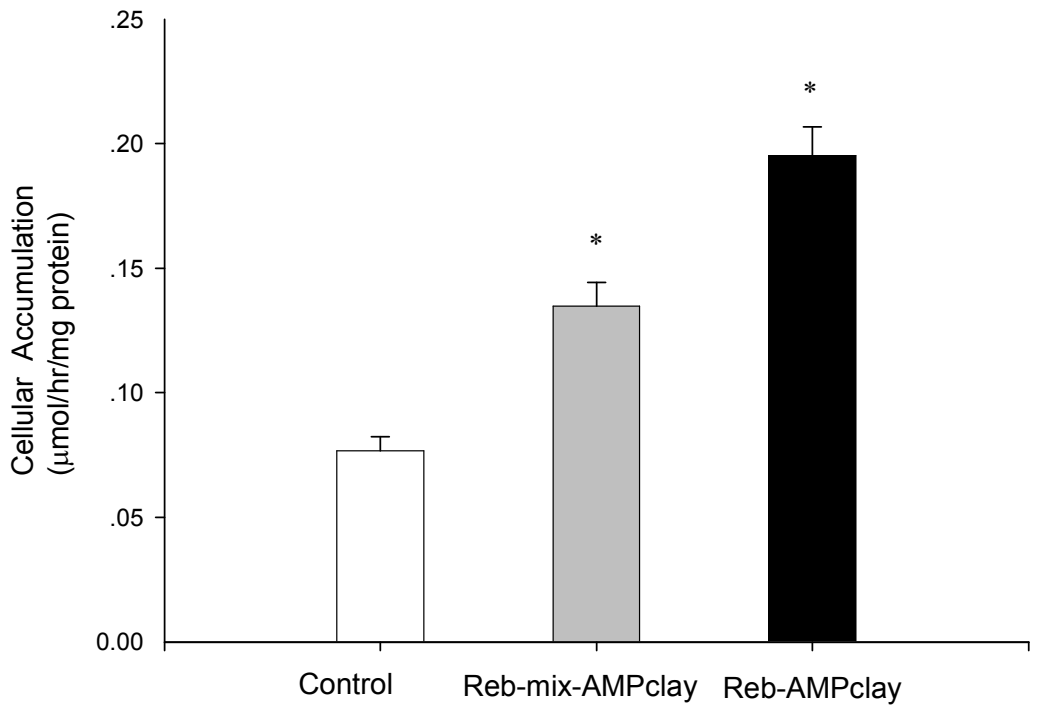

Fig.9. Cellular accumulation of rebamipide in Caco-2 cells (mean±S.D., n = 6). *p < 0.01, compared with the control given rebamipide alone.

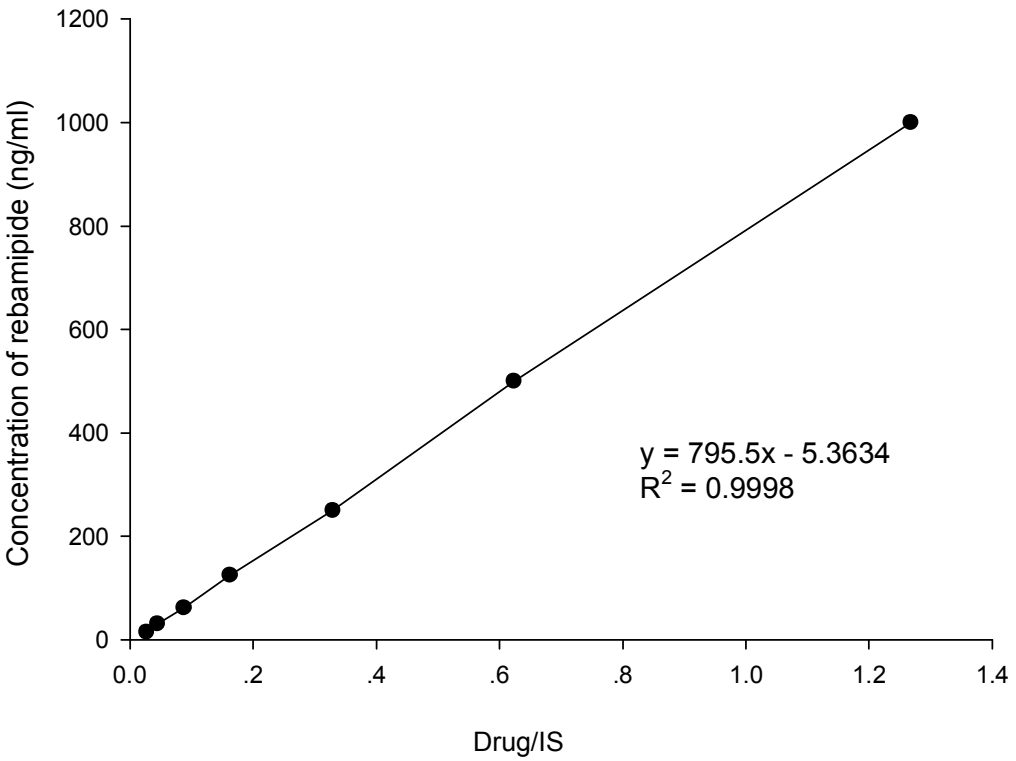

Fig. 10 The standard curve of rebamipide in pharmacokinetics study

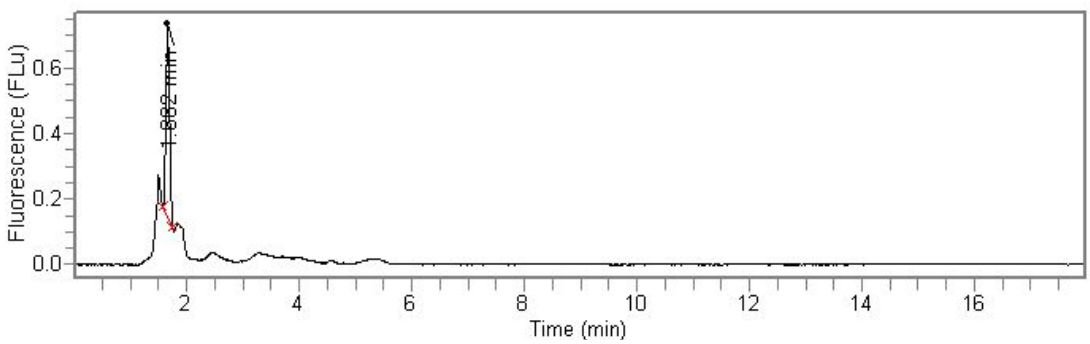

(A)

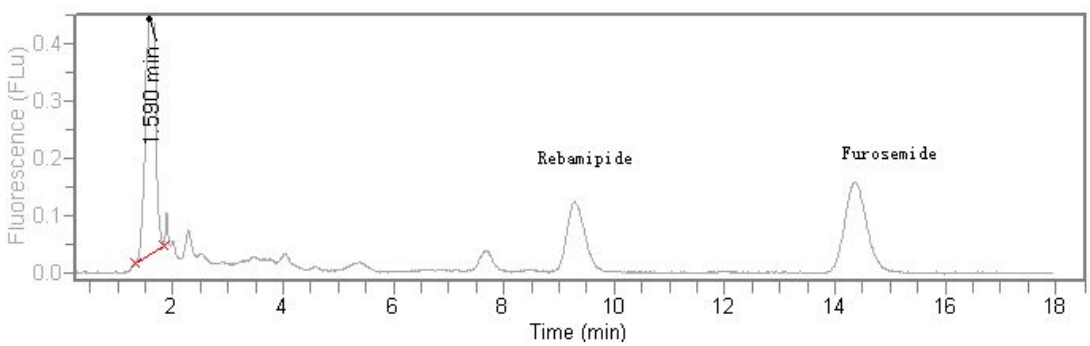

(B)

Fig.11 Two representative chromatograms including an intact blank plasma (A), and a plasma sample supplemented with lower range of rebamipide and the internal standard furosemide (B).

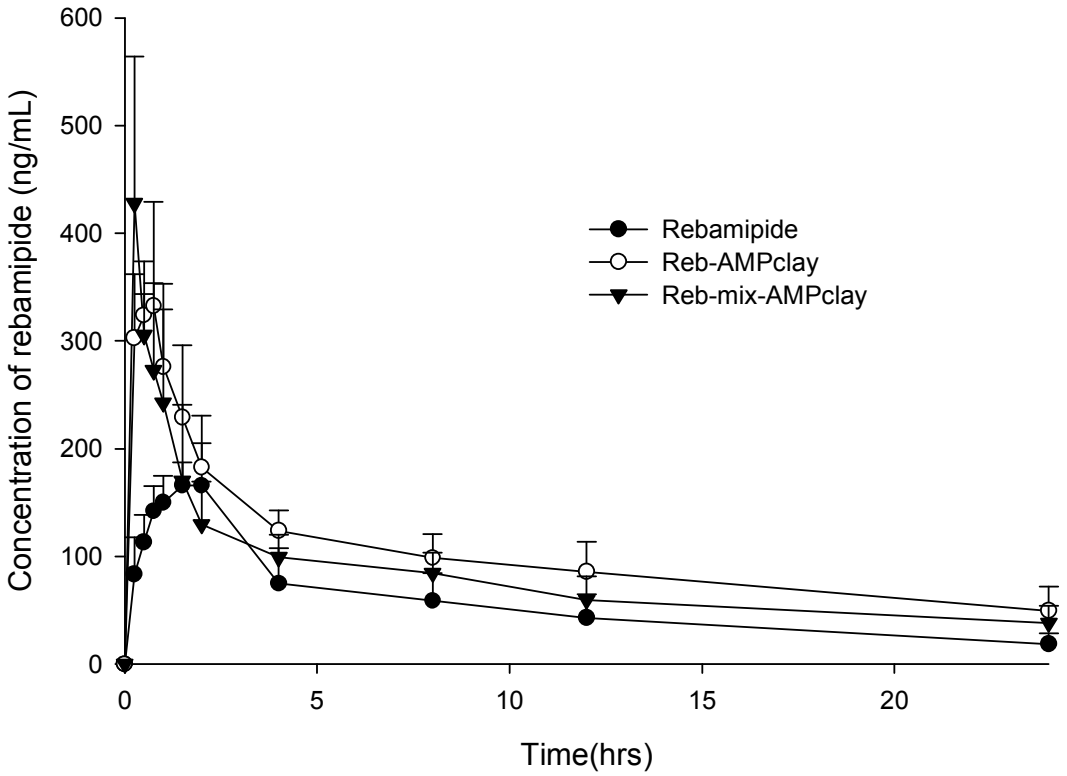

Fig.12 The mean plasma concentration–time profiles of rebamipide after oral administration (20mg/kg rebamipide) Rebamipide power, Reb-AMPclay and Reb-mix-AMPclay.

Table 1. Solubility of rebamipade with different excipients(μg/ml).

Excipient	Solubility of rebamipade		
	D.W	SIF	SGF
control	23.91±1.35	3775.83±102.06	0.92±0.09
chitosan	155.78±2.27	4353.45±103.53	244.09±5.23
Methyl cellulose	37.29±0.90	3316.96±78.04	0.87±0.04
HPMC 4000	47.43±3.52	3506.63±72.96	0.96±0.06
carbopol	5.28±1.36	2383.77±37.43	0.79±0.14
sodium alginate	336.39±10.55	3515.61±107.59	2.35±0.32
Lactose	26.05±1.20	3532.33±90.9	0.8±0.02
PEG6000	38.38±1.87	3772.1±34.33	0.99±0.06
AMP-clay	510.67±8.65	5095.05±119.01	535.39±34.66

Table 2. Solubility of rebamipide and nanoclay rebamipide with different buffers, DW, SGF and SIF(μg/ml).

	Solubility of rebamipade	
	Reb-AMPclay	Rebamipide
DW	510.67±8.65	23.91 ± 1.35
pH= 2.0	922.19 ± 35.19	0.84 ± 0.01
pH= 6.8	9409.04 ± 130.84	1152.97 ± 37.35
pH= 10.0	1838.76 ± 147.22	9504.78 ± 73.76
SIF	8589.12 ± 150.39	3775.83 ± 102.06
SGF	686.80 ± 28.12	0.92 ± 0.09

Table 3. Pharmacokinetic parameters of rebamipide, Reb-AMPclay and Reb-mix-AMPclay after oral administration in rats

	C_{max}(ng/ml)	T_{max}(h)	$T_{1/2}$(h)	AUC(ng.h/ml)
Rebamipide	177.81±19.03	1.75±0.42	9.81±3.75	1345.03±423.43
Reb-AMPclay	375.05±70.63*	0.58±0.20*	9.57±2.17	2435.39±459.66*†
Reb-mix-AMPclay	427.81±136.13*	0.25*	10.61±3.99	1928.72±306.31

All data are expressed the means ± standard deviation (n = 6)

*$p < 0.05$ compared with rebamipide alone.

†$P < 0.05$ compared with Reb-mix-AMPclay alone

Acknowledgements

I would like to take this opportunity to express my gratitude to all the people who have ever helped me in this paper.

My sincere and hearty thanks and appreciations go firstly to my supervisor, Dr. Hyo-Kyung Han, whose suggestions and encouragement have given me much insight into these scientific research. It has been a great privilege and joy to study under her guidance and supervision. Furthermore, it is my honor to benefit from her personality and diligence, which I will treasure my whole life. My gratitude to her knows no bounds. I am also extremely grateful to Dr. Hoo-Kyun Choi. He as my advisor in Chosun university who has kindly provided me assistance and guidance in the course of preparing this paper.

I also like to express my thanks to all my lab mates of life pharmacology department who co-worked in 4 years of my studying and helped me to adapt new environment: Mingji Jin, Youngbin Im, HyoungKyu Lee, Seongjin Yoo.

In addition, many thanks to my parents and my wife for their unfailing love and unwavering support. From the bottom of my heart, I will ever always wish and pray for them.

Finally, I am really grateful to all those who devote much time to reading this thesis and give me much advice, which will benefit me in my later study.